AD 640988

AD

USAAVLABS TECHNICAL REPORT 66-60

INVESTIGATION OF LIGHTWEIGHT STRUCTURAL DESIGN TECHNIQUES FOR LIGHTWEIGHT FANS

CLEARINGHOUSE
FOR FEDERAL SCIENTIFIC AND
TECHNICAL INFORMATION
Hardcopy | Microfiche
$5.00 | $1.25 | 145 pp
ARCHIVE COPY
Code 1

By

G. Boehler

W. Foshag

E. Deutsch

J. Balciunas

September 1966

U. S. ARMY AVIATION MATERIEL LABORATORIES
FORT EUSTIS, VIRGINIA

CONTRACT DA 44-177-AMC-250(T)

AEROPHYSICS COMPANY
WASHINGTON, D. C.

Distribution of this document is unlimited

U S ARMY MATERIEL COMMAND

DDC
RECEIVED
OCT 31 1966
TISIA

DISCLAIMER NOTICE

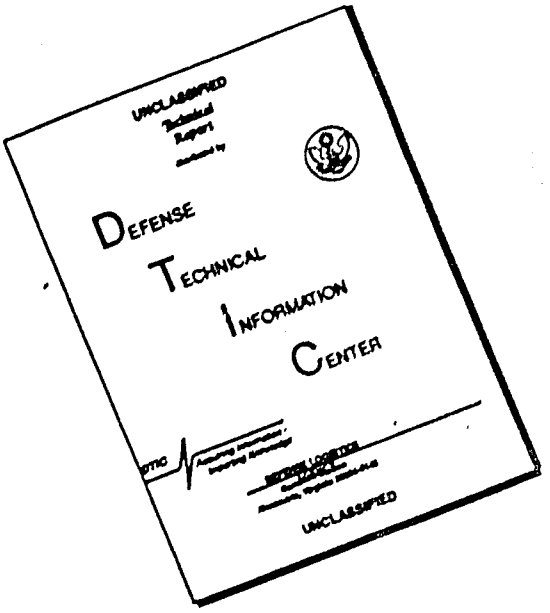

THIS DOCUMENT IS BEST QUALITY AVAILABLE. THE COPY FURNISHED TO DTIC CONTAINED A SIGNIFICANT NUMBER OF PAGES WHICH DO NOT REPRODUCE LEGIBLY.

BLANK PAGES
IN THIS
DOCUMENT
WERE NOT
FILMED

Disclaimers

The findings in this report are not to be construed as an official Department of the Army position unless so designated by other authorized documents.

When Government drawings, specifications, or other data are used for any purpose other than in connection with a definitely related Government procurement operation, the United States Government thereby incurs no responsibility nor any obligation whatsoever; and the fact that the Government may have formulated, furnished, or in any way supplied the said drawings, specifications, or other data is not to be regarded by implication or otherwise as in any manner licensing the holder or any other person or corporation, or conveying any rights or permission, to manufacture, use, or sell any patented invention that may in any way be related thereto.

Trade names cited in this report do not constitute an official endorsement or approval of the use of such commercial hardware or software.

Disposition Instructions

Destroy this report when no longer needed. Do not return it to originator.

DEPARTMENT OF THE ARMY
U. S. ARMY AVIATION MATERIEL LABORATORIES
FORT EUSTIS, VIRGINIA 23604

The investigation covered by this report was sponsored jointly by the U. S. Bureau of Ships and the U. S. Army Aviation Materiel Laboratories. It was undertaken to determine if rotating diffuser fans could be fabricated light enough in weight to be used in aircraft applications and to develop methods for prediction of operating stresses.

The report has been reviewed by this command and is considered to be technically sound.

Project 1P125901A142
Contract DA 44-177-AMC-250(T)
USAAVLABS Technical Report 66-60
September 1966

INVESTIGATION OF LIGHTWEIGHT STRUCTURAL DESIGN TECHNIQUES FOR LIGHTWEIGHT FANS

by

G. Boehler, W. Foshag,
E. Deutsch and J. Balciunas

Prepared by

AEROPHYSICS COMPANY
Washington, D. C.

for

U. S. ARMY AVIATION MATERIEL LABORATORIES
FORT EUSTIS, VIRGINIA

Distribution of this
document is unlimited

SUMMARY

The efficiency of an air mover for air cushion vehicles (ACV's) is a function not only of the aerodynamic efficiency but also of the weight per air-horsepower delivered at the nozzle. Earlier work had indicated aerodynamic advantages of the rotating diffuser (RD) fan for ACV's. This report presents the results of an investigation of the design and fabrication problems of a minimum-weight rotating diffuser ACV lift system.

Because such an analysis does not exist in the literature, a numerical method for the stress analysis of an indeterminate rotating diffuser centrifugal fan structure was reduced to practice and programmed for the IBM 1620 computer. This method was used as a tool for the analytical design of a minimum-weight RD fan. This fan, with a 64.5-inch overall diameter, was built of aluminum and was structurally tested in the fan test facility of the Joy Manufacturing Company, New Philadelphia, Ohio. Stress levels throughout the fan were measured by means of 21 strain gages.

Results of the test are very encouraging and vindicate the analytical approach to fan design. Based on measured weights and stress levels, it is concluded that RD fans for ACV applications, for ratings between 100 and 1000 horsepower, can be built for 0.5 pound per horsepower.

The stress analysis developed in this contract appears to yield accurate numerical data except at the base of the rotating diffuser and in regions of large shroud curvature. Its extension to account for three-dimensional effects appears feasible.

The method of fan fabrication used in this program is relatively expensive and time-consuming. It was determined, however, that plastic fabrication of RD fans with approximately the same weight and strength characteristics as the aluminum fans is both possible and practical, with very significant cost reduction.

FOREWORD

The study presented in this report was undertaken by Aerophysics Company, Washington, D. C., as the prime contractor and Joy Manufacturing Company, New Philadelphia, Ohio, as the subcontractor. The study was cosponsored by the U. S. Army Aviation Materiel Laboratories (USAAVLABS), Fort Eustis, Virginia, and the U. S. Navy Bureau of Ships and was monitored by USAAVLABS. Mr. William Sickles was the Project Officer.

The study is a continuation of the work reported in USATRECOM Technical Report 64-33 (Reference 2). The report contains a summary of the work performed between November 1964 and February 1966.

CONTENTS

ILLUSTRATIONS

TABLES

LIST OF SYMBOLS *

a	axial length of section, inches
d	ratio of radial to tangential stresses
E	Young's modulus
F	force acting on portion of body, pounds
G	shear modulus, $inch^4$
g	gravitational constant, $ft./sec.^2$
K	stress concentration factor
l	length of blades along ray
L_v	vane straight length, inches
N	number of blades, rotating speed, r.p.m.
N_v	number of vanes
R	radius of section, inches
r	radial thickness of station, inches
S	station
t	tangential blade width, inches
T_v	vane thickness, inches
w	length of blade section along mean passage line, inches
W_v	vane width, inches
α	coefficient of thermal expansion
β	diffuser angle, degrees
δ	deflection of member, inches
ΔR	radial distance between means with adjacent stations, inches
ΔT	temperature rise of section above starting temperature, $^oF.$

*See Figure 2, page 5, for identification of stations and symbols.

θ	angle between ray and axis, degrees
λ	vane angle
ν	Poisson's ratio
ρ	density, slugs/ft.^{3}
σ	normal stress, pounds per square inch (p.s.i.)
Σ	energy of deformation
τ	shear stress, p.s.i.
ψ	spring rate
ω	angular velocity

SUBSCRIPTS

b	blade
c	value obtained by energy-balance method
d	inner diffuser
f	fictitious value for calculation
h	hub
i	assumed value for calculation
m	value obtained from finite-difference method
o	outer radius of disc
r	radial
s	shroud
t	tangential
u	ultimate strength
v	vane

INTRODUCTION

The efficiency of an air mover for air cushion vehicles is a function not only of the aerodynamic efficiency but also of the weight per air-horsepower delivered at the nozzle. Work performed under Contract DA 44-177-AMC-886(T) by Aerophysics Company and by its subcontractor, Joy Manufacturing Company, verified the aerodynamic performance of the rotating diffuser fan and indicated a method of designing a lightweight unit. Since the rotating diffuser lift system appears to offer improved performance for presently contemplated air cushion vehicles, Aerophysics Company, again in association with Joy Manufacturing Company, was awarded Contract DA 44-177-AMC-250(T) to conduct an investigation to verify the lightweight structural design techniques developed under the previous contract, with a view to permit substantial reductions in the weight, cost and manufacturing time of rotating diffuser fans. The results of this investigation are contained in the present report.

The program discussed in this report consisted of five phases. Under Phase I, a detailed stress analysis of a lightweight RD impeller was prepared, the analysis was coded on a 1620 IBM digital computer and a method of fabrication, based on an aluminum riveted type of construction, was selected and its choice was justified.

Under Phase II, a detailed design analysis of the aluminum fan proposed in Phase I was performed. This analysis was based on the results of the computer-programmed stress analysis developed in Phase I. Fabrication drawings of a 64.50-inch-diameter lightweight RD fan were also prepared.

Under Phase III, two identical units of the design completed under Phase II were fabricated. Under Phase IV, the first unit was structurally tested in November and December 1965 in the fan test facility of the Joy Manufacturing Company, New Philadelphia, Ohio. Elaborate steps had been provided in advance for the speedy substitution of the second fan, properly modified, in case of a failure of the first fan during test. Since there was no such occurrence, there was no need for modifying the second wheel or for testing it; it was simply sent to New Philadelphia for dynamic balancing.

This report presents an evaluation of the results obtained under Phases I through IV of the contract. In order to insure maximum clarity of the report, the report sections do not each exactly correspond to one phase of the program. The report is thus organized as follows: Phase I is discussed in Sections I and II. Phases II and III are reported in Section III. The report on Phase IV, which was handled completely by Joy Manufacturing Company, was written by Joy and is presented as Section IV. The last two sections of the

report do not correspond to specific phases. In Section V, a comparison is made of the calculated stress levels, discussed in Sections I and III, and the measured stress levels, discussed in Section IV. In Section VI, two preliminary design studies of air cushion vehicles representative of potential uses of RD fans as internal-flow air movers are made and the specific weight of the RD fan (weight per horsepower) is obtained.

SECTION I

STRESS ANALYSIS OF A LIGHTWEIGHT RD IMPELLER

GENERAL

Extensive coverage is given in the literature to the theoretical stress analysis of rotating profiled discs with applied rim, bore and blade loads; however, there has been little work done on the analysis of the disc with an integrally attached shroud, such as the RD wheel shown in Figure 1. For wheels operating at low stress levels, application of the loaded profile disc method (Stodola method) for the hub stresses has generally sufficed for a workable approximation of the stresses. This method was used for the stress analysis of the 20-inch fan analyzed under an earlier Aerophysics Contract (Reference 2). It will always give a conservative value for the stresses, and therefore can be used with confidence.

However, if a serious attempt is made to design a minimum-weight RD fan, the need for a more exact method of analysis is apparent.

The problem is complicated by the fact that the shrouded wheel is an indeterminate structure. An energy-balance method that properly apportions deformation energy between the hub and shroud must be used. In addition, an exact solution is impossible, and a computer solution using an iterative scheme must be obtained.

Fortunately, a method of stress analysis for shrouded discs has been devised recently (1961) by Deutsch at Fairchild Stratos (Reference 5). With proper modifications, the Deutsch analysis is quite suitable for the analysis of RD fans. In the fall of 1964, Aerophysics Company secured the consulting services of Mr. Deutsch to help prepare the detailed stress analysis of a lightweight RD impeller required under Phase I of Contract DA 44-177-AMC-250(T). The results of the extension of the Deutsch analysis to RD fans are presented in this section, as well as the listing of the corresponding computer program.

NOTATION

The notation, fully described in the List of Symbols and in Figure 2, is basically the same as that of Reference 5. However, additional notation is introduced to describe the diffuser geometry and to account for the fact that, to allow for the calculation of wheels of composite construction, provision must be made to vary hub, shroud and blade density independently at each station.

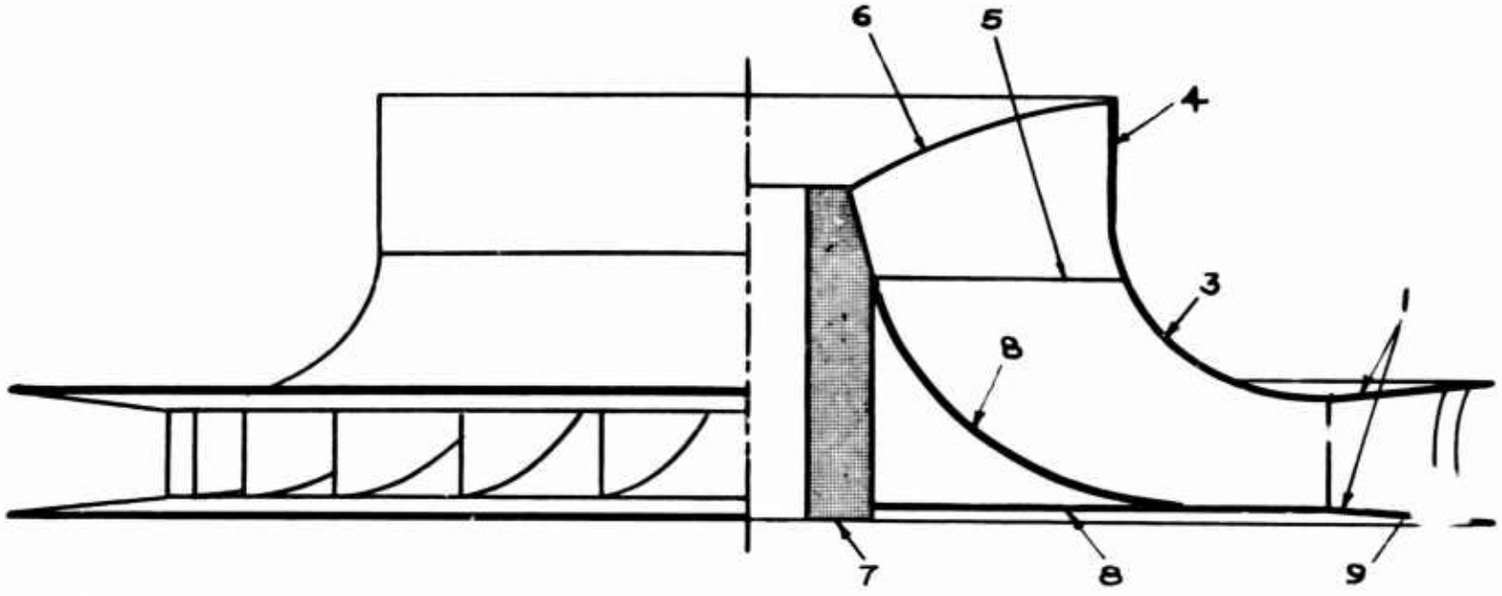

① DIFFUSER
② BACKPLATE (BACK DIFFUSER)
③ CONE
④ INLET CYLINDER
⑤ BLADE
⑥ INDUCER
⑦ HUB
⑧ FAIRING
⑨ MODULATING VANES

Note:

①③④ FRONT SHROUD
①② BACK SHROUD
⑦⑧ INNER SHROUD

Above components may be made as complete units.

Figure 1. Impeller Nomenclature.

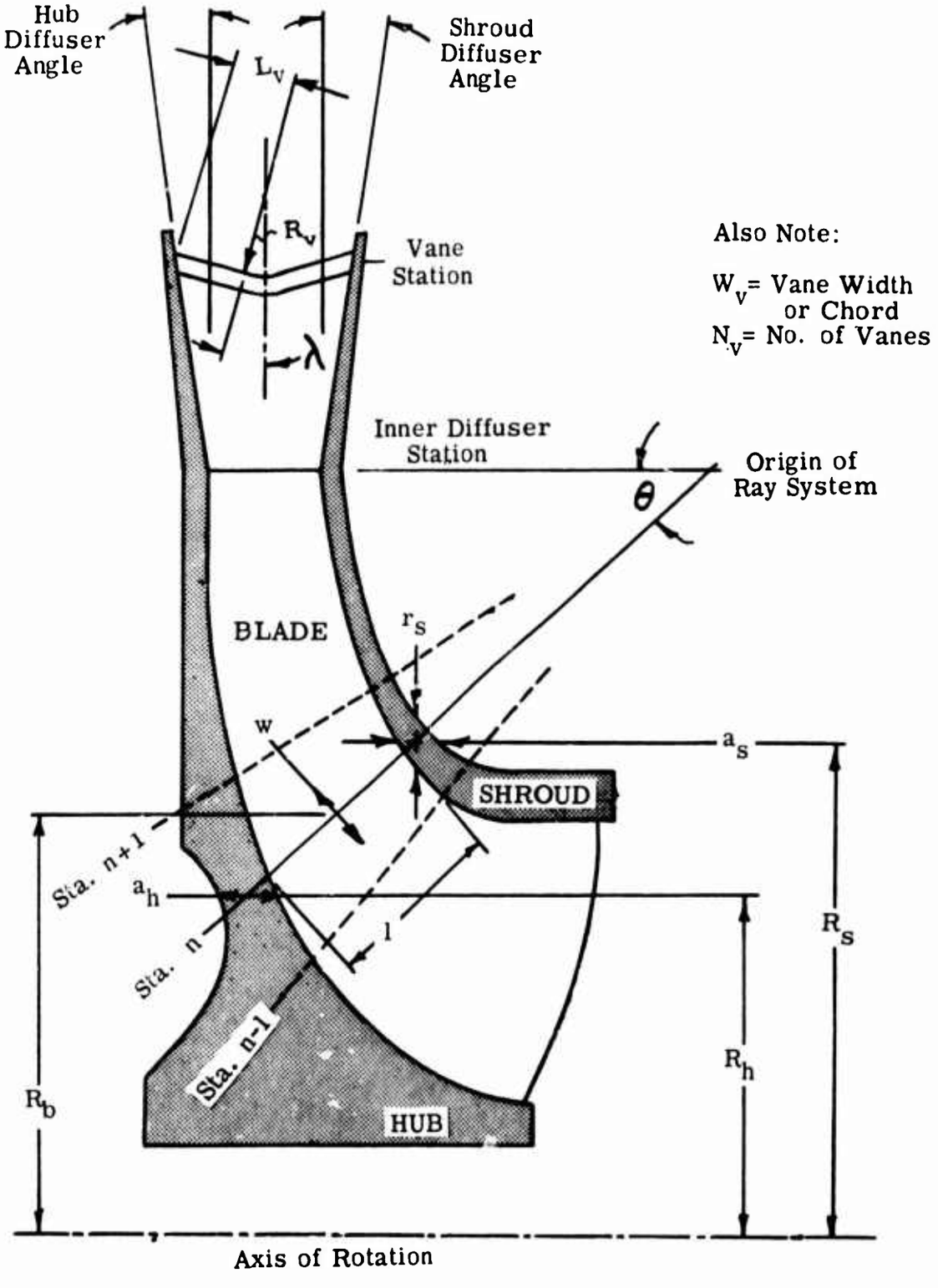

Figure 2. Symbols.

EXTENSION OF THE DEUTSCH ANALYSIS OF REFERENCE 5 TO RD FANS

To understand the following discussion, the reader must be familiar with the original Deutsch paper (Reference 5), which is extended, rather than superseded, herein. To be applicable to RD fans, however, the Deutsch analysis must be modified as follows:

1. One of the differences between the original Deutsch paper and the present one is that, in the original analysis, the densities of the hub, of the shroud and of the blades are assumed to be the same, while here it is found useful to differentiate between them.

   Equation (1) of the original paper is then rewritten as

   $$\rho_{f_h} = \rho_h + \rho_b (Nt\,\ell / 2\pi R_h a_h) .$$

   Similarly, the equation giving the fictitious density for the shroud can be written as

   $$\rho_{f_s} = \rho_s + \rho_b (Nt\,\ell / 2\pi R_s h_s) .$$

   Equation (4) similarly becomes

   $$F_b = w\,\ell\,t\,\rho_b R_o w^2/g .$$

   Now, as shown in Figure 2, modulating vanes may be incorporated in the diffuser region of the fan. In such a case, the hub and shroud densities at the hub and shroud stations where the diffuser vanes are attached must be increased to allow for the weight of the vanes. This is accomplished by assigning half of the vane weight to the hub and half to the shroud.

   The vane mass is given by (Figure 2): $N_v W_v T_v \rho_b (L_v + R_v \lambda)$. The hub volume affected by the vane mass (that between the vane station and the next inner station, provided they are not too radially distant) is

   $$2\pi R_h a_h \left[R_h(N) - R_n(N-1) \right] .$$

   Therefore, the hub fictitious density becomes

   $$\rho_{f_h} = \rho_h \left[1 + \frac{N_v W_v T_v (L_v + \lambda R_v)}{2\pi R_h a_h \left[R_h(N) - R_h(N-1) \right]} \frac{\rho_b}{\rho_h} \right] .$$

Similarly, the shroud fictitious density is

$$\rho_{f_s} = \rho_s \left[1 + \frac{N_v W_v T_v \left[L_v + \lambda R_v \right]}{2\pi R_s a_s \left[R_s(N) - R_s(N-1) \right]} \quad \frac{\rho_b}{\rho_s} \right].$$

2. The basic centrifugal stress analysis neglects the bending stress imposed upon the disc because of its conical shape. Only the average radial and tangential stresses at any radius are calculated.

While this bending stress is in general of a secondary nature it should be considered at the base of the diffuser section of the wheel. Accordingly, the diffuser section of the wheel will be considered as a circular plate with a hole of uniform radial and axial thickness having its inner edge fixed and having a uniformly distributed load applied. The bending stress found at the inner radius can be calculated from Reference 9 , page 200, case 21. That bending stress will be added to the centrifugal stress at the base of the diffuser to obtain the maximum tensile stress.

For the case of a simple diffuser without vanes, the centrifugal force is resolved into two components, one acting in the plane of the diffuser wall, the other acting axially. It is this axial component which is used to determine the bending stress acting at the diffuser base.

From Reference 9, using Roark's nomenclature, the radial bending stress σ_r is given by

$$\sigma_r = \frac{3w}{4t^2} \left\{ \frac{4a^2(m+1) \frac{2}{b} - a^2(m+3) + b^2 \left(\frac{b^2}{a^2} (m-1) + 4 \right)}{m + 1 + \frac{b^2}{a^2} (m-1)} \right\}$$

where w is the distributed unit load
t is the thickness of the plate
a and b are outside and inside radii of the circular plate
m is the reciprocal of Poisson's ratio

For our case, w, the unit load, is given by

$$w = \frac{\text{centrifugal force}}{\text{area}} \times \tan\beta$$

or

$$w = \frac{(t_i + t_o)(r_i + r_o) \rho w^2 \sin\beta}{4g \cos\beta}$$

where the subscripts i and o refer to the inside and the outside of the diffuser ring, respectively.

By considering the diffuser sections of the hub and shroud as composed by cantilevered beams of unit width, we can calculate an equivalent bending moment per inch that would produce the bending stress just found for the vaneless diffuser:

$$M = \frac{b\,t^3 \quad \sigma_r}{12\ t/2} = \frac{t^2 \quad \sigma_r}{6}.$$

This will be of particular interest when the shroud or hub is of composite construction. It will also be of immediate use in the following paragraph.

3. Analysis of the diffuser vanes -- The shape of the diffuser is such as to cause the sides to deflect toward one another under centrifugal stress. When the diffuser is fitted with vanes, however, each vane acts to overcome this tendency. To account for this action, we shall make use of the elastic equilibrium of the three members.

Let us return to the cantilever beam analogy for the hub and the shroud.

We shall consider the beam width as the peripheral distance between diffuser vanes. For a cantilever beam, the deflection per unit load δ is given as

$$\delta = \frac{\ell^3}{3\ EI}$$

where ℓ is the length of the beam. For the case of the hub,

$$\ell = R_{h\ 220} - R_{h\ 203}$$

(Station 220 corresponds to the inner diffuser station; Station 203, to the vane station)

$$I = \frac{2\ \pi\ R_{203}\ (a_{h220})^3}{12\ N_v},$$

and the hub compliance is thus

$$\psi_H = \frac{(R_{h200} - R_{h203})^3\ N_v}{\pi\ (R_{203})(a_{h200})^3\ E},\ \text{in inches/l}$$

ψ_s is found similarly.

The compliance of the diffuser vane is obtained by considering the half-blade as a cantilevered beam built in at the centerlineof vane symmetry. Applying a unit load in the axial direction produces a force of (1) x ($\sin\lambda$) normal to the vane, acting at the junction of the vane and of the diffuser wall. At the end of the straight portion of the vane, a bending moment of $L_v \sin\lambda$ acting at the end of a curved beam of radius R_v and a central angle of λ will be produced. The change of slope at the end of the curved beam due to an end moment is

$$\theta = \frac{M R_v \lambda}{EI} .$$

Substituting the value of the moment $M = L_v \sin\lambda$, and solving for this deflection normal to the vane at the diffuser wall ($\delta_M = L_v \theta$), we obtain

$$\delta_M = \frac{L_v^2 R_v \lambda \sin\lambda}{EI} .$$

In addition, the straight portion of the vane will undergo a further deflection in the same direction. This may be considered as a cantilevered beam, of length L_v, loaded with an end load of $\sin\lambda$. The end point deflection is

$$\delta_L = \frac{L_v^3 \sin\lambda}{3\,EI} .$$

The total end point deflection normal to the end of the vane is thus

$$\delta_N = \delta_M + \delta_L = \frac{L_v^2 \sin\lambda}{EI} \left(R_v \lambda + \frac{L_v}{3}\right)$$

and the total vane deflection in the direction of the unit force is

$$\frac{2 L_v^2 \sin\lambda \cos\lambda}{EI} \left(R_v \lambda + \frac{L_v}{3}\right)$$

Substituting

$$I = \frac{W_v T_v^3}{12} ,$$

we have the expression for the compliance of the vane:

$$\psi_v = \frac{24\, L_v^2 \sin\lambda \cos\lambda}{W_v T_v^3} \left(R_v \lambda + \frac{L_v}{3}\right)$$

Drawing a free-body diagram of the forces acting on the diffuser vane, we obtain

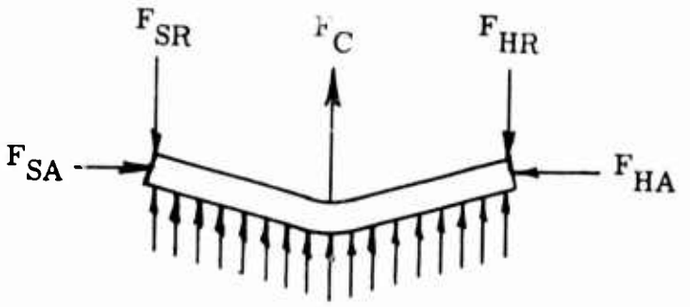

Resolving the centrifugal force into two components, one axial and one along the vane, gives the following equation or equilibrium:

$$F_{HA} = F_{SA} = \frac{F_c}{\tan\lambda}$$

where

$$F_c = \frac{2(L_v + R_v\lambda)\, T_v W_v \rho}{g}\, \bar{R}\, w^2 .$$

Now

$$F_{HA} = \delta_H (K_H + K_v)$$

where δ_H is the deflection in the direction of F_{HA} and K_H and K_v are the spring rates (reciprocal of the compliance) of the hub and vane. Substituting

$$\delta_H (K_H + K_v) = \frac{F_c}{\tan\lambda} = \delta_s (K_s + K_v)$$

and

$$\delta_H = \frac{F_c}{\tan\lambda\,(K_H + K_v)},$$

$$\delta_s = \frac{F_c}{\tan \lambda (K_s + K_v)} .$$

The external force which must be applied to the hub and shroud to produce these deflections is

$$F = \frac{\delta}{\psi} .$$

This force produces a bending moment at the base of the diffuser opposed to that produced by the conicity of the diffuser. Converting the moment into inch-pounds per running inch, we have

$$\Delta M_{Hv} = \frac{\delta_H}{\psi_H} (R_{vane} - R_{diffuser}) \frac{N_v}{2\pi R_{diffuser}} .$$

Thus, the diffuser bending moment and its related stress increment, found in the above paragraph, are reduced, because of the modulating vanes, by the amount

$$1 - \frac{\Delta M_{hv}}{\Delta M_h} .$$

The shroud can be treated in the same manner as the hub.

One final stress must be considered in this analysis. The vane is acted upon by two opposing side forces, found previously to be

$$\frac{F_c}{\tan \lambda} ,$$

acting at a distance $L_v \sin \lambda$ from the midpoint of the vane. This produces the following bending stress in the vane:

$$\sigma_v = \frac{F_c \cos \lambda \, L_v \sin \lambda \, T_v}{\sin \lambda} \times \frac{12}{2 W_v T_v^3} .$$

DISCUSSION OF THE COMPUTER PROGRAM

The computer program originally written by Deutsch in 1962 at Fairchild Stratos to solve the type of problems discussed in Reference 5 was extended to the general case of the RD fan shown on Figure 2. Revised input and output sheets were also prepared to adapt in an optimum manner to the RD fan configuration.

The program is written in FORTRAN language and is normally run on the IBM 1620 computer. Because of its length, it had to be broken down into two decks. The first deck is run first with the input cards; the output of the first deck is added to the initial input data and forms the total input for the second deck. The two decks are listed as Appendixes I and II of this report, respectively. For an understanding of the program, it must be noted that the notation "CO", say CO 48, stands for "Column" and corresponds to the same column of the appendix of Reference 5. So, CO 48 is the variable defined in column 48 of the appendix. Those items which were not defined in Reference 5 and are not self-explanatory are defined in the List of Symbols.

A blank revised input sheet is shown as Appendix III. As the program is compatible with all types of wheels, only necessary data need be filled in. For example, wherever there is no shroud, shroud input is left blank. It is easy to find the computer symbol for each of the data inputs by referring to the source program.

SECTION II

LIGHTWEIGHT MATERIAL AND TECHNIQUES REVIEW

INTRODUCTION

For construction of the RD fan, the Aerophysics Company considered structural materials from the major metallic, nonmetallic and mixed groupings. Of these, aluminum and reinforced plastics were selected.

The first two test fans were constructed of aluminum. A suggested innovation would be an alternate RD fan of glass cloth or preimpregnated reinforced plastic.

STRUCTURAL MATERIALS

Aluminum

Aluminum was chosen from the structural materials because, handled in the classic manner at this prototype level, the fabrication techniques and strength characteristics are predictable.

A prime concern was choosing aluminum alloys that exhibit corrosion resistance necessary to the RD fan operating in a marine environment. The particular selection exhibits its superiority by its weight-to-strength ratio and relative obvious ease of fabrication. (The obvious alternatives, steel and magnesium, could measure up to aluminum only in certain properties.)

The stress levels of the test fans have, from the preliminary stress analysis, proven to be uniformly low. Hence, it has been unnecessary to investigate materials of unique mechanical properties or mixed structural materials of metals and plastics.

The aluminum alloys selected for the test fans are as follows:

1. Full Outer Shroud - 6061-0, before fabricating, which is heat-treated to the T-4 condition after forming. Because of the depth of the outer shroud, considerable work hardening of the piece will occur during spinning. As the spinning progresses, the metal must be continually annealed. To insure definite available stress levels, following spinning, the shroud must be heat-treated to the T-4 condition.

2. Blades - 6061-T6 formed cold by routing, rolling and joggling.

3. Backplate - two possibilities were considered:

a) In anticipation of possible warping of the backplate during heat treatment, because of its size, leave the backplate in the 0 condition. This forces the use of a high-strength alloy, such as 5052 aluminum. The difficulty is that such an alloy in the 0 condition is not easily available commercially. This solution was therefore rejected.

b) Use 6061-T6 and take chances that some warping may occur during the forming of the diffuser annuius but that it can be corrected.

4. Hub - 6061-T6 billet.

Preimpregnated Reinforced Plastics

As suggested, an attractive RD fan, exceptionally well adapted to marine environment and with a superior strength-to-weight ratio (as compared to aluminum) could easily be constructed of preimpregnated plastics. In considering both the evolution of the RD fan to a larger structure and the properties of preimpregnated reinforced plastics, it can readily be foreseen that future RD fans could be of such plastics.

Preimpregnated reinforced plastics are usually formed in sheets of combined fabric webbed with resin. When subjected to heat and pressure, the resin is cured, and the molded parts are remarkably uniform. Such plastics can be used to build up the local structural areas of the fan.

Aerophysics Company chooses the preimpregnated reinforced plastic for the alternate RD fan because of its suitable epoxy resin, which lends itself to bonding with conventional epoxies and other materials at room temperatures. (This suggests the use of honeycomb and aluminum sheet combined with Scotchply construction.) Tooling requirements for this material can be similar to those for aluminum forming. The preimpregnated reinforced plastics lend themselves to many molding processes.

As with other preimpregnated reinforced plastics, Scotchply is easily stored and handled, reducing material inventory and eliminating in-shop formulation control. It allows for only a minimum of material waste.

The tolerance of the final layed-up Scotchply component will correspond to that of the mold or tools on which it is fabricated. It is available in one-, two- and three-ply filament orientation, which allows an orientation of the direction of the fibers to achieve maximum directional strength. This is a unique quality difficult to achieve with the conventional fabric-glass-resin combinations.

Glass Cloth Reinforced Plastics

There is no basic difference in materials between preimpregnated reinforced plastics and glass cloth plastics reinforced with epoxy or phenolic resins. The difference is in the way the materials are used. As the name indicates, in preimpregnated plastics, the resin is incorporated into the glass cloth at the plastic supplier's factory. In glass cloth reinforced plastics, this is done at the time of fabrication of the end product. Significant differences in fabrication techniques result. The preimpregnated plastic must be cured at temperatures of 350-400° F. This usually requires an oven large enough to accommodate the whole fan to be built. The glass cloth reinforced plastic is cured at room temperature, but the reaction between the epoxy and the hardener takes place in a very short time, often forcing the buildup of cloth layers in several steps, which easily becomes time-consuming.

FABRICATION TECHNIQUES IN ALUMINUM

Spinning

The main circular structure of the aluminum RD fan lends itself naturally to fabrication by the spinning technique. The initial tooling is comparatively inexpensive.

Aluminum lends itself well to the spinning process because of its excellent ductility and its need of only a few intermediate anneals during spinning. This technique is usually reserved for limited-quantity production. Moreover, spinning gives a fine, aerodynamically smooth surface.

In spinning the outer shroud of the RD fan, certain dimensional problems arise from the spring-back characteristics of the piece, from work thinning and from subsequent heat treatment; i.e., the tolerances on the diameter, depth and wall thickness may vary from piece to piece. A final acceptable outer shroud depends on the skill of the spinning operation. No two deep spinnings of the shroud will be identical, thus creating certain assembly and fastening problems. The solution of these problems will be discussed in the section dealing with assembly.

The spinning of the hub (optional) presents similar problems. In one consideration, the RD fan would be driven from a structural hub formed by the spinning techniques. In this instance, the blades extend inwardly only as far as this spinning. These blades are fastened to and driven by this hub.

An alternate design is the use of a hub spider, which is a lathe and milling machine piece. The hub area replaced by the hub spider may be faired in with "foam-in-place" plastics and sheet metal fairing surfaces.

Hydropress

The RD blades may be fabricated by the rubber die forming technique. This process (particularly the Guerin process) provides low-cost tooling of small shallow, flanged and ribbed parts of irregular shapes. The hydropress tooling is relatively inexpensive for short runs, for which conventional tooling would be uneconomical. This process may provide for simultaneous blanking and piercing of flat pieces.

At the prototype level, such as in the present program, an alternate method of fabrication of the blades is by hand-forming. The blade is routed out by using a template and bent by using conventional sheet-metal brake and roller equipment.

Forgings

Only the hub or a hub spider of the RD fan may be fabricated by forging in aluminum. In the industrial practice of RD fan fabrication, the hub is generally forged or cast in steel. Industrial experience indicates that, of the two techniques, the forged hubs of this type are stronger and more durable.

A small RD fan hub may be hand-forged in the simple biscuit shape. Certain outstanding properties of aluminum hand forgings may be here noted -- their high weight-to-strength ratio, toughness, and ability to withstand shock and repeated applications of stress. Such forgings provide a desirable combination of directional properties allowing thinner structural sections, and thus a lightweight hub.

Aluminum forgings maintain the advantages of aluminum previously discussed; i.e., they are lightweight and corrosion resistant, and have excellent machineability to achieve a smooth aerodynamic surface.

It is most important to the forging process that a suitable aluminum alloy be selected. For the RD fan, the alloy 6061 at the standard T6 temper combines a moderate tensile strength with good ductility and gives excellent corrosion resistance and forgeability. Moreover, it particularly offers excellent welding characteristics possible for the joining of the fan blades. Before the blades are adjoined, the forged biscuit must be machined to the operational outline of the working hub.

This latter machining, plus other factors, has led Aerophysics to examine other methods for fabricating the hub. Despite the attractiveness of hand forgings, design studies and weight analysis for the two prototype fans show that the initial costs of hand forging and machining are high, as compared to spinning. Spinning eventually eliminates the additional costs of machining to achieve a smooth surface. Moreover,

for the medium-sized projected RD fans, the forged hubs are not as light as spun hubs, because of machining problems. The aluminum properties and advantages remain essentially the same as indicated for the forged product.

Assembly Methods

Inert gas welding would be one acceptable method of assembly. In this process argon or helium is used to shield the molten weld. However, accumulated distortions arise from the heat of welding, causing warping. As in the case with all welding fabrication in aluminum, the thin, lightweight metal areas are prone to distortions under welding, and thus it is difficult to maintain a uniform structure.

During welding assembly, the fan may be held in a complicated fixture, but despite this, localized stresses occur at all the weld junctions. There is no concise way to determine the stress levels at the welds; thus, these areas will remain indeterminable under stress analysis.

In addition, gaps may form from possible tolerance buildup between the RD components. These would prohibit the welding of necessarily joined surfaces.

Bonding is another possible assembly method. The assembly of helicopter techniques applicable to the RD fan production indicates a need for elaborate clamping and holding fixtures. The entire blade bonding technique must be closely quality controlled. The elaboration of this method would eliminate its use for a small run of RD fans.

Riveting is a classical and accepted form of structural assembly. It is a traditional sheet metal fastening method and appears attractively adaptable to the RD fan. The layout for the riveting is straightforward and accessible. Conventional shop tooling is readily available and adaptable. This method of assembly is extensively used by the British for assembly of their large lightweight centrifugal GEM fans (Rotol fans).

The output from the Aerophysics stress analysis can be applied in a conventional manner to the detail design of the fan. Therefore, fastenings between components can be accurately determined and fabricated. The tolerance buildup can be anticipated by the detailed arrangement of local support and rivet fastenings.

TECHNIQUES IN PREIMPREGNATED REINFORCED PLASTICS

A review of 3M Scotchply indicates that it is well-suited to larger RD fan fabrication. The entire fabrication may be accomplished through the vacuum bag technique; i.e., the uncured Scotchply is fitted over

the mold tooling, and these are encased in a plastic vacuum sack. The vacuum is thus applied between the mold and the plastic sheet. The surrounding atmospheric pressure forces the reinforced plastic firmly over the mold. This technique is economical for short runs and allows control over the surface finish.

The curing time for the Scotchply fabric can be as short as 4-1/2 minutes at 325° F. Scotchply may be re-added to the RD structure by reheating at 325° F. without affecting the basic RD structure.

As previously discussed, the Scotchply is available in three fiber orientations. In the outer shroud of the RD fan, the filament orientation may progress from filaments wound circumferentially at the inlet area to filaments cross-mixed and blended from circumferentially to radially at the curving shroud to filaments laid out radially in the diffuser disc area. The inner shroud arrangement should be the same for the curving area.

The overlapping of ply direction in the curving area is an attractive use of Scotchply. This development of patterns will also insure stress uniformity in this area. (All uncured Scotchply may be overlapped. Upon heating and curing, this overlap will diffuse into the adjoining surface.)

In the diffuser disc area of the shroud, a supplementary layer may be required with fibers laid tangentially to stiffen the RD ring against waviness.

An important feature of the Scotchply preimpregnated plastic is its use in patches where stresses are high or concentrated. In particular, the area of bending that runs circumferentially around the root of the RD rings may be increased in depth by progressively building up this juncture with blended, stepped and laminated Scotchply segmented rings.

Similarly, the areas where the blades join the shrouds are points of load concentration and can be accordingly thickened by a Scotchply buildup.

Although the attachment of the fan blades to the inner and outer shrouds is always a difficult fabrication problem, Scotchply offers good solutions for blade attachment -- either by direct epoxy bonding or by routing and slotting the molds so that the slots can be incorporated into the faces of the shrouds.

Because Scotchply may be built up, layer upon layer, a logical means of fabricating the blades is offered. The blades are made over molds, which insures uniformity of blade from blade to blade; thus, this

tooling technique appears to be superior. In bonding the blades to the shrouds, a heavily filled semiflexible epoxy will be suitable.

TECHNIQUES IN GLASS CLOTH REINFORCED PLASTICS

During Phase I of the contract, the review of lightweight materials and techniques was not meant to be all-inclusive, but only to be sufficient to permit, without preconceived ideas, an intelligent choice of the materials and techniques for the fabrication of the two demonstration fans to be built under the contract. At the end of Phase I, it was recommended by Aerophysics that the two test fans be built of aluminum. Additional studies of plastic fans were not made, therefore, during the remainder of the contract, and the rest of this report deals only with metal fans.

As a follow-on to the contract, Aerophysics initiated additional design studies of plastic fan fabrication during the summer and continued them during the fall of 1965. Since they are directly pertinent to a discussion of lightweight fan fabrication techniques, they will be briefly reported below.

The studies started from the considerations developed in the section above, in which an all-Scotchply fan is proposed. Additional reflection indicated that a plastic fan incorporating some elements made of Scotchply and others made of glass cloth reinforced plastics was possibly preferable. The idea was to retain Scotchply wherever its use appeared advantageous and to use glass cloth reinforced plastic elsewhere. In particular, inner and outer shrouds do not need to be made of Scotchply; the blades, which provide dimensional accuracy of the fan, do. It is thus necessary to have available a small oven for blade fabrication, but the need for the large oven for outer shroud fabrication disappears.

A design study of this composite plastic fabrication using the same fan that was built of aluminum under the contract and is described in Section III, fan Model RD 51-.50-1.3-75^{0}, was made. This design, shown in Figure 3, will be described here. The fan is built around five components, which are bonded together. These components are as follows:

1. A main drive shaft which consists of a constant-section cylindrical aluminum tube, to which are fastened bulkhead extensions which support the inner shroud.

2. A backplate, made of fiber glass or aluminum honeycomb, which acts as foundation for the structure of the whole fan.

3. An inner shroud made of conventional reinforced glass-fiber overlay, laid up by hand over a concave die. This die or mandrel is a large piece of hardwood, similar to that which one would use for turning an aluminum spinning of the same size. It can be obtained fairly economically by going to the spinning people, who have available large gluing presses and large wood turning saddle lathes. Three to six layers of cloth may be required. This is made possible by the recent development of new resins, with over 1-hour pot time. The curing can be done at room temperature, under pressure obtained by means of the vacuum bag technique, for example.

4. An outer shroud, the fabrication of which is similar to that of the inner shroud. The outer shroud is reinforced, as shown in Figure 3, at circumferential stiffeners which take part of the hoop stress.

5. Eighteen blades made of 3M preimpregnated 1002 Scotchply material. The reason for using Scotchply as blade material is quite significant and basic to the whole design and will be discussed in some detail.

   First, each blade is quite small (20 inches is the maximum dimension) and does not require the same huge oven as the shroud pieces.

   Second, the blades are viewed as providing the dimensional accuracy of the fan and must therefore be built using the best materials and the best possible mold. It is possible to make blade flanges integral with the blades; these flanges are essential to bind the blades to the inner and to the outer shroud, respectively.

   For assembly of the finished blades to the shroud surfaces there are a multitude of good epoxy bonding agents on the market, such as 3M EC2216.

The major advantage of plastic fabrication, in terms of simpler fan assembly, will now become apparent. Not shown on the earlier sketches, it is intended to provide both blade and shroud molds with locating grooves, alignment tongues and indentations which will permit the immediate and accurate positioning of blade with respect to shroud (in a manner similar to that in which some childrens' plastic models are assembled). Thus, the tedious lofting, layout and alignment of the metal fan can be eliminated. The hub can be much simplified, since the central spider is not required any more.

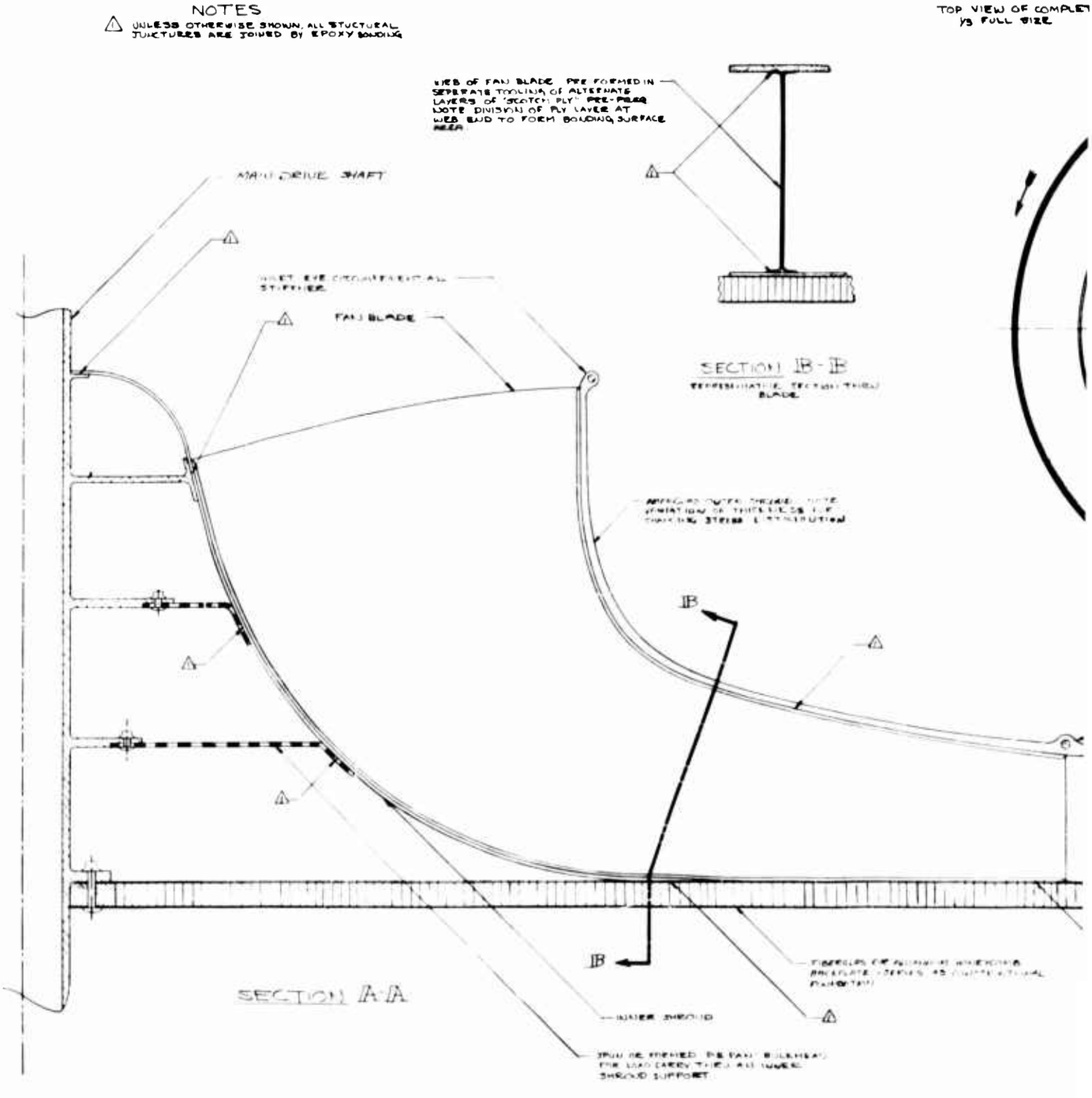

Figure 3. Plastic Fan Design, Fan RD 51-.50-1.3-75

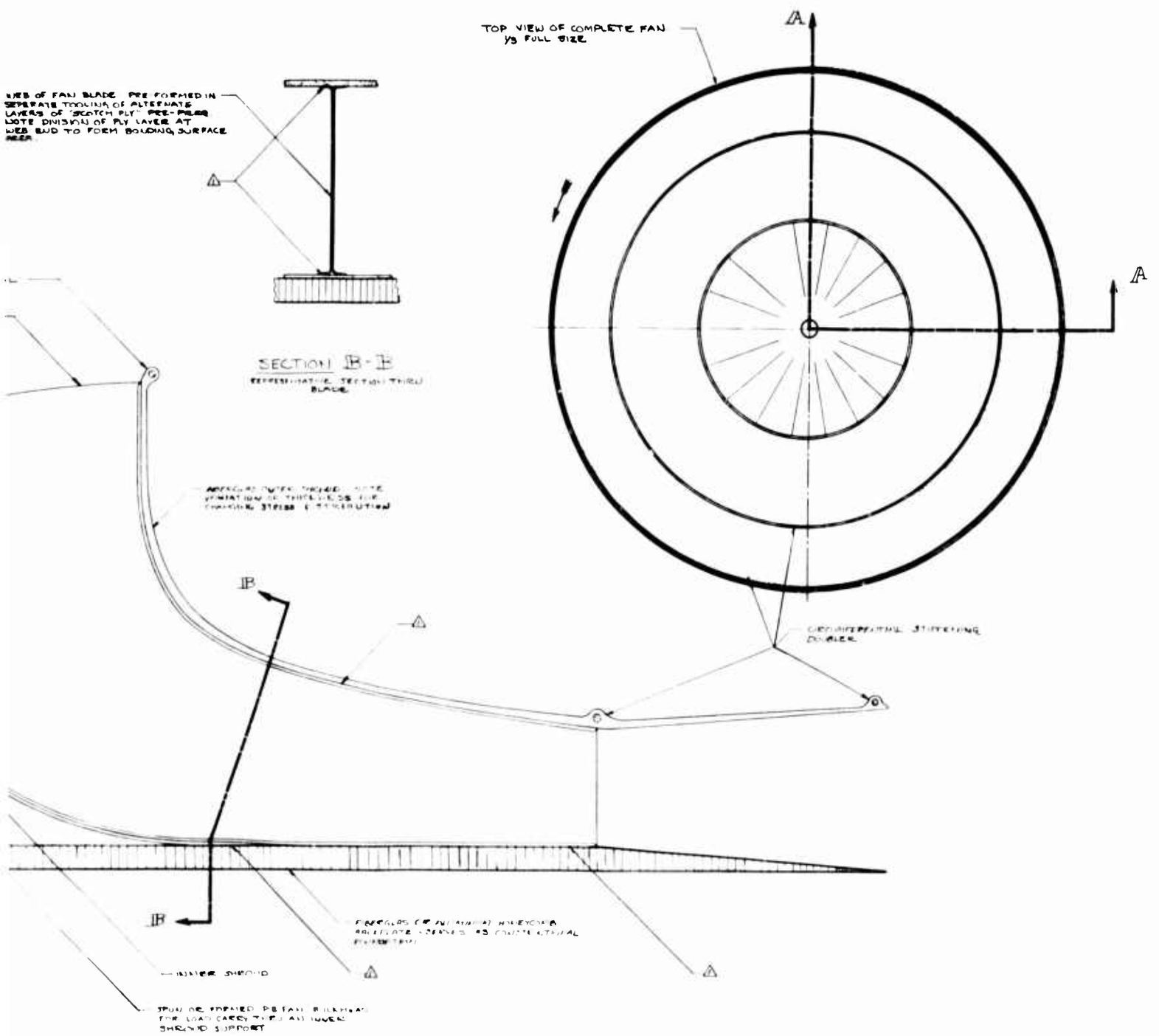

Figure 3. Plastic Fan Design, Fan RD 51-.50-1.3-75°.

Surprisingly, the total cost of plastics materials for a given fan (even if made entirely of Scotchply) is lower than that of the corresponding aluminum fan. One reason is that for the aluminum hub, a lot of "hogging out" and material removal are required. Only a fraction of the original material is used in the final plastic structure.

The main advantages of the plastic over the metal approach to fan design are therefore seen to be cost and time of fabrication. (Subcontracting delays for an aluminum shroud spinning can be quite substantial.) Standard advantages of plastics mentioned earlier may also be briefly recalled here: lighter weight and resistance to fatigue, impact and corrosion.

SECTION III

DETAILED DESIGN OF RD FAN

AERODYNAMIC SELECTION OF THE RD FAN

The contract specified the design and fabrication of "a 60-inch-diameter fan that will absorb approximately 100 shaft horsepower." It was intended that this fan be representative of a family of internal-flow air movers for potential ACV's or STOL aircraft in the range of 100 to 1,000 horsepower. It was first decided that a total pressure rise of 20 inches of water would be representative. Correspondingly, the volume flow was fixed to 25,000 c.f.m. Several RD fans were considered, and the choice was narrowed down to two: RD 51-.50-1.3-75^{0} and RD 51-.70-1.3-75^{0}. The aerodynamic characteristics of these two fans are shown in Figures 4 and 5, respectively (for an explanation of RD fan indexing, the reader is referred to Reference 2).

It was decided to build the former fan (Figure 4). The reason was that, for the same overall diameter, the air passage is narrower, and that fan, therefore, is harder to assemble than the other one. If anything, this results in weight penalties. As a redeeming feature, the aerodynamic features of the fan of Figure 4 are such that no modulating vanes are required. Vanes would most likely be required for the other fan.

The fan which was built (RD 51-.50-1.3-75^{0}) is representative of ACV's with high cushion pressures (50 to 100 pounds per square foot), such as the landing craft described in Section IV. The other fan (51-.70-1.3-75^{0}) is representative of ACV's with lower cushion pressures (25 to 50 pounds per square foot), such as the Bell Skimmer 5 (Westland SRN5).

GENERAL FAN CONFIGURATION

The assembly drawing of the two identical fans which were built is shown as Figures 6 and 7. Detailed fabrication drawings were also prepared and submitted to USAAVLABS in accordance with the contract. A list of the detailed drawings is given in Appendix IV. The general features of the fan will be summarized here.

First, the final fan design is an all-aluminum structure.

Second, the fan components are formed by the processes of spinning, sheet metal forming (including stretch-forming) and conventional lathe and milling machine work.

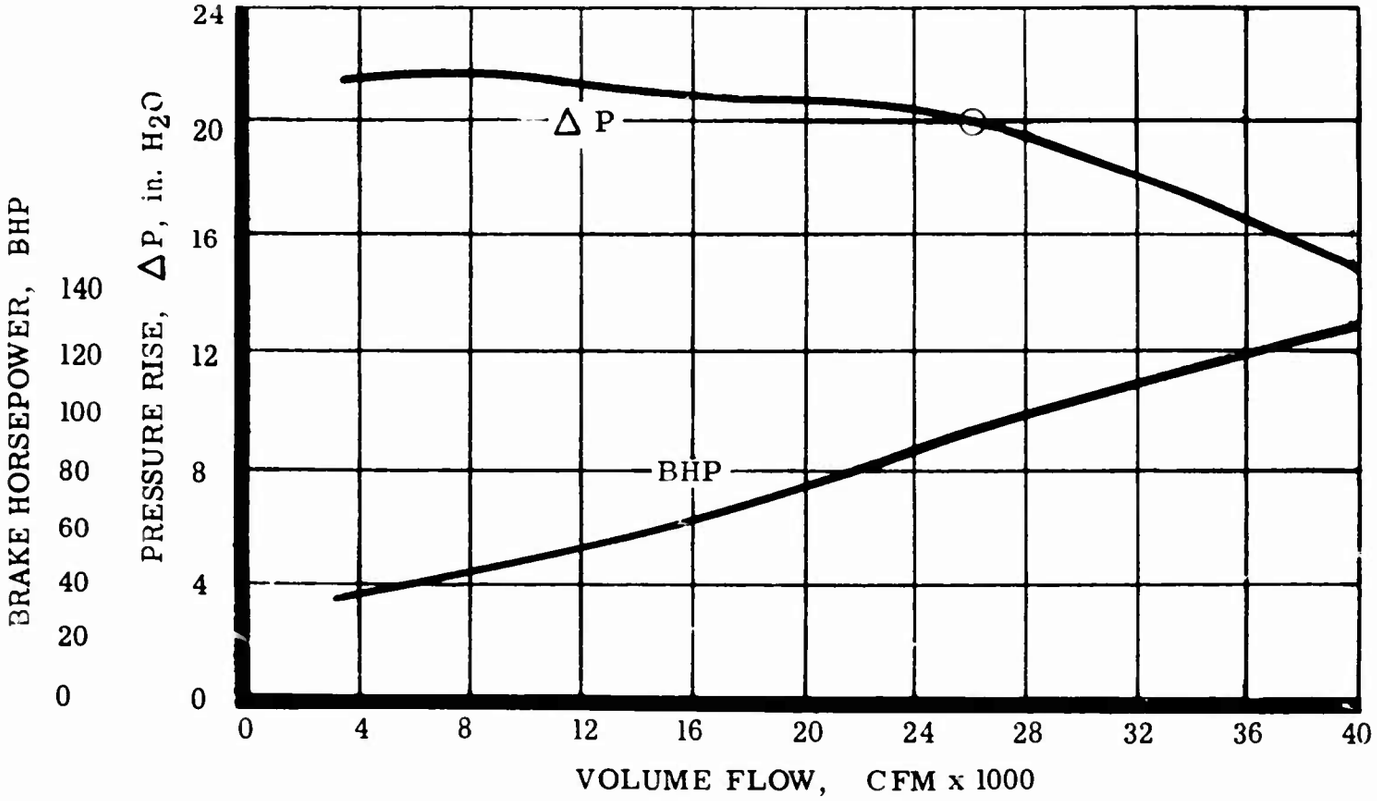

Figure 4. Aerodynamic Performance, Fan RD 51-.50-1.3-75° (1,180 RPM).

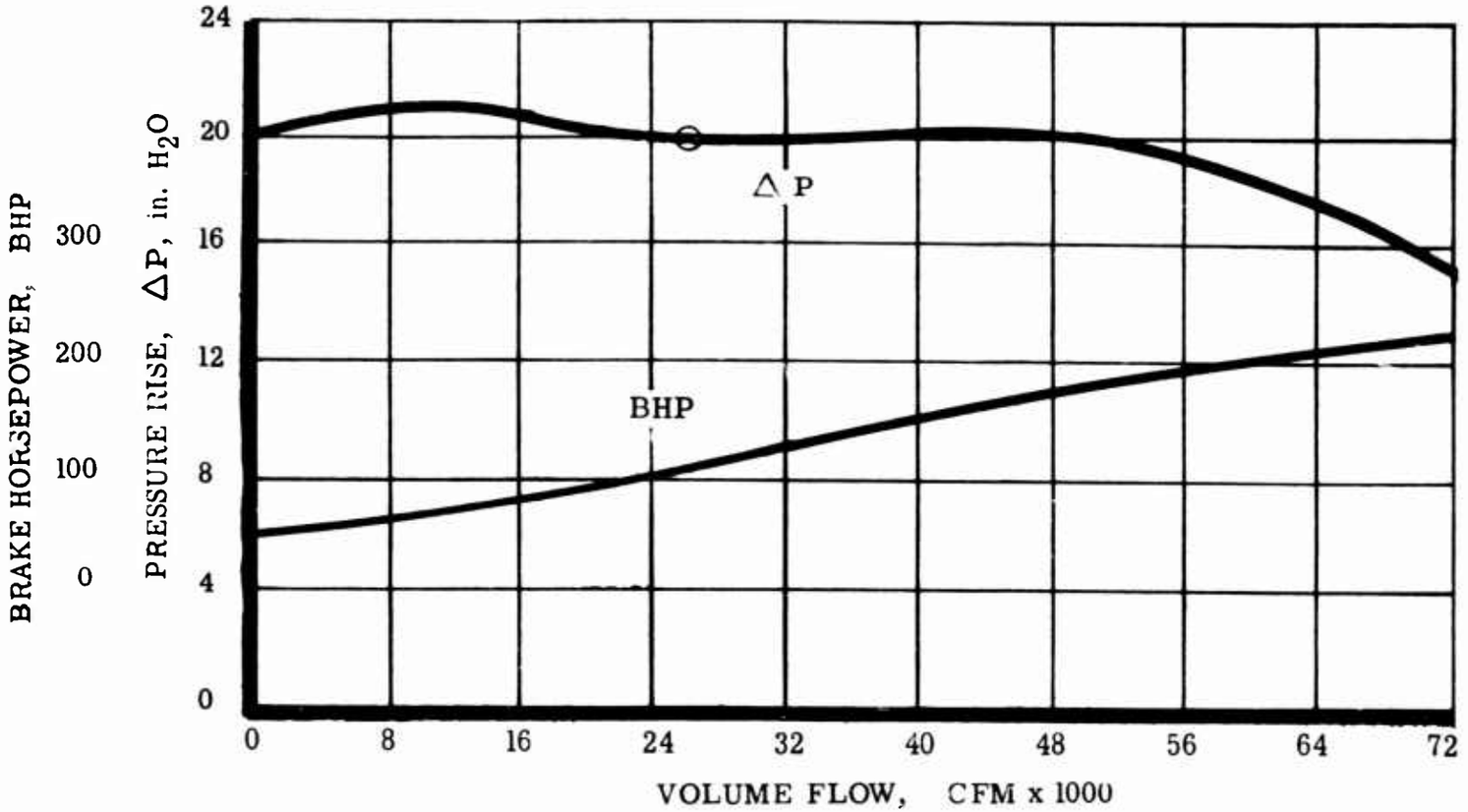

Figure 5. Aerodynamic Performance, Fan RD 51-.70-1.3-75°, (1, 180 RPM).

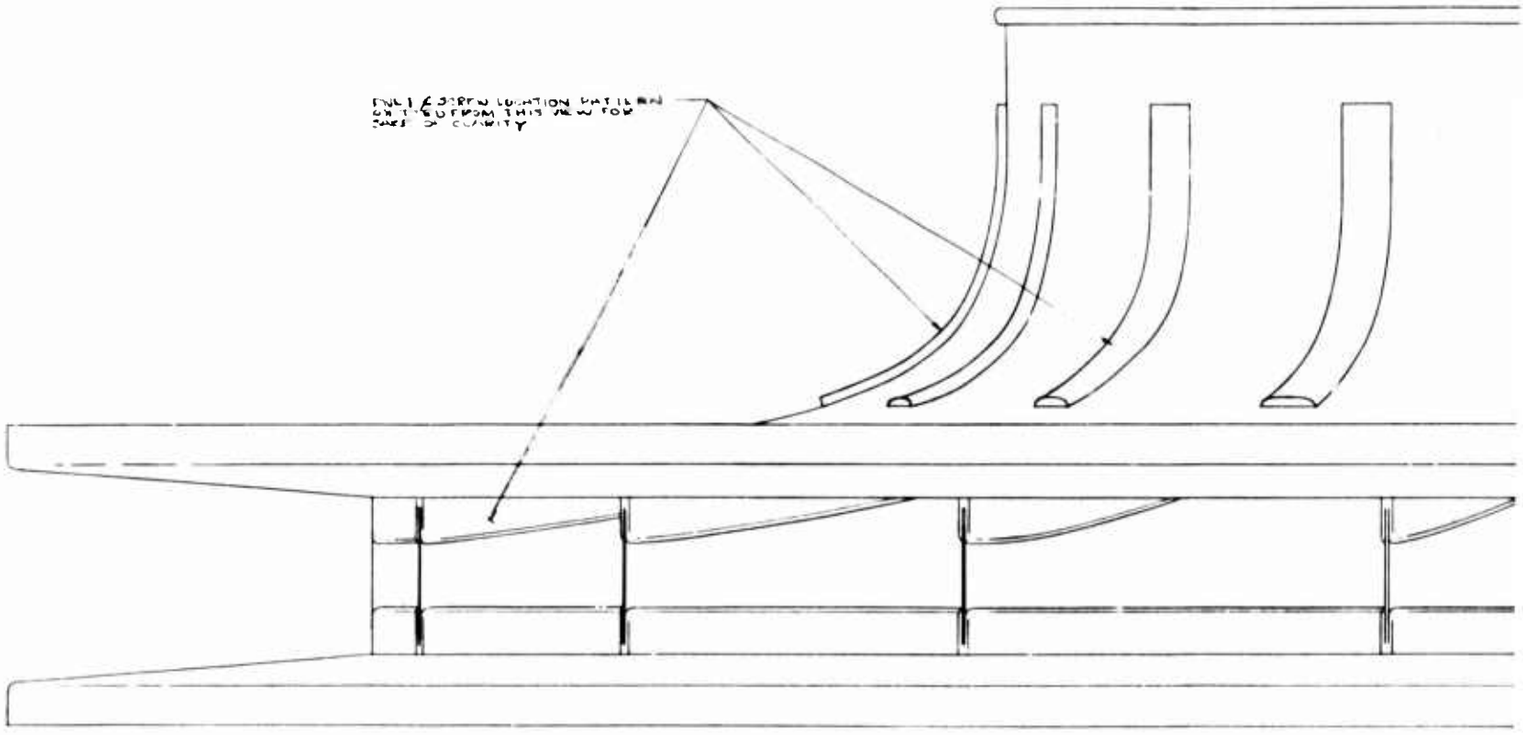

Figure 6. Assembly Drawi

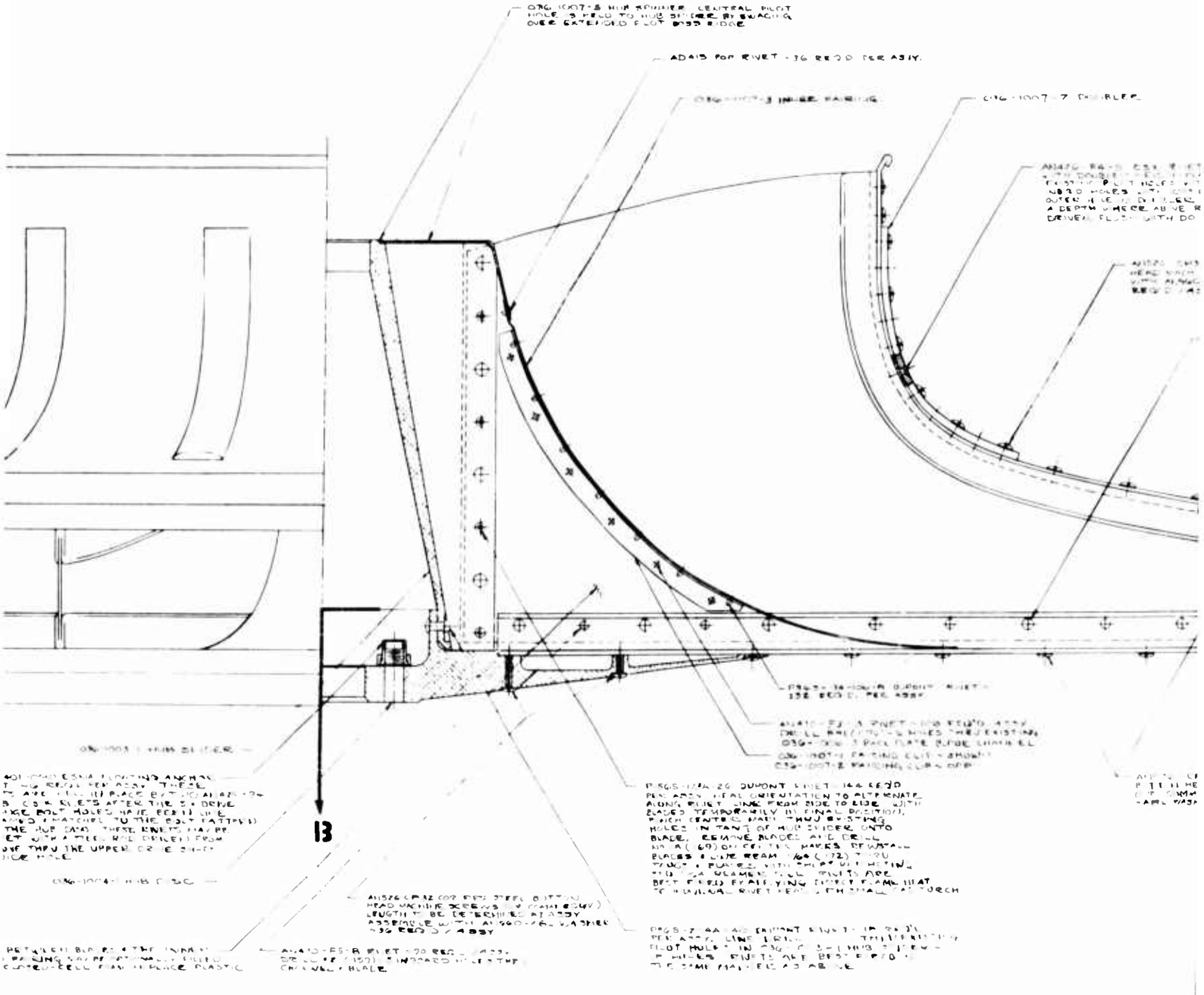

ssembly Drawing of Aluminum Fan RD 51-.50-1.3-75^{0}, Side View.

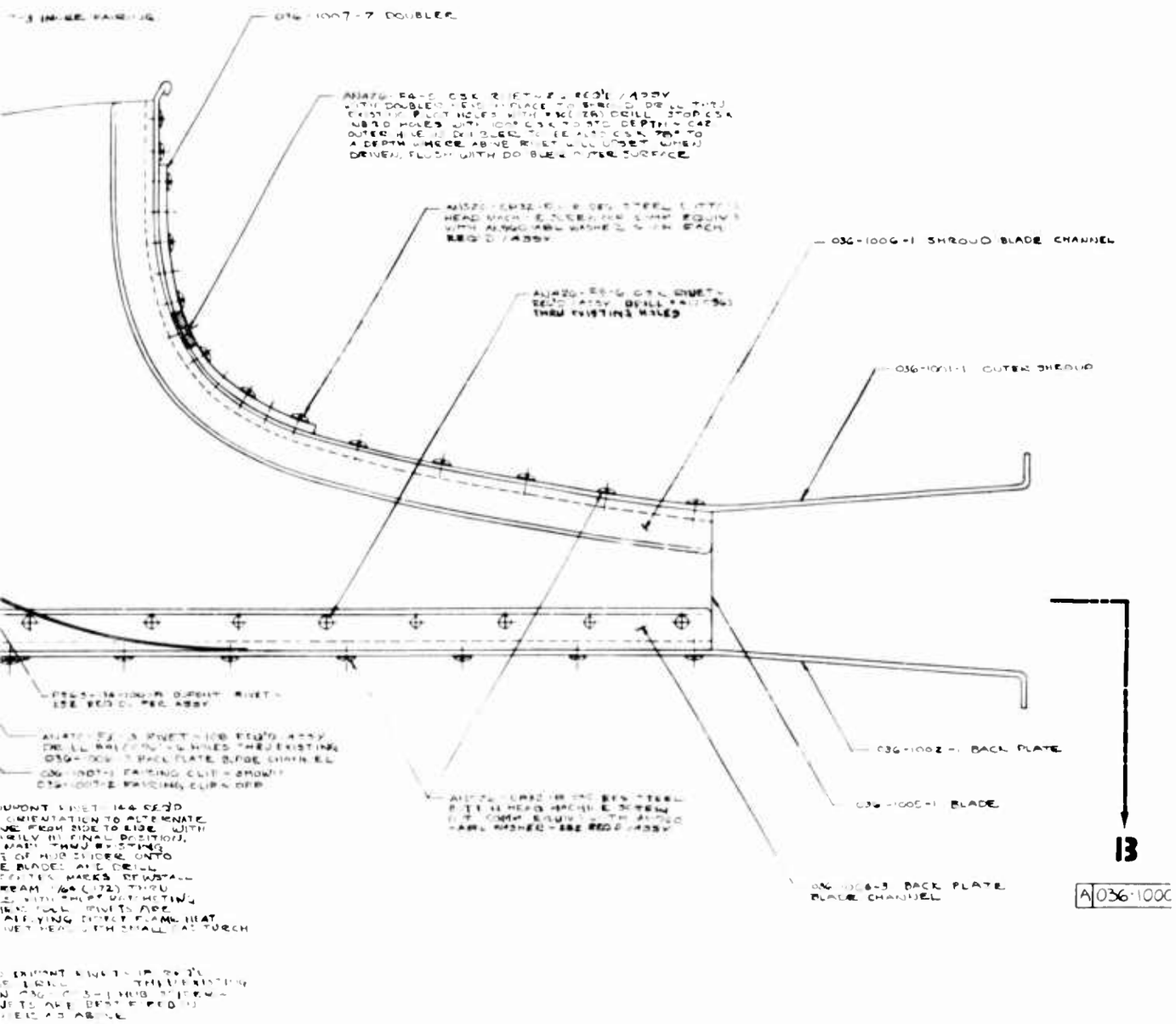
036-1007-7 DOUBLER
036-1006-1 SHROUD BLADE CHANNEL
036-1011-1 OUTER SHROUD
036-1002-1 BACK PLATE
036-1005-1 BLADE
036-1006-3 BACK PLATE BLADE CHANNEL
B
A 036-1000

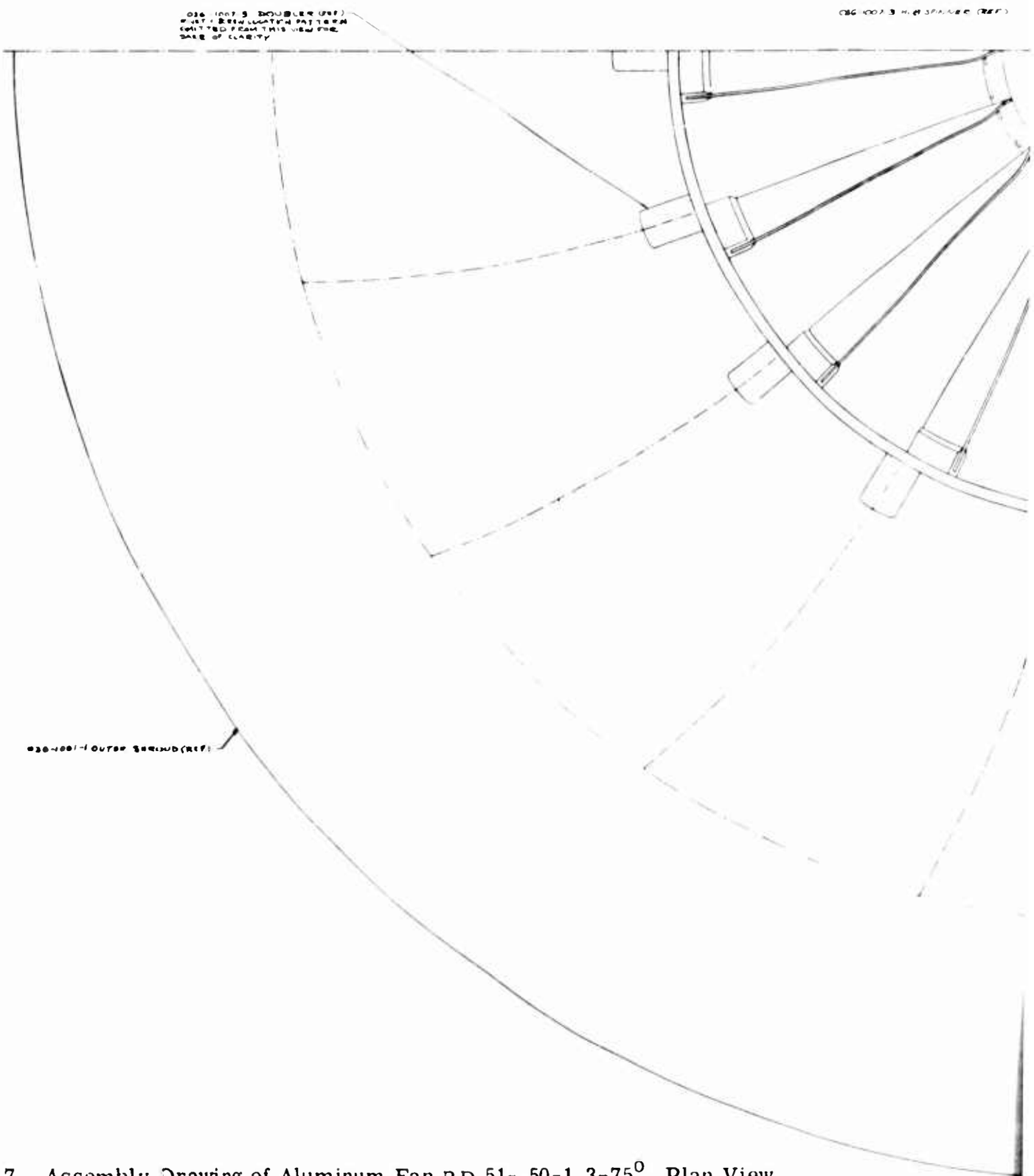

Figure 7. Assembly Drawing of Aluminum Fan RD 51-.50-1.3-75^{0}, Plan View.

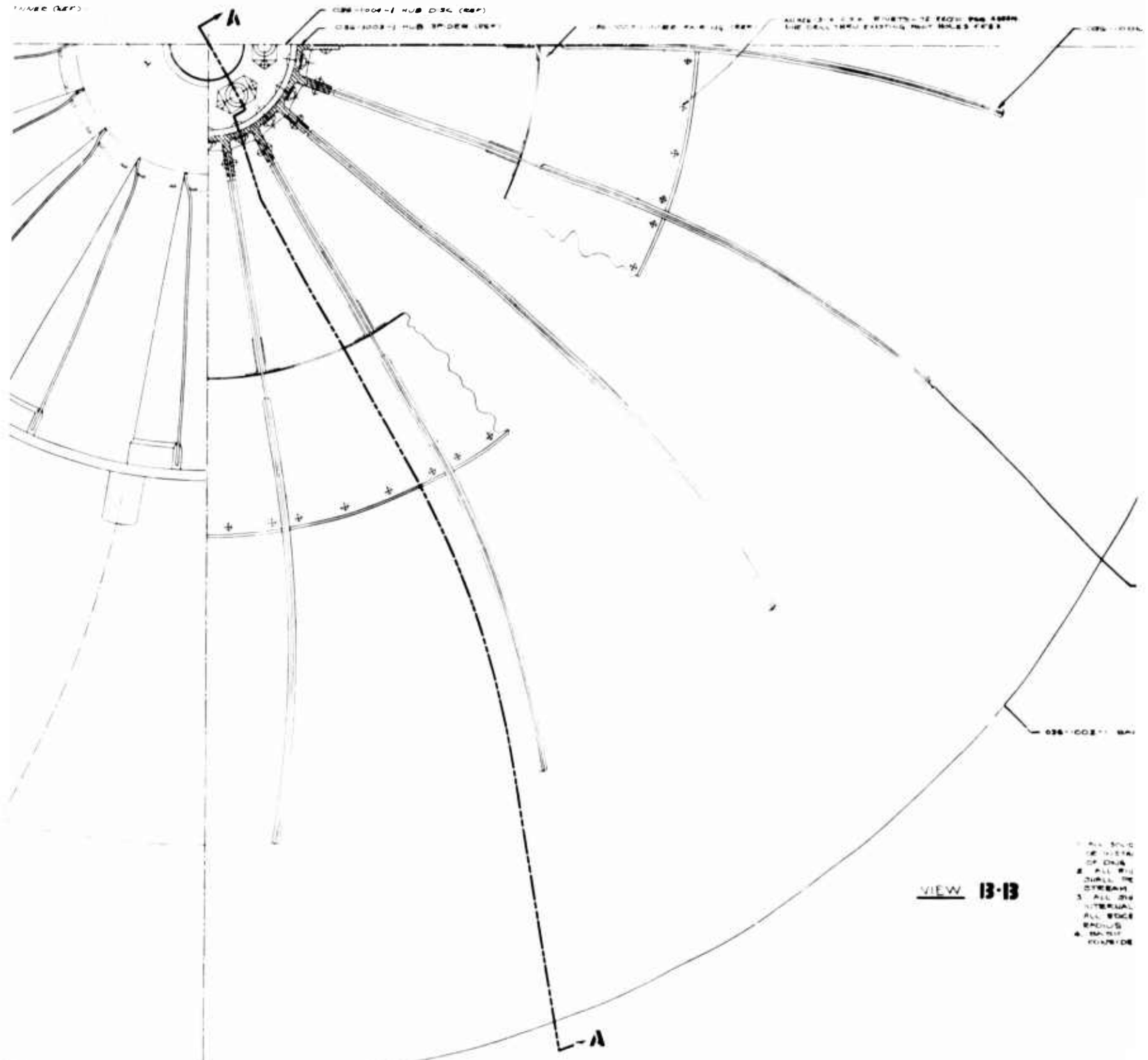
A
A
VIEW B-B

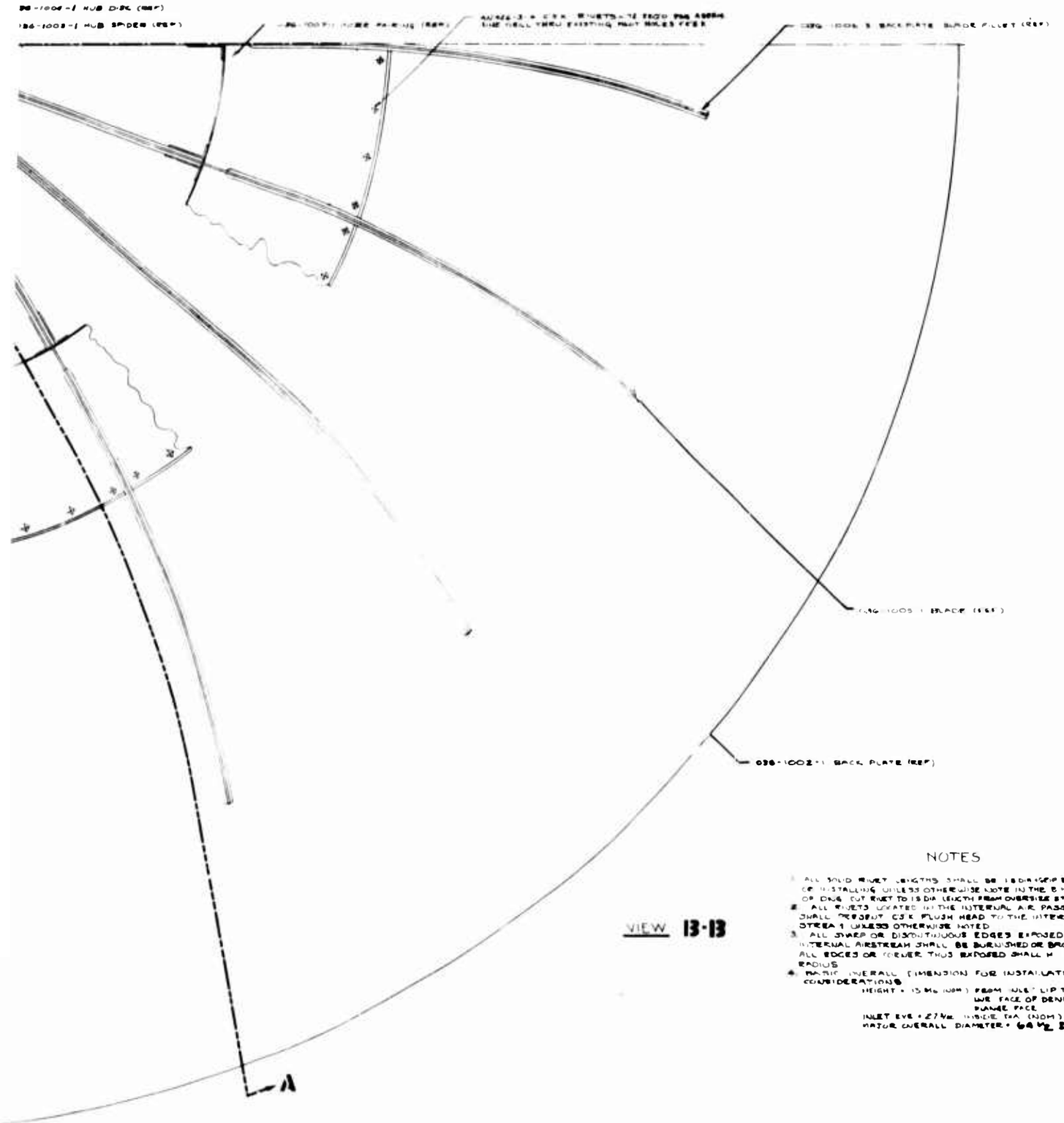

VIEW **B-B**

NOTES

1. ALL SOLID RIVET LENGTHS SHALL BE 1 DIA GRIP BEFORE UPSETTING OR INSTALLING UNLESS OTHERWISE NOTE IN THE B.M. OR FIELD OF DWG. CUT RIVET TO 1.5 DIA LENGTH FROM OVERSIDE STOCK.
2. ALL RIVETS LOCATED IN THE INTERNAL AIR PASSAGE-WAY SHALL PRESENT C.S.K. FLUSH HEAD TO THE INTERNAL AIR-STREAM UNLESS OTHERWISE NOTED.
3. ALL SHARP OR DISCONTINUOUS EDGES EXPOSED TO THE INTERNAL AIRSTREAM SHALL BE BURNISHED OR BROKEN SMOOTH. ALL EDGES OR CORNER THUS EXPOSED SHALL HAVE .020-.040 RADIUS.
4. BASIC OVERALL DIMENSION FOR INSTALLATION CONSIDERATIONS

HEIGHT = 13.84 (NOM.) FROM INLET LIP TO AFT FACE OF DRIVE FLANGE FACE.

INLET EYE = 27 Dia. INSIDE DIA. (NOM.)

MAJOR OVERALL DIAMETER = 64 1/2 DIA.

Third, the final fan design is completely assembled by aircraft fastener technique: rivets, aluminum bolts and stainless steel bolts.

FAN DESIGN PHILOSOPHY

Because of the availability of the computer-programmed stress analysis discussed in Section I, great strides could be made toward the orderly development of an "analytical design". Following the debugging of the computer program, 44 computer runs were made, representing about 30 different configurations. It was possible to vary systematically such things as blade thickness; for example, for a given configuration, one would try successively blade thicknesses of 0.125 inch, 0.1 inch, 0.09 inch, 0.08 inch, and 0.07 inch. Similarly, the conical hub spider could be evaluated against the cylindrical hub spider, the variable-thickness shroud against the constant-thickness shroud, etc. This permitted the selection everywhere of the minimum-weight component compatible with the structural integrity of the fan. Since the centrifugal loads on the fan are proportional to the mass of the fan, a lighter fan has lower centrifugal loads; therefore, it is stronger than a heavier one, if properly designed. The analytical approach thus allows one to put material in the load-carrying elements, where it is needed, and to remove it elsewhere. It also allows the designer to choose between several fabrication techniques and to optimize not only for weight, but for cost and ruggedness.

In the present program, the emphasis was placed on two qualities: light weight and structural integrity of the fan. In order to achieve a light weight and to minimize risks of structural failure, great sophistication was used in the detailed design and assembly of the fan. In particular, the hub was machined from a solid piece of aluminum in the form of a spider to insure accurate positioning of the blades. Backplate and blades on the one hand, and blades and shroud on the other hand, were fastened using stainless steel screws with helicoil inserts; welding which could introduce distorsions in thin elements and reduce strength of the heat-treated elements was not used anywhere. The result was an expensive fan. This should be viewed only as a necessary step at the prototype level. With the knowledge gained in the present program, it is possible to do either of two things: (a) redesign the metal fan for production, for the same weight, by simplifying the hub, or (b) as indicated in Section II, mold the fan of plastics. However, neither of these steps could be taken within the funding limitations of the present contract.

However, all of the objectives of the program -- the establishment of an improved stress analysis, the analytical design of the fan and the demonstration of the structural feasibility of lightweight RD fans of large size -- were fully met.

COMPUTER PROGRAM INPUT AND OUTPUT

As shown in Appendix III, 15 stations were chosen for describing the fan configuration. The final fan configuration which was analyzed and for which the results are shown in Appendix V is that of Figure 7. However, rather than drawing the rays corresponding to the 15 stations on Figure 7, Figure 7 was redrawn with only the outline needed for the determination of the input physical characteristics shown. The input drawing is shown as Figure 8. The definition of the various input quantities was shown in Figure 2. It can be seen that the mass elements corresponding to station n, for example, for the hub and for the shroud are those extending on each side of ray n, half-way to rays (n - 1) and (n + 1), respectively. It can be seen from Figure 8 that the determination of the "mean" values for the quantities a_h, a_s, r_s is not as obvious in practice as would appear from Figure 2. For example, for Stations 1 to 6, a_h is obtained as the sum of two quantities, one corresponding to the axial length of the hub disc and the other to that of the hub spider. Also, the axial length of the spider tangs must not be counted into the input, since the tangs do not resist any tangential stresses. Similarly, the thickness of the shroud doublers is not counted, in the mathematical analysis, as part of the shroud thickness, since they are not continuous in the peripheral direction. However, both the weight of the tangs and that of the doublers must be introduced in the input. This is accomplished by calculating a fictitious density for the hub or shroud station to which the tang or the doubler element belongs. This was done for each station in tabular form. Details of the input determination are not reproduced here. The reader is warned that great care must be exercised in the determination of the input, since the output is critically dependent upon the input. No matter how good the stress analysis method is, the results will be incorrect if the input "modeling" is not done correctly. For example, to add the axial length of the tang, at Station 7 on Figure 8, to that of the hub disc amounts to replacing the tangs by a solid cylinder and results in an input value which is wrong by a factor of five. Fortunately, with practice, an input error can be immediately detected by looking at irregularities in the plots of output tangential and radial stress distributions against radius.

It may be noted also that the outer shroud outline was drawn, double size, on Figure 8. The reason is that, as explained in Section II, spinning is an art and not a science, and no two spinnings are alike. It was therefore decided by Aerophysics that a separate stress analysis computer run should be made, as a matter of routine, for each newly built fan, prior to running it, using as shroud thickness the measured thickness of the shroud of that particular fan rather than the nominal thickness. The shroud thickness shown in Figure 8 is that of shroud no. 1, belonging to the same fan for which experimental stress analysis results are reported in Section IV.

The input layout for fan RD 51-.70-1.3-75^{o} is shown in Figure 9, for reference. However, results of the computer program for that case are not shown.

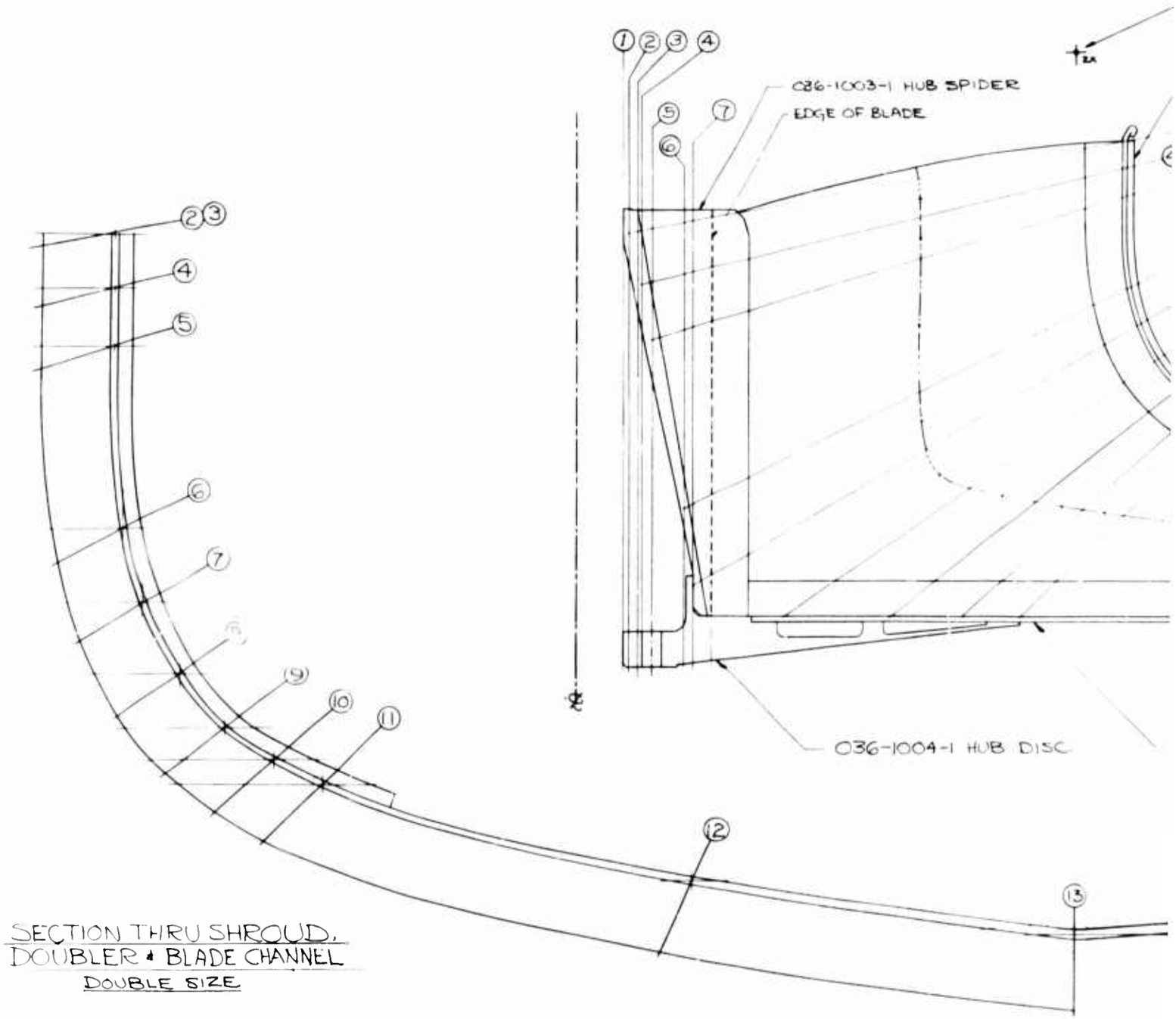

Figure 8. Fan RD 51-.50-1.3-75°, Drawing Used fo

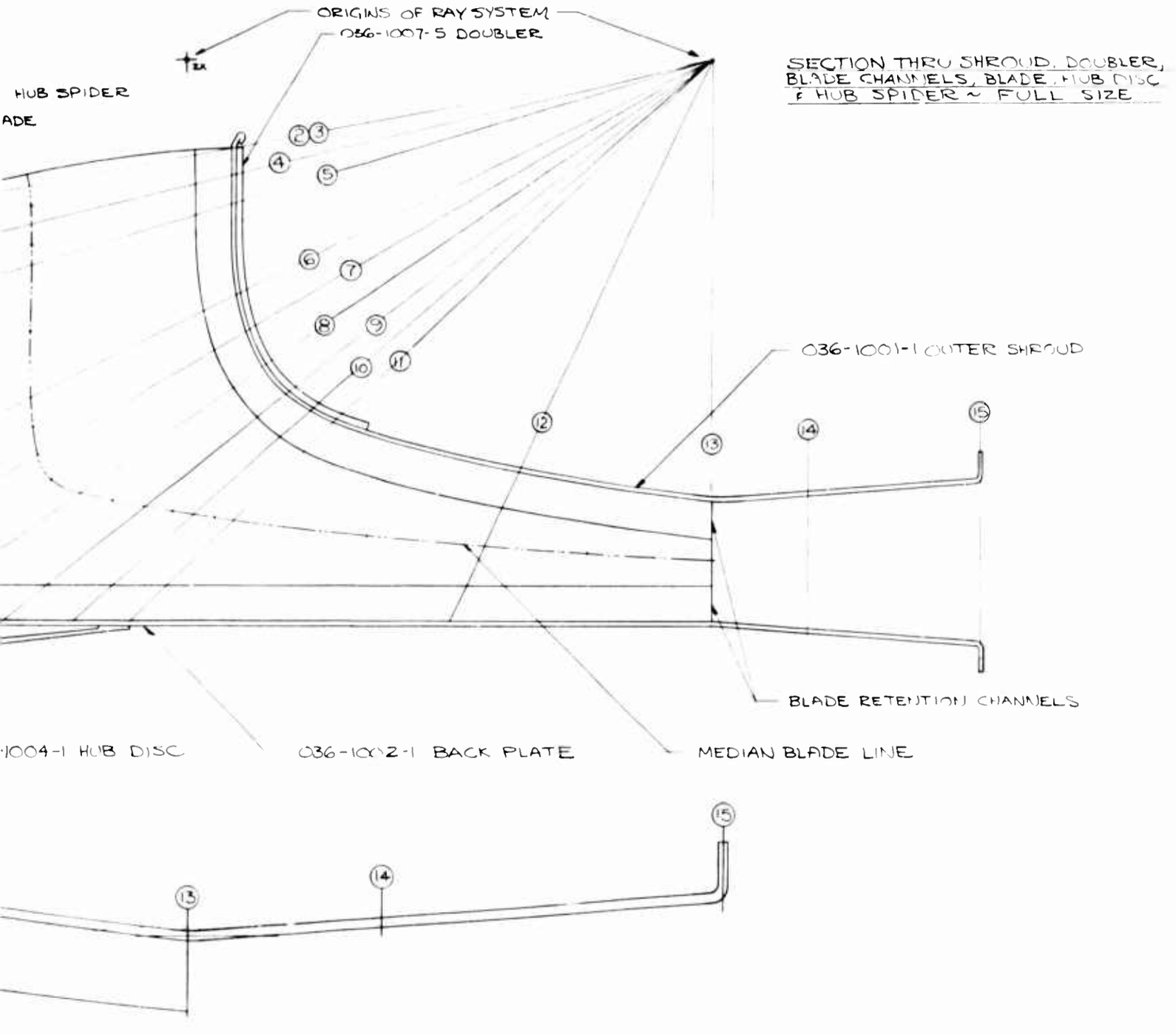

1.3-75°, Drawing Used for Computer Program Input.

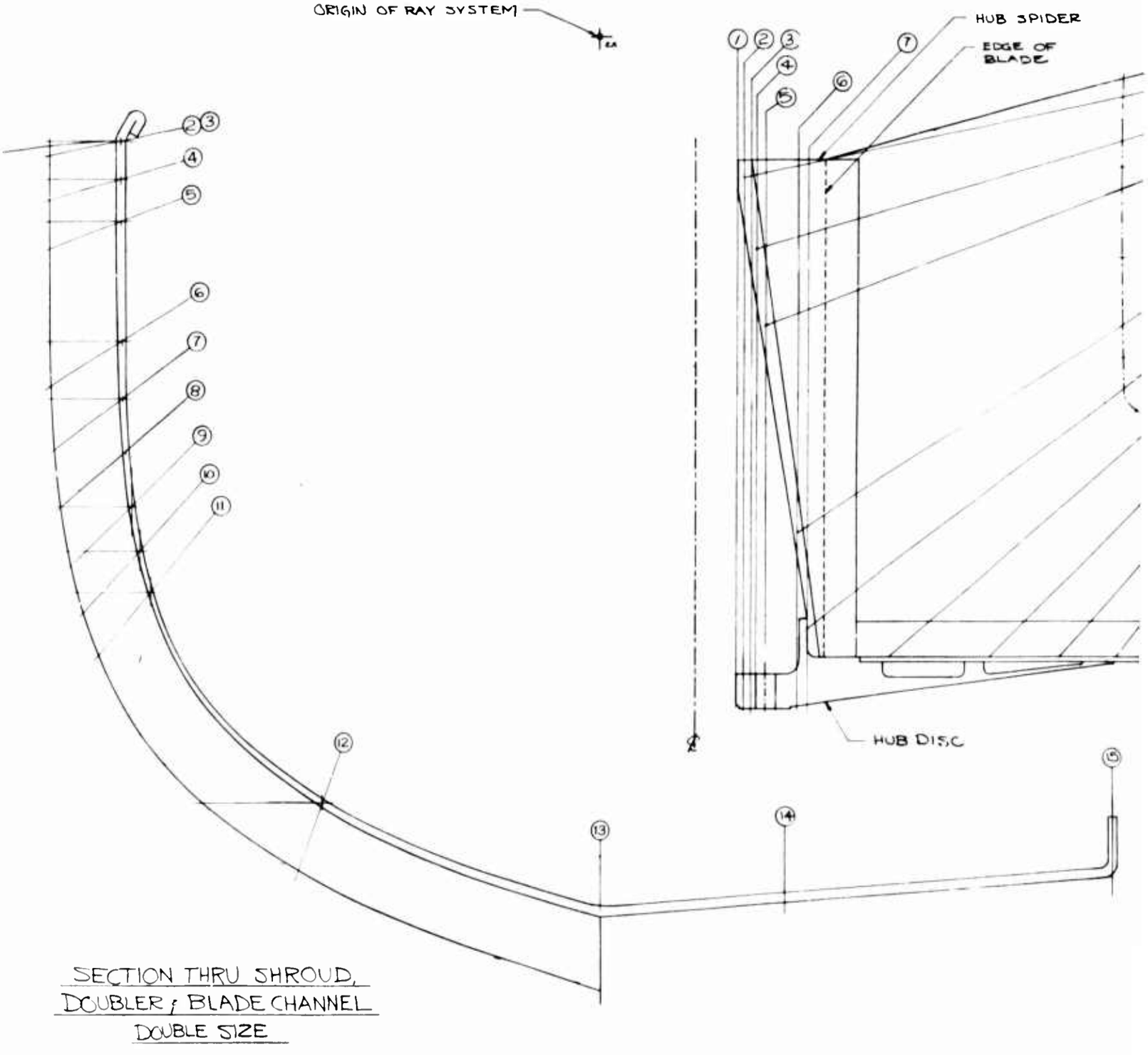

Figure 9. Fan RD 51-.70-1.3-75°, Drawing Used for (

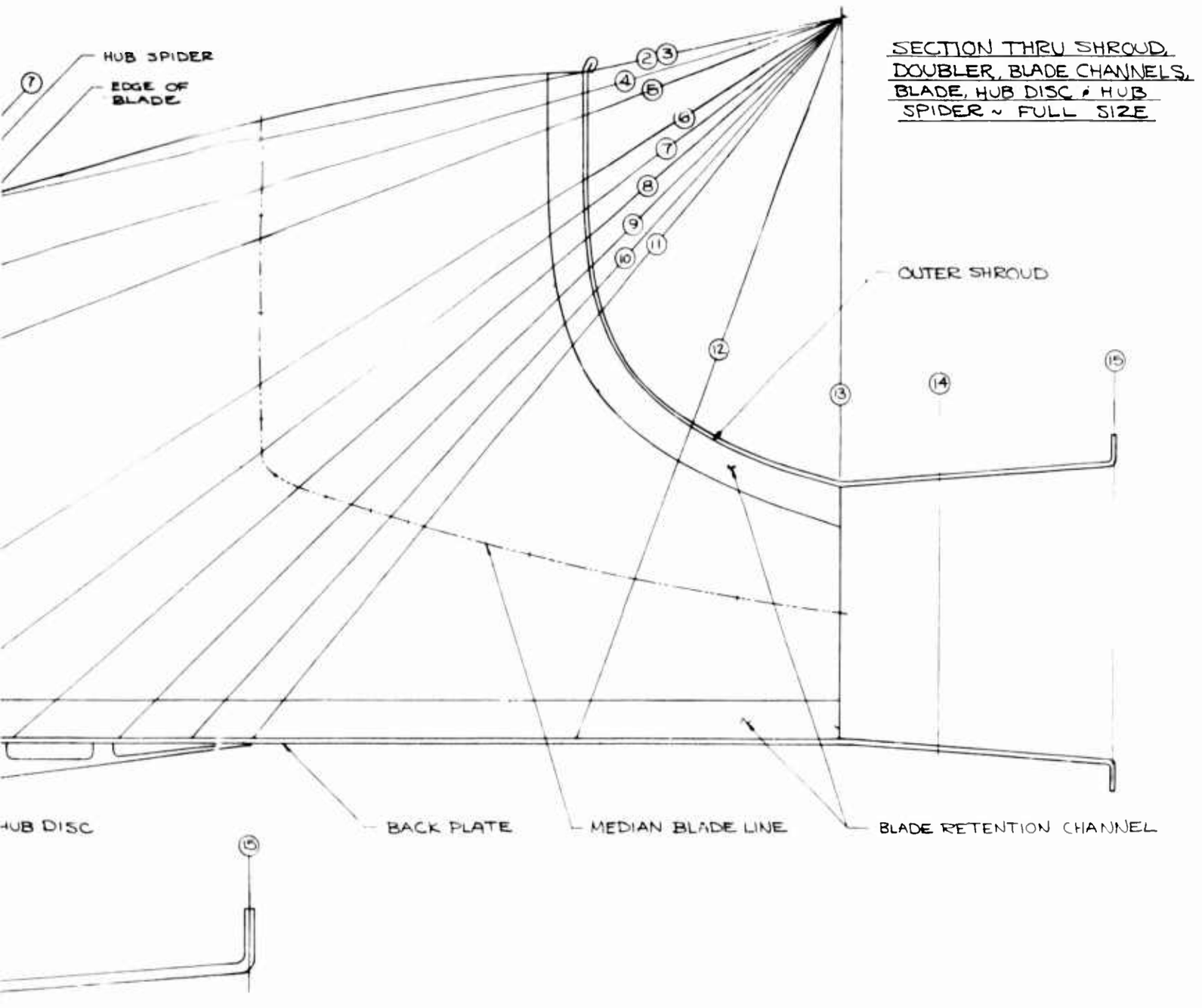

3-75°, Drawing Used for Computer Program Input.

A typical output for the RD fan stress analysis is shown in Appendix V as "Run 44. No Radial Thickness". This case corresponds to the configuration shown in Figures 6 and 7 and to the input shown in Figure 8. configuration shown in Figure 6 and to the input shown in Figure 7. The calculated stresses for this case are used later in this section for the detailed stress analysis of the fan and in Section V for a comparison with the stresses determined experimentally by Joy Manufacturing Company, as reported in Section IV. The output lists the calculated values of the hub stresses, shroud stresses and blade stresses at the 15 stations shown on Figure 8 and defined mathematically by the value of the ray angle. In accordance with the notation of Reference 5, hub and shroud stresses are prescribed as tangential and radial stresses, and the corresponding values of hub and shroud radius are also shown. Blade stresses are shown as shear and tensile stresses.

It is mentioned in Reference 5 that once the stresses are obtained for the fan structure by application of the Deutsch analysis, an additional effect must be considered for the shroud; i.e., the additional stress caused on the shroud by blade restraint. It is a tangential shroud stress and it is maximum at the shroud-blade function. To represent this effect, the following formula was proposed by Deutsch:

$$\sigma_{addit.} = (\pi F_b R_s) / (4N r_s^2 a_s).$$

The computer program was prepared with an option to include the above additional stress. Practically, this was done by tying in $\sigma_{addit.} = 0$ together with $r_s = 0$. Therefore, each case was run for $r_s \neq 0$ and $r_s = 0$ (the "No Radial Thickness" heading). A comparison of computed and experimentally-determined stresses definitely indicated that the above formula did not hold for the lightweight fan which was built. The following explanation is advanced: The above formula assumes that the blade acts as a rigid support. Since the blade gage is very thin, the blade restraint is very small, as the blade deflects together with the shroud; hence, $\sigma_{addit.}$ is very small. As a consequence, the computer runs with $r_s \neq 0$ were discarded, and only the run with "No Radial Thickness" is shown in Appendix V.

DETAILED DESIGN AND FABRICATION PROBLEMS

The assembly drawings of the two identical fans which were built under the contract are shown in Figures 6 and 7. The detailed drawings are not reproduced here, but are listed in Appendix IV. Instead, a few photographs of the fan components are included. A discussion of the detailed design and fabrication problems of the fan components will first be made; next, the procedure for the assembly of the fan will be described, with extensive use of photographs.

Outer Shroud

It was found from the computer analysis of the early designs that the shroud stresses were running consistently higher than the hub stresses; hence, the need to pay great attention to the outer shroud structural design. Also, any foreign objects which might be ingested by the fan would, because of centrifugal force, strike the shroud, not the hub.

It was also decided early that the shroud fabrication would lend itself very naturally to the spinning technique. In final analysis, this proved to be a correct view, since the fan which was built possesses exceptional strength characteristics for its weight. However, the shroud design and fabrication presented extremely bothersome developmental problems, which at one time threatened the whole program with failure. These problems were due to two causes: first, the fact that the ratio of the thickness of the shroud to its maximum diameter was much smaller than current practice in the spinning art, thus pushing the state of the art; second, the carelessness of the spinning subcontractor. Both aspects will be reviewed briefly.

A spinning such as the outer shroud is made by starting from a circular plate of constant thickness which rotates on a saddle lathe and progressively changing its shape by flowing the metal into the shape of a mandrel also rotating on the lathe. The greater the curvature of the final piece, the greater is the difficulty of the operation. Also, the thickness distribution of the final piece is such that maximum thickness is at the outer radius and minimum thickness is at the point of maximum curvature (on Figure 8, this corresponds to the region between Stations 5 and 11). On the other hand, the computer analysis discloses that the point of maximum curvature usually corresponds to maximum stress. Consideration was given to making a thick shroud and grinding it down to a prescribed thickness distribution. This was rejected as too expensive. Finally, starting from a plate 0.25 inch thick, a criterion was set for the minimum acceptable thickness of the shroud as 0.065 inch at the point of maximum curvature. To play it safe, and because it was cheap, it was decided to reinforce the shroud by means of doublers (see Figure 14) to take the in-between-blade bending.

The other potential problem area was the lack of rigidity of the shroud of the fan because of its very small thickness and the possible distortions coming from the fact that the shroud had to be spun in the 0-condition and heat-treated to the T-4 condition afterwards. The first shroud was rejected as having a minimum thickness below 0.065 inch. The next two shrouds were received by Aerophysics at its Brentwood, Maryland, plant on 10 August 1965. They satisfied the minimum thickness requirement. However, upon inspection at Brentwood and careful mating to the Aerophysics assembly fixture, it was determined that neither of the two shrouds satisfied prescribed dimensional specifications as shown on Aerophysics Drawing 036-1001; i.e., $\pm$ 1/8 inch off nominal dimensions,

in the restrained condition. In particular, the diffuser angle was found to be 9 degrees on the average, compared to a nominal value of 4 degrees 15 minutes. What had happened, naturally, was that the spinnings in the 0 condition probably complied with the dimensional requirements, but the distortions had set in as a result of the subsequent heat-treat to a T-4 condition.

Ultimately, the problem was solved by redesigning the spinning mandrel from a convex to a concave shape, turning a flange outward at the tip of the diffuser (Station 15 on Figure 8) and insuring that the shroud was partially reworked and the distortions removed immediately after the heat-treat operation, when the metal was still soft. The final shroud dimensions fell well within the original specifications.

Inner Shroud

It was decided that the inner shroud should be nonstructural, as an examination of Figures 6 and 7 will immediately disclose. Therefore, the inner shroud is only a fairing for the air passage, and there was no reason to use a spinning. It consists of 18 pieces of 0.025-inch-thick aluminum, bent and joggled by hand, which are attached to the blades by means of clips and are riveted directly to the backplate and to the hub spinner.

It was decided originally to fill the void between the inner shroud and the hub with foam-in-place "rensulate" plastic. Problems were encountered with the foam-in-place, and the space inside the inner shroud was finally left hollow.

Backplate

The backplate was made of a 6061-T6 aluminum sheet, as shown on Figures 6, 7, and 8. The computer program had indicated that a sheet thickness of 0.100 inch was acceptable. However, a thickness of 0.125 inch was used, because a 0.100 sheet could not be procured in width greater than 5 feet.

The backplate diffuser annulus was originally bent, using an Aerophysics-built roller, on the table which had been built for the assembly of the fan. However, the plate showed a certain amount of waviness for both fans. After it had been decided to turn the shroud flange up to increase its rigidity, as explained in the previous section, it became necessary to perform the same operation on the backplate. Thus, it became convenient to use the same mandrel as for the shroud. As an experiment, one backplate was annealed, the flange was turned, and the plate was heat-treated again. The other plate had the flange turned while it was in the T-4 condition. The latter one gave better results than the former one, but both were acceptable.

Blades and Blade Attachment

A blade thickness of 0.07 inch was chosen, following the results of the stress analysis. This was a much lower gage than the designer would spontaneously use. A consequence was that even partial blade attachment by welding was out of the question. Blade attachment is entirely by rivets.

The blades, shown on Drawing 036-1005, were cut with a router, following a template. They were bent individually on a brake, which was both cheap and accurate. No special problems were encountered.

Blade attachment to backplate and shroud is achieved by using a channel piece (Drawing 036-1006), milled from a 5/16-x-1-inch piece of bar stock, which is bent to shape in the case of the backplate and bent and stretch-formed in the case of the shroud. Channel-to-blade attachment is by means of countersunk rivets. Channel-to-backplate attachment and channel-to-shroud attachment are by means of stainless steel bolts, held tightly to the channel by means of helicoil inserts. This has the advantage of making the shroud and the backplate removable. This type of blade-to-fan attachment requires a lot of precise fitting, but is extremely strong.

Hub Spider

Two different considerations led to the design of the center hub as a "spider" machined conical piece. First, for ease of assembly of the fan a simple blade positioning device is desirable. Having a spider-type hub, with the blades held on both sides at the root, this goal is achieved simply. Second, the shroud dimensions hold true only within ± 1/8 inch. It is therefore desirable to be able to "slide" the blade to match the shroud. Hence, again, the slotted arrangement has an advantage.

The basic hub spider is a conical tube. This configuration was proved by computer analysis to be superior to the cylindrical tube. Originally, the tangs were designed to have conical edges. In the meantime, from the results of the computer analysis, the blade thickness was reduced from 0.125 inch to 0.07 inch and welding of the blades to the tangs become impossible (0.1 inch is about the minimum thickness that can be welded routinely). The design then reverted to an all-riveted arrangement. It was then necessary to have the tang edge cylindrical, rather than conical, to provide clearance of the drill for drilling the rivet holds through the tangs above Station 7.

Fabrication of the hub spider for the two fans was subcontracted to Applied Science Industries, Falls Church, Virginia.

Hub Disc

The hub disc for both impellers, shown on Drawing 036-1004, was subcontracted to Ray B. Watson Co., Baltimore, Maryland. The two pieces were received on schedule and were acceptable.

It may be noted that both hub spider and hub disc are very functional, being both light and strong and appropriate for a prototype fan; however, they are much too expensive for a production article (total cost of about $1,500 for each fan). As mentioned elsewhere, there is no problem in redesigning, for the same weight, both spider and disc for easier and cheaper fabrication.

FAN ASSEMBLY

Before discussing the fan assembly, a pictorial review of the fan components to be assembled will be made. The hub spider is shown in Figures 10 and 11. Typical blades with channels riveted in place are shown in Figures 10 and 13. A blanked blade is shown in Figure 12. The hub disc is shown in Figure 12. The outer shroud spinning is shown in Figure 14.

There are actually several ways to assemble the fan. The following is shown only as a general procedure, and covers the most important steps.

First, it is assumed that the fan components have been readied in accordance with Drawings 036-1001 to 036-1007, with the exception of hole drilling in the backplate, the shroud and the blades, which is done as part of the assembly.

A key element in the accurate assembly of the fan was the design and fabrication of a circular fixture table, which was used as basic dimensional reference for the lofting and the final assembly. The table was horizontal, and a dummy shaft extended axially above it. The shaft was strictly perpendicular to the table, thus permitting repeatable accurate positioning of the fan assembly (Figures 17, 18, and 19). The table was 20 inches high, providing a convenient working height (Figure 17).

The steps for the assembly of the fan can be described as follows:

1. Using templates rotating around the shaft for the backplate, and also a height gage using the table top as reference, loft the blade channels on both the backplate and the shroud, for all 18 blades (see Figure 12 for the marks on the backplate).

2. Bend and position the backplate blade channels. Pilot drill through the backplate (Figure 15). Drill the final holes and screw the channels in place. They will be removed and replaced many times during the assembly.

3. Stretch form, bend and position the shroud blade channels.

4. Rivet the shroud doublers to the shroud (Figure 14).

5. Drill and tap holes for helicoil in the backplate channel and in the shroud channel. Install the helicoil inserts.

Figure 10. Basic Blade, With Channels Riveted in Place, Attached to Hub Spider.

Figure 11. Major Fan Machined Components, Hub Spider and Hub Disc.

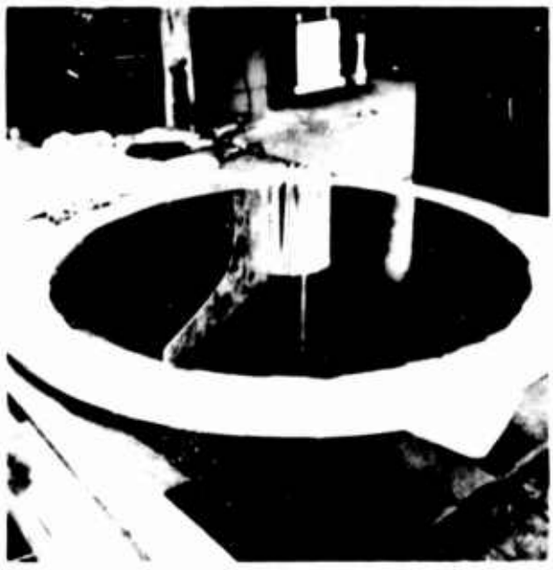

Figure 12. Backplate and Hub Spider With Blanked Blade in Place.

Figure 13. Three Completed Blades With Channels Riveted in Place.

Figure 14. Outer Shroud Spinning With the 18 Doublers Riveted in Place.

Figure 15. Positioning and Pilot Drilling of Backplate Blade Channels.

Figure 16. Individual Hand Fitting of Completed Blade to Backplate and Hub Spider.

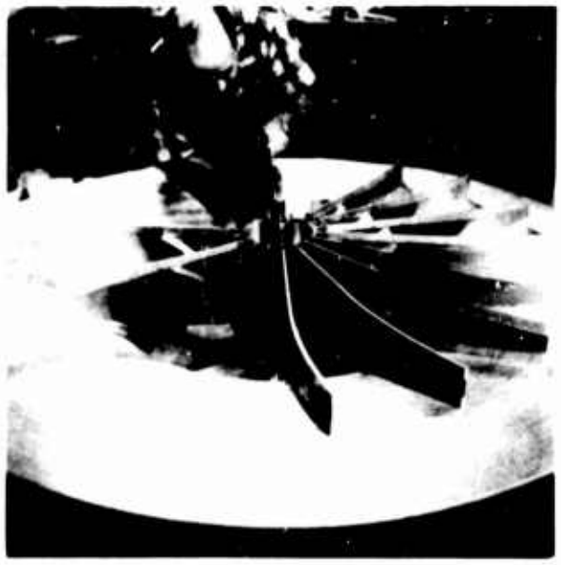

Figure 17. Individual Hand Fitting of Completed Blade to Inverted Outer Shroud and Hub Spider.

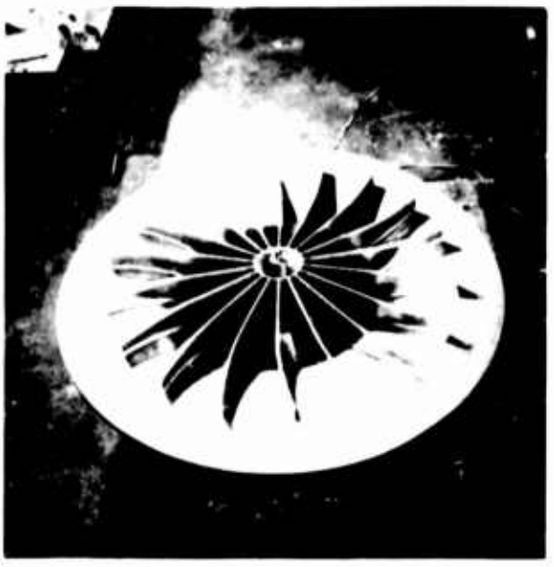

Figure 18. Blades in Final Position With Respect to Inverted Outer Shroud.

Figure 19. Final Fan Assembly; Backplate, Hub Disc and Shroud Screwed to the Blades.

6. Pilot drilling of the shroud from the shroud channel in place is not practical. Pilot drill the shroud from the lofting on the shroud instead.

7. As a bench subassembly, drill and rivet both channels to the blade. Rivet two inner shroud clips to the blade. Ea blade is then in the condition shown in Figure 17 (but not attached to the spider yet).

8. Rivet hub disc to backplate.

9. Loosely assembly backplate, spider hub and blades. Present the shroud to insure a good fit and remove it. Locate the blade holes through the tangs with a specially designed tool.

10. Remove the blades. Undersize drill the located holes.

11. Put the blades back in the fixture. Line ream the holes for the explosive rivets attaching the blades to the hub spider.

12. Install the shroud in the inverted position on the fixture table. Mount hub spider and blades. Finish drilling the shroud holes. Insure hand fitting of all blades, one by one, by alternating between the inverted position (Figure 17) and the upright position (Figure 16). When all blades fit, as in Figure 18, insert the rivets tying in the hub spider and the blades and explode them.

13. Unscrew the shroud. Screw the backplate and rivet the inner fairing (18 pieces) to the backplate and to the clips.

14. Screw the shroud back and rivet the inlet spinner (it can be seen in Figure 21).

15. Remove the backplate. As the last step, pop the 18 explosive rivets that fasten the hub spider and the hub disc.

16. Screw the backplate on for the last time (Figure 19).

Figure 20. Completed Fan, Model RD 51-.50-1.3-75^{0}, Edge-On View.

Figure 21. Completed Fan, Model RD 51-.50-1.3-75^{0}, General View.

DETAILED STRESS ANALYSIS

The detailed stress analysis of the fan was made for a number of conditions corresponding to various computer runs. Since the detailed stress analysis indicates which and how many fasteners (rivets, screws, bolts) to use, the most significant detailed stress calculation is that which was made just prior to freezing the fan design; i.e., here, at the end of Phase II of the program. The fan configuration as it stood at the end of Phase II is embodied in the input of Runs 41 and 42. Runs 41 and 42 had the same physical input, but Run 41 corresponded to $r_s \neq 0$ (in-between-blade bending included) and Run 42 corresponded to $r_s = 0$ (no in-between-blade bending). It was stated earlier in this section that a comparison of calculated and measured stresses made at the end of Phase IV of the program had indicated that the fan actually behaved with negligibly small in-between-blade bending. The input for the detailed stress analysis should therefore be the results of Run 42, not of Run 41. However, this was not known at the end of Phase II, and the detailed stress analysis, as shown in what follows, is based on the output of Run 41. To be complete, both input and output for Run 41 are shown in Appendix VI, as well as a sketch of the ray system for Run 41, which differs slightly from that shown on Figure 8 for Run 44.

As explained earlier, after the fan was built, Runs 43 and 44 were made, and they incorporate the very minor changes made between final design of the fan and fabrication. Therefore, the output of Run 43 is very close to that of Run 41, and the output of Run 44 is very close to that of Run 42. Therefore, to save space, input and output for Runs 42 and 43 are not included among the Appendixes.

So, again, the detailed stress analysis which follows is based on the output of Run 41. Since the stresses for Run 41 (Appendix VI) are higher than those for Run 44 (Appendix V), the results of the analysis are certainly conservative.

Shroud Stresses

By inspection (shroud stresses for Run 41, Appendix VI), the maximum stress, at Station 9 is

$$\sigma_t = 6,717 \text{ p.s.i.} \qquad \sigma_r = 328 \text{ p.s.i.}$$

From equation 31, Reference 5,

$$\sigma_u = \sqrt{\sigma_r^2 + \sigma_t^2 - 2\nu(\sigma_r \sigma_t)}$$

$$= 6,620 \text{ p.s.i. limit,}$$

assume that ultimate stress = 1.5 x limit stress and design for 125 percent overspeed; therefore,

$$\sigma_u = 1.56 \times 1.5 \times 6,620$$

$$= 15,500 \text{ p.s.i.}$$

From the ALCOA manual (Reference 3, page 78) for 6061-T4 sheet,

$$\sigma_{ty} = 16,000 \text{ p.s.i.}$$

$$\text{M.S.} = \frac{16,000}{15.500} - 1 = 0.03.$$

Another section which may be critical is section 13, the base of the diffuser:

$$\sigma_r = 3,889 \text{ p.s.i.} \quad \sigma_t = 1,509$$

$$\sigma_u = 3,790.$$

Hence,

$$\text{M.S.} = \frac{16,000}{3,790 \times 1.56 \times 1.5} - 1 = 0.81.$$

Hub Stresses

By inspection, the maximum stress at Station 11 is

$$\sigma_t = 2,892 \text{ p.s.i.}, \quad \sigma_r = 3,831 \text{ p.s.i.}$$

Again using equation 31 of reference 5, one finds that

$$\sigma_u = 3,950 \text{ p.s.i.}$$

From the ALCOA manual (Reference 3, page 78) for 6061-T6 sheet,

$$\sigma_{ty} = 35,000 \text{ p.s.i.}$$

Hence,

$$\text{M.S.} = \frac{35,000}{3,950 \times 2.34} - 1 = \text{high}.$$

Blade Stresses

By inspection, the maximum stress is on the hub side of the blade at Station 3:

$$\sigma_t = 1,462 \text{ p.s.i.}, \quad \tau = 284 \text{ p.s.i.}$$

Hence, M.S. = high.

Shroud Rivet Design

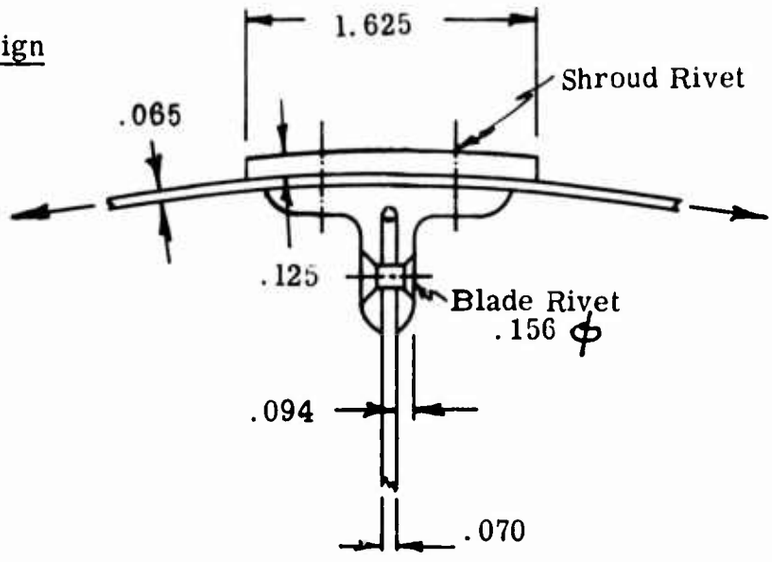

As shown above, Station 9 is critical:

$$\sigma_t = 6,717 \text{ p.s.i.}$$

Assume that the rivets are spaced radially .75 inch apart. The shear load is

$$p = 6,717 \times .75 \times .065 = 328 \text{ pounds.}$$

Using 5/32-inch rivets and 78° head angle, the allowable shear strength is 670 pounds (24 ST).

Hence, in shear, M.S. = $\frac{670}{328} - 1$ = high; in bearing, M.S. = $\frac{670}{328} - 1$ = high.

Allowable tensile strength = 683 pounds; M.S. = high. Therefore, the use of 5/32-inch rivets throughout is permissible. However, for extra safety, 3/16-inch rivets can be used wherever there is a doubler.

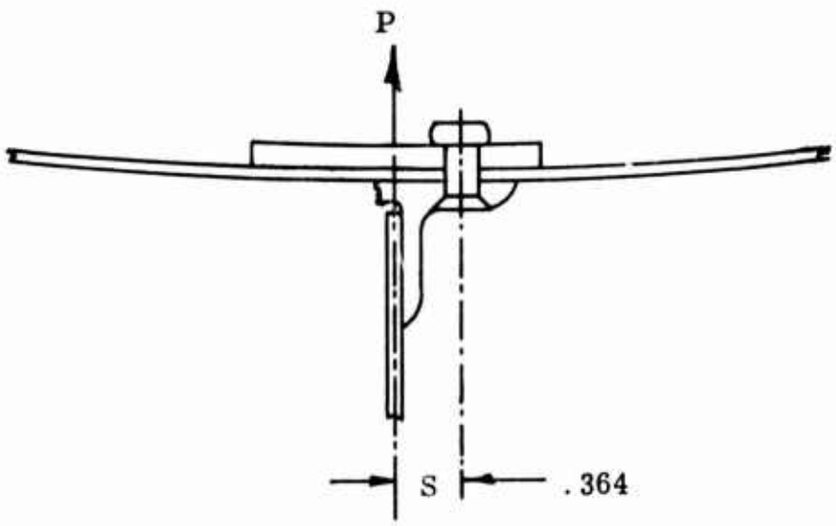

Check now the rivet at the upper flange on direct tension. The blade load at Station 7 is

$$P = \sigma_t \times A = 826 \times .75 \times .070 = 43.3 \text{ pounds, which is carried on two rivets of .156-inch dia.}$$

$$A_{rivet} = .0192 \text{ inch square;}$$

hence,

$$\sigma_t = \frac{P}{A} = \frac{43.3}{2 \times .0192} = 1,130 \text{ p.s.i.,}$$

$s = \frac{.070}{2} + .094 + 1.5 \times \frac{5}{32} = .364$ inch, assuming that the rivet is at a distance equal to 1.5 x diameter of rivet from the flange of clip.

The bending moment in doubler and shroud is

$$M = 21.6 \times .364 = 8 \text{ inch-pounds.}$$

$$\sigma_b = \frac{6M}{b h^2} = \frac{6 \times 8}{.75 \times .125^2} = 4,100 \text{ p.s.i.}$$

Check now the bearing stress on the rivet and the shroud:

$$\sigma_b = \frac{F}{A} = \frac{328}{.094 \times .156} = 22,400 \text{ p.s.i.}$$

Finally, check the stress concentration in the shroud around the rivet holes. At the rivets, the maximum loading occurs in pure tension. The effective area between two rivets is that left after the metal is removed for the holes. Now, at this point there is hardly any bending stress, and the tensile stress is that from Run 42 (Station 9):

$$\sigma_{t\ equiv.} \quad 1817 \times \frac{.750}{.750 - .156} = 2,300 \text{ p.s.i.}, \quad \sigma_r = 328 \text{ p.s.i.}$$

Stress concentration at hole (Reference 9, page 387) is

$$\sigma_e = 3\ \sigma_t - \sigma_r = 5,123 \text{ p.s.i.}$$

Rivets, Lower Flange to Blade

Select 5/32-inch countersunk rivets, spaced 1.5 inches apart.

Shear load due to blade tension load, using Station 7 (stresses computed are nearly normal to passage wall) is

$$\sigma_t = 826 \times 1.5 \times .070 = 87 \text{ pounds}.$$

Shear load due to shear is

$$\tau = 421 \times 1.5 \times .07 = 44 \text{ pounds}$$

$$P_{total} = \sqrt{87^2 + 44^2} = 97 \text{ pounds}$$

M.S. = high.

Hub Spider Rivets

By inspection, the maximum stress along the hub spider is at Station 7 and is

$$\sigma_r = 1,364 \qquad \tau = 695 \qquad \sigma_e = \sqrt{1,364^2 + 695^2} = 1,520$$

$$t_{blade} = 0.07 \text{ inch}$$

The shear load is therefore $1,520 \times .07 = 108$ pounds per inch

Use 5/32-inch explosive rivets. In single shear, they can withstand 590 pounds per rivet. They are in double shear.

Bearing Failure

The rivets were originally spaced 1.25 inches apart (eight rivets). It was decided to add one rivet. The spacing thus became 1.1 inches.

$$f_{br} = \frac{P}{t\,d} = \frac{108 \times 1.1}{.07 \times .156} = 9,900 \text{ p.s.i.}$$

Tear-out Failure

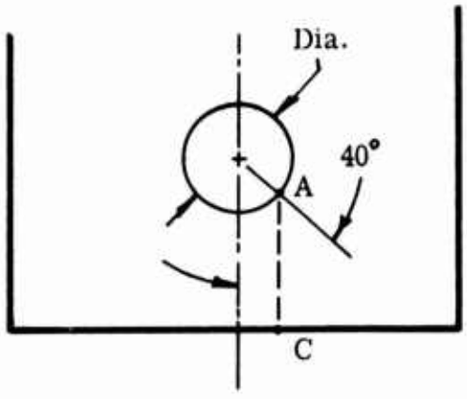

The tear-out failure is based on the distance AC. The rivet center is assumed to be two diameters from the edge of the blade.

$$AC = 2 \times .156 - .078 \quad \cos. 40^{o}$$

$$= .273 \text{ inch}$$

$$f_s = \frac{108 \times 1.1}{2 \times .07 \times .273} = 3,125 \text{ p.s.i.}$$

By inspection, it is seen that the maximum combined blade stress along the hub backplate is 1,050 p.s.i. at Station 12. Therefore, the same rivets can be used for the backplate as for the hub (5/32 inch).

FAN WEIGHT BREAKDOWN

The weight breakdown of the fan, as it was actually built, is given in Table I.

TABLE I
FAN WEIGHT BREAKDOWN

Component	Number	Weight (lb.)	Total Weight (lb.)
Hub Disc	1	13.00	13.00
Blades	18	1.025	18.45
Inner Shroud Fairing	18	.109	1.96
Shroud-Blade Channel	18	.344	6.19
Fairing Clip	36	.0375	1.35
Backplate Channel	18	.406	7.31
Hub Spider	1	11.75	11.75
Outer Shroud	1	32.50	32.50
Backplate	1	40.00	40.00
Hub Spinner	1	.30	0.30
Shroud Doubler	18	.120	2.16
Bolts, Rivets		2.00	2.00
			136.97

SECTION IV
LIGHTWEIGHT RD IMPELLER TESTING

INTRODUCTION

Joy Manufacturing Company of New Philadelphia received a subcontract from Aerophysics Company to conduct the following tests on a lightweight rotating diffuser fan impeller:

1. Balancing
2. Brittle Coating Stress Analysis
3. Strain Gage Stress Analysis
4. Proof Test
5. Sound-Excited Vibration Analysis

Before any of the tests could be conducted, the impeller was mounted on the shaft and statically balanced. Then the impeller was mounted on its bearing pedestals and coupled to the fan test lab dynamometer (see Figures 22 and 23). Next, a protective shed was built around the impeller to protect lab equipment and personnel in case of impeller failure. The testing then proceeded in the same order as given above.

Each of the above procedures will be discussed in this section. The stresscoat stress analysis and sound-excited vibration analysis techniques are supplemented with Joy reports listed in the Bibliography. The strain gage stress analysis technique using radio telemetry equipment will be the primary topic of this section, since obtaining the strain gage test data is the primary objective of the subcontract.

To avoid mix-up in nomenclature of different parts of an RD-type impeller, the nomenclature is the same as that given in Figure 1, Section I.

BALANCING

There are two types of unbalance; thus, there are two types of balance: static and dynamic. They may be present in a rotor individually, but normally an unbalanced rotor includes some of each. The balancing procedure for static unbalance is quite simple and will be discussed next.

By definition (Reference 1, page 7), "Static unbalance is that condition of weight distribution of a rotor where the center of gravity does not lie on the rotating centerline of the rotor." Static unbalance gets its name from the fact that it can be detected by placing

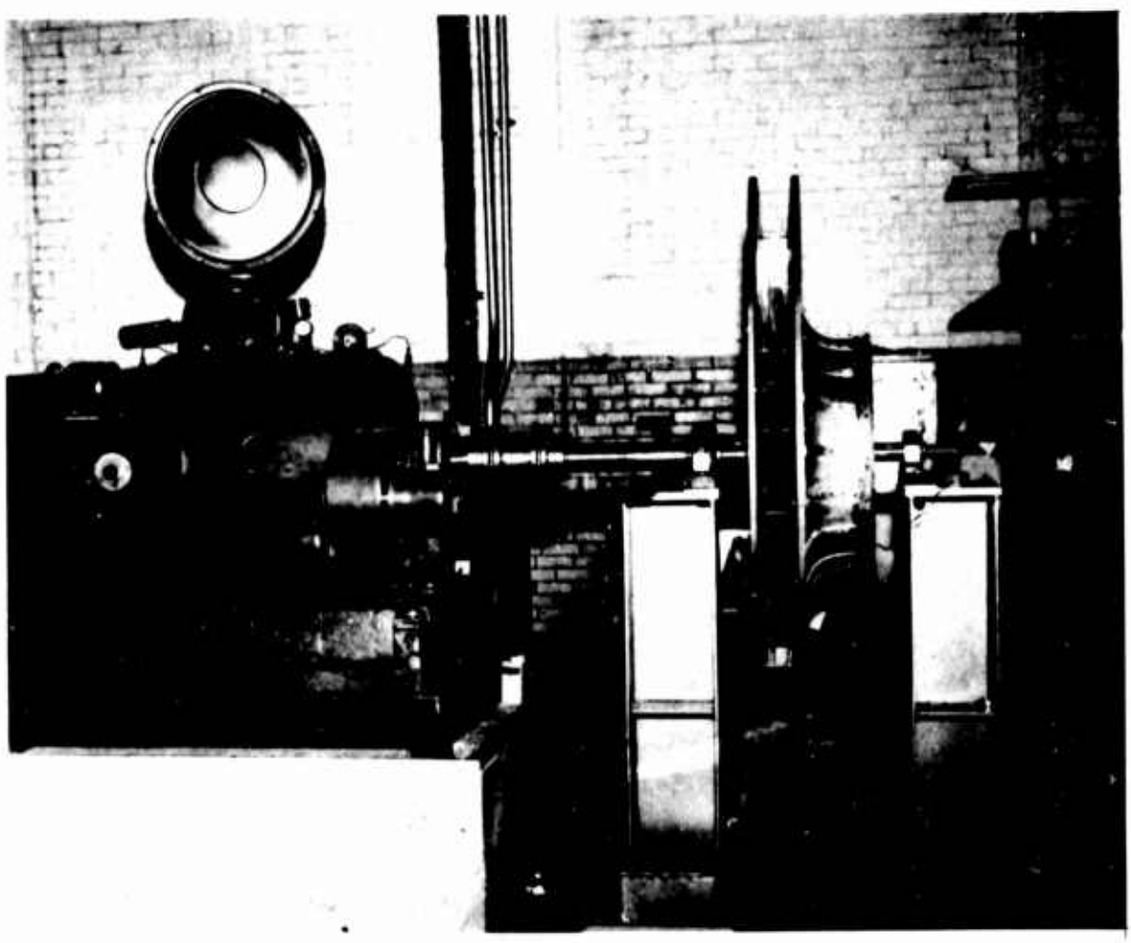

Figure 22. Impeller Test Setup.

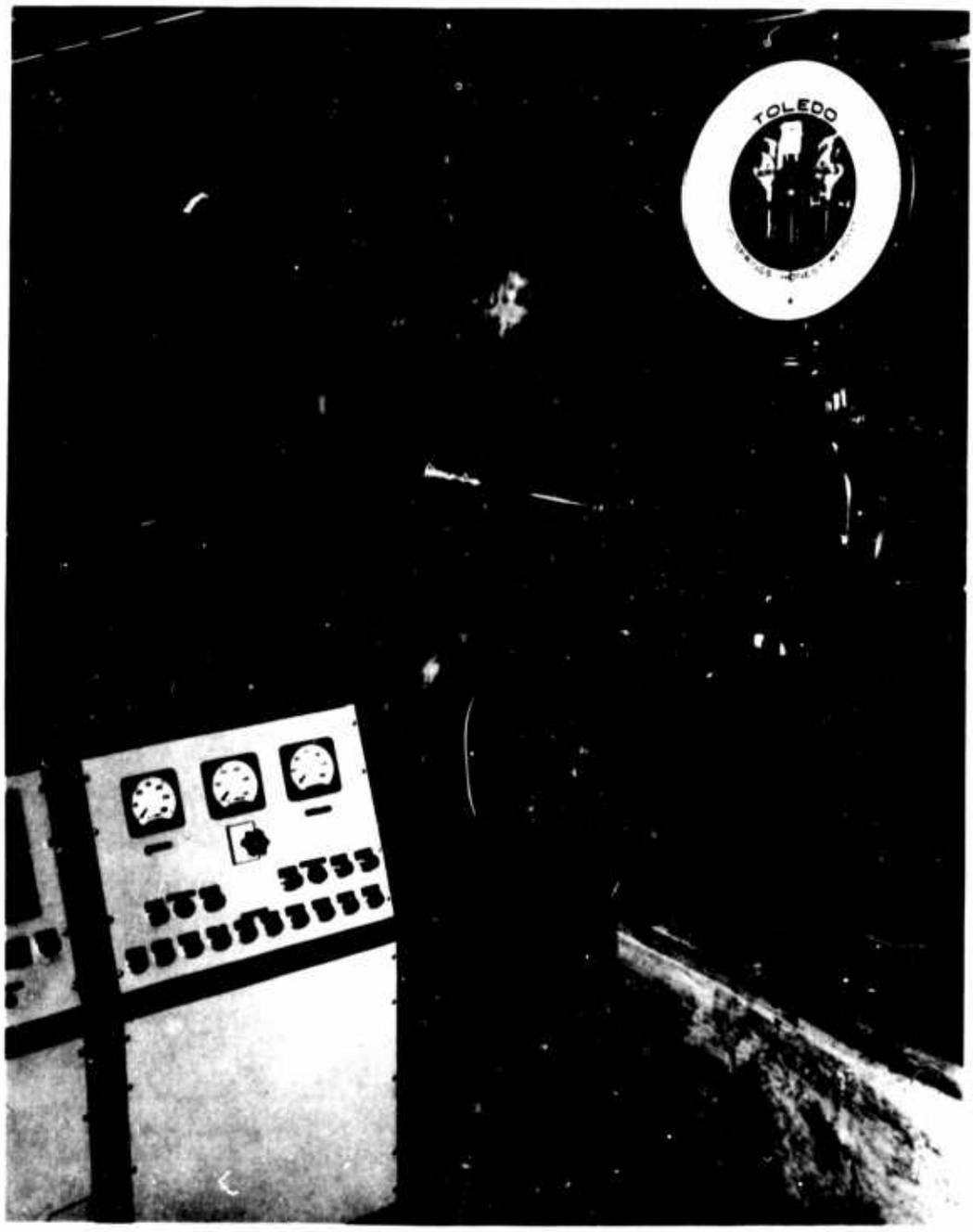

Figure 23. Joy 100 Horsepower Dynamometer.

the part on level parallel knife edges. The heavy side of the rotor will swing to the bottom. Corrections can be made and the part is considered balanced when it does not rotate on the knife edges when placed in any position. The Aerophysics RD rotor was statically balanced by supporting each side of the rotor shaft on a "knife edge" device. The "knife edge" device consisted of two hardened steel wheels with bearing on a support. The rotor then could rotate very easily and thus be statistically balanced, as described above. Approximately 4 ounces of static weight were required to statically balance the rotor.

It is known (Reference 1, pages 7 and 8) that the center of gravity of a part is the point about which all of the weight of a rotor is equally distributed. If we were to slice a rotor into a series of small slices, the line through the center of gravity of each slice would be the principal inertia axis. This is the axis about which any rotor will try to rotate. When a rotor is restricted in its bearing, vibrations result if the rotating centerline and the principal inertia axis do not coincide.

Thus, by definition, the dynamic unbalance is that condition of weight distribution of a rotor which causes the principal inertia axis to intersect the rotating centerline. The intersection will occur at the center of gravity of the rotor. Such a condition is created by a heavy spot at each end of the rotor on opposite sides of the centerline so as to produce two forces acting in opposite directions on opposite ends of the rotor. Dynamic unbalance cannot be detected on knife edges as static can, and does not become apparent until the part is rotated.

The equipment used to balance the Aerophysics lightweight RD rotor dynamically is shown in Figure 24. The equipment consists of an International Research and Development Company (IRD) Model 314 Portable Vibration Analyzer, additional vibration pickup (for rear bearing), selector switch, scale and balancing weights. The IRD Model 314 Portable Vibration Analyzer consists of amplitude meter, variable frequency filter, vibration pickup and stroboscopic light. The amplitude meter registers the peak-to-peak displacement of vibration. The variable frequency filter measures individual vibrations by separating them from other vibrations in the machine. The vibration pickup picks up vibrations in the machine. The stroboscopic light measures the relative phase of vibration. It is a flashing light whose flash rate is determined by the vibration frequency or an internal oscillator in the instrument.

A wheel such as the RD wheel running at more than 1,000 r.p.m. is usually balanced in two planes. One plane is the back shroud and the other is the front shroud. The balancing procedure, which will be described next, is for the single-plane balancing. The procedure

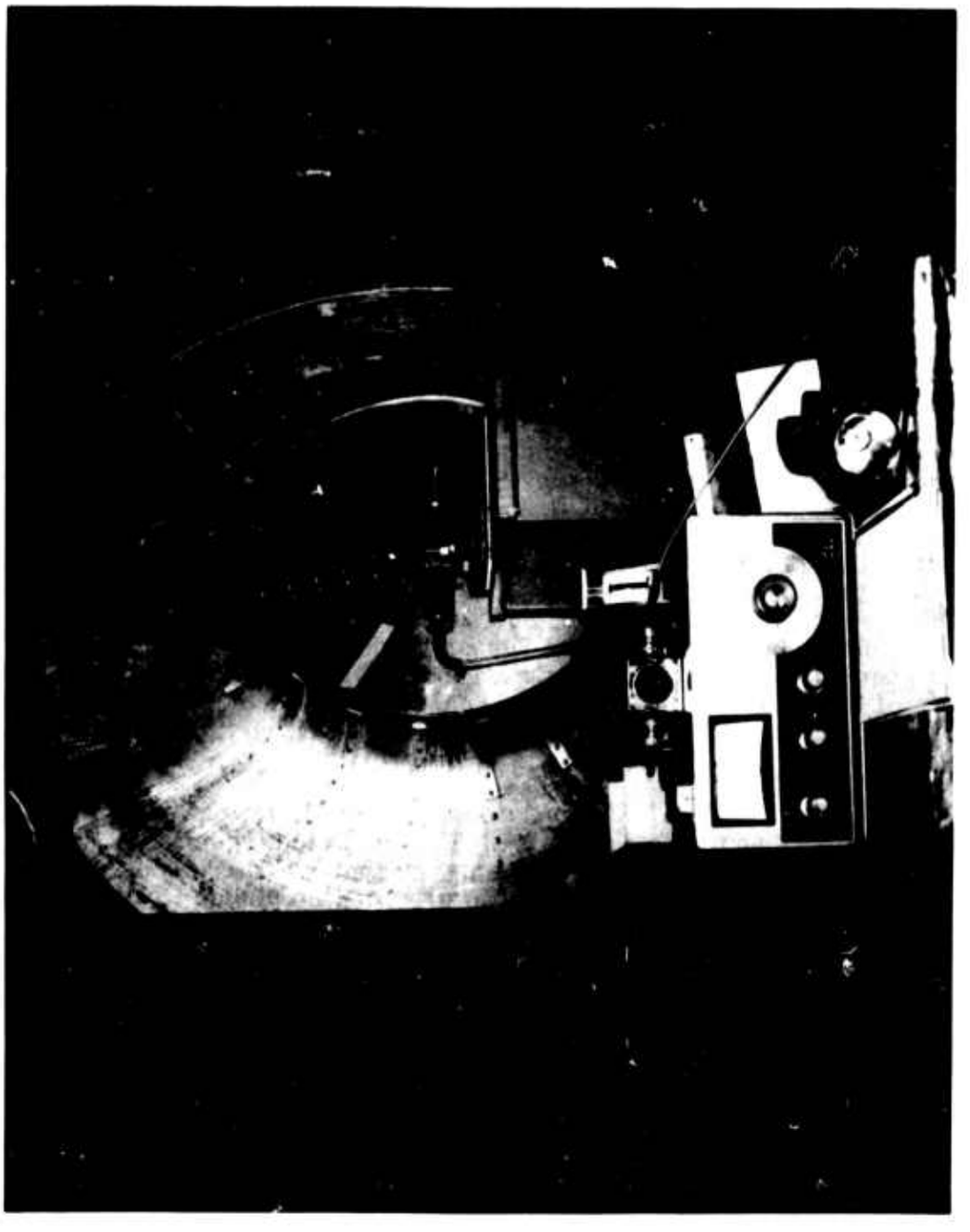

Figure 24. IRD Balancing Equipment.

for single-plane balancing is used for two-plane balancing. First, one plane is balanced and then the other. Normally, some effects of balancing one plane affect the balance of the other, and the balancing process is then repeated by trial and error until both planes are balanced.

The balancing equipment described (see Figure 24) is used in the following manner to balance a wheel dynamically in a single plane.

1. The wheel is run up to balancing speed.
2. The analyzer filter selector knob is set on OCS and the filter oscillation frequency knob is turned until the stroboscopic light stops a mark on the wheel from rotating (for example, the tape on the inlet cover shown in Figure 24).
3. The filter selector knob is then turned on IN, and the vibration readings are taken from the displacement scale of the analyzer for one bearing. The selector switch is then switched to get vibration readings for the other bearing.
4. The vibration displacement (mils-peak-to-peak) is then recorded, and a trial weight is attached on the diffuser.
5. The wheel is then again run up to balancing speed, and the new vibration displacement and phase angle shaft readings are recorded for both bearings.
6. A vector diagram is then drawn on a polar coordinate paper calculation sheet, and the location and amount of the balancing weight are determined.
7. The new calculated balancing weight is placed at the calculated location, and the wheel should theoretically be balanced in a single plane. Usually, however, it takes at least three runs with trial weights before the wheel is balanced.
8. Permanent balancing weights are attached, and the balance is checked.

After the wheel was mounted on the dynamometer, it was dynamically balanced at 500 r.p.m. and the balance was checked at 700 r.p.m. The results are given in Table II. The wheel was finish balanced at 1,180 r.p.m. after the completion of strain gage tests, and the results are given in Table II.

From Figure 25, T. C. Rathbone curves, it is seen that final dynamic balance of .22 and .44 mils-peak-to-peak is "very smooth".

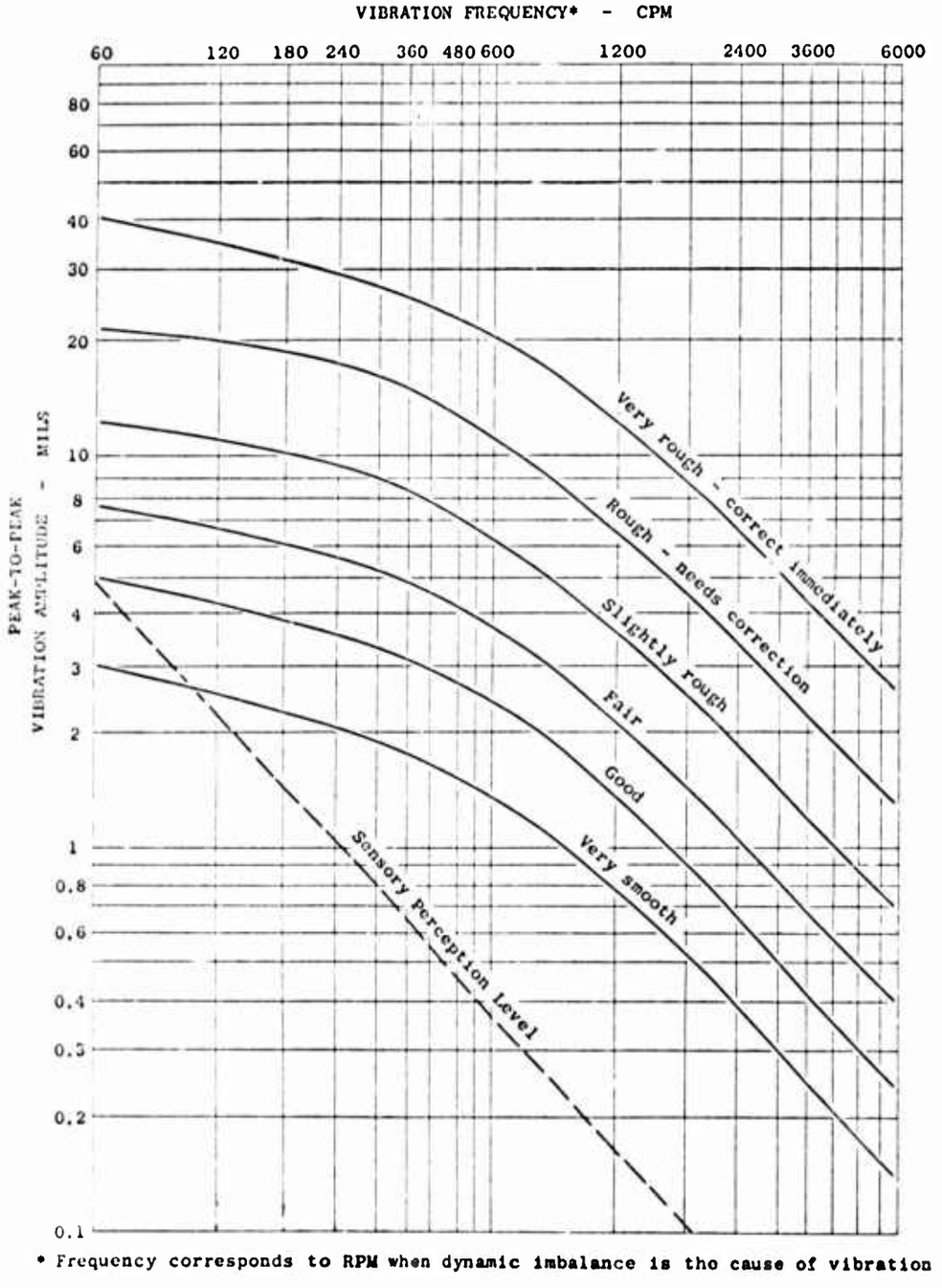

Figure 25. T. C. Rathbone Balance Criteria Curves.

TABLE II
BALANCE DATA

Speed (r.p.m.)	Vibration Amplitude (Mils-Peak-to-Peak)		Permanent Balance Weights (Ounces)	
	Initial Balance			
	Front Brg.	Rear Brg.	Front Shroud	Back Shroud
500	.30	.40	6.5	7.5
700	.30	.40	6.5	7.5
	Final Balance			
500	.48	.78	3.2	8.1
700	.40	.78	3.2	8.1
900	.30	.42	3.2	8.1
1180	.22	.40	3.2	8.1

STRESSCOAT TESTING

The brittle coating (Stresscoat) technique consists of little more than applying a coating of brittle lacquer to the structural member under test, loading the member, and analyzing the resultant cracks for information about surface strains. The coatings fracture at a predetermined value, and cracks occur normal to the principal tension strain. The values at which the coatings fracture are determined by calibration. The stresscoat lacquers are calibrated by coating the part and a calibration test bar. The bar is deflected a fixed amount in a cantilever beam test fixture. By placing the test bar in a strain scale, the least amount of strain required to fracture the coating is determined. Thus, the first crack on the coated test part occurs at the same value of strain as appears on the calibration bar. Once the correspondence between load and strain is established, the strain at any load is determined so long as the entire piece stays within the elastic range. This is based on the premise that all load strains vary in direct proportion to the load under the prescribed conditions of complete elasticity. More complete description of brittle coating technique under dynamic loading is given in Reference 6.

The stresscoat equipment, purchased from Magnaflux Corporation, is standard. It consists of a cabinet with built-in air compressor spray guns, gas mask, cantilever beam calibration device, and assorted stress coatings and undercoatings.

A Joy 18-14-3450 Series 1000 fan with flexible ducting was used to exhaust the stresscoat fumes to the outside of the test lab. The stresscoat fumes are toxic and explosive.

The wheel was sprayed over three sectors about 30 degrees wide, with three different stresscoat coatings: 1204, 1205 and 1206. The calibration bars were also sprayed with the same coatings at the same time, and they were kept with the wheel. After a drying period of about 20 hours, the wheel was run at the following r.p.m.'s: 300, 500, 700, 900, 1,150, 1,350 and 1,450. After each run, careful observation was made of the appearance of new cracks, as well as of the propagation of old cracks from one run to the next at a higher r.p.m. The calibration bars were placed in the cantilever beam calibration device, and the stresscoat sensitivity was recorded before the wheel was run.

STRAIN GAGE TESTING

Selection of Strain Gage Locations

The stresscoat results were not sufficient to locate all the strain gages. Therefore, a meeting was held on December 13, 1965, between Aerophysics and Joy personnel to review the results of the stresscoat testing and to agree on the location of strain gages. It was decided to apply strain gages primarily where past experience with RD fans and the computer program indicated that the maximum stresses should be. A few additional strain gages were located where the few stresscoat cracks had been found. Fifteen strain gages were installed. They were distributed as follows: eight on the front shroud, two on the blades and five on the back shroud. The strain gage locations are shown schematically in Figure 26 and are described in Table III.

After the above fifteen strain gages had been run and their data analyzed, it was decided by Aerophysics that another six gages should be mounted and run. The location of the gages is shown in Figure 26 and Table III.

Since strain gages measure strain and not stress, and because of Poisson's effects (strains unaccompanied by stresses), two gages set 90 degrees apart are required in biaxial stress field. Therefore, a number of gages were mounted in pairs: one at 90 degrees to the other, one in hoop (tangential), and one in meridional (radial) direction. For uniaxial field, or where stresses in the direction perpendicular to gage direction are known, only one gage is required.

Instrumentation

There were two sizes of strain gages used: 1/2 in. by 1/2 in. and

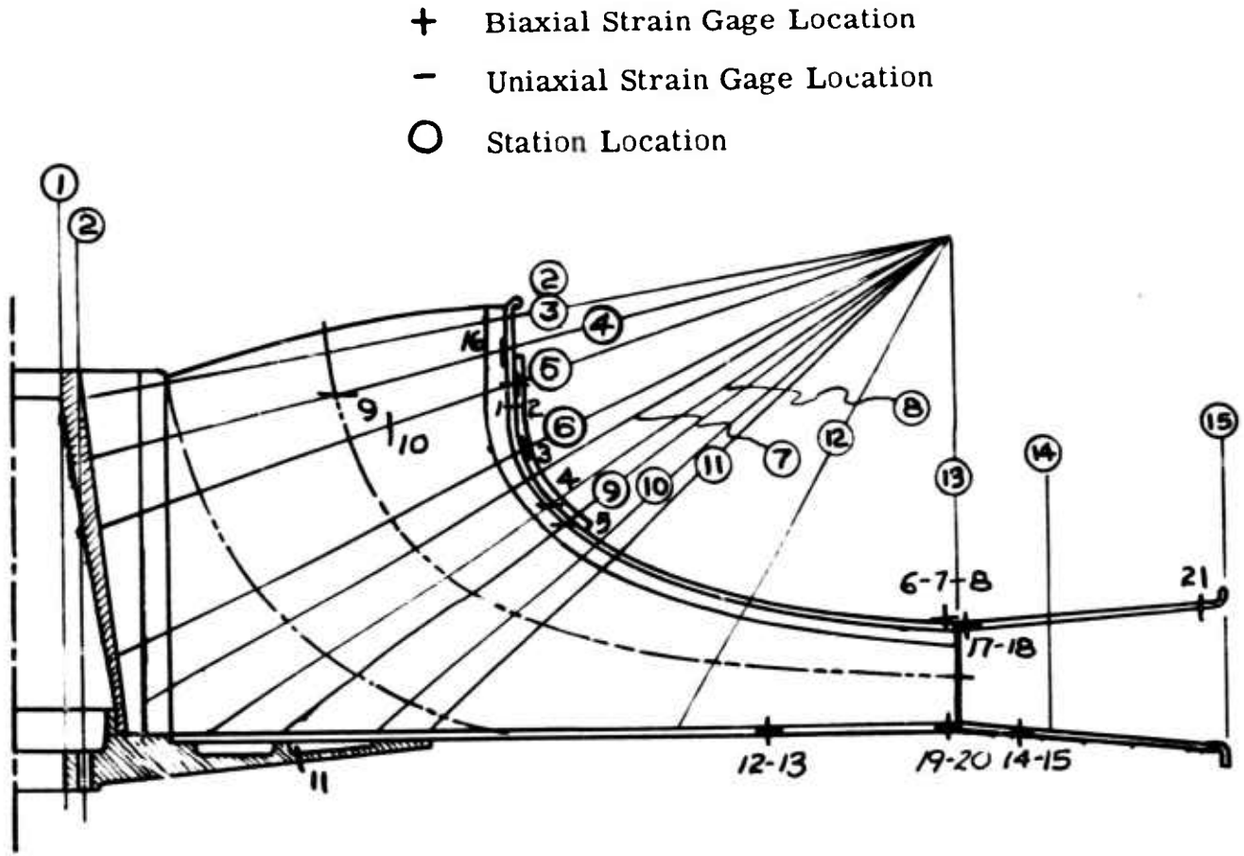

Figure 26. Strain Gage Location.

TABLE III
MEASURED STRAIN GAGE LOCATION

Fan Element	Station and Measured Location					Gage Number and Direction	
	Station	Distance (In.)	Reference	Distance (In.)	Reference	Radial (Meridional)	Tangential (Hoop)
Front Shroud	5	1	Blade	2	Edge of Inlet Cylinder	1	
	4	7/8	"	1-3/8	"		2
	6	1-1/4	"	3-7/8	"	3	
	8	1-1/2	"	5-1/2	"		4
	9	3-3/8	"	6-1/8	"		5
	13	3/8	Top Blade Screw	7-1/4	Top of Diff. Edge	6	
	13	5-1/4	Blade	7-1/4	"	7	
	13	4-1/2	"	7-3/8	"		8
	15			3/4	"		21
	Between 4 and 5	9/16	Projection of Blade Edge	1-3/8	Edge of Inlet Cylinder		16
	Inside of Front Shroud						
	13 Inside Diffuser	3	Blade	6-1/2	Top of Diff. Edge	17	
	"	4-1/8	"	6-1/2	"		18
Blade	4 on Blade 4	1-1/8	Front Edge of Blade	4-7/8	Inside of Inlet Cylinder	9	
	5	2-1/8	"	3-1/4	"		10 (Axial)
Back Shroud	9			1/2	Above Screw		11
	Between 12 and 13	2-1/2	Blade	11	Top of Diff. Edge	12	
	"	3-1/2	"	11	"		13
	Between 13 and 14	2-1/2	"	5	"	14	
	"	1-1/4	"	5	"		15
	13	4-1/2	"	6-7/8	"	19	
	13	5-1/2	"	6-7/8	"		20

1/4 in. by 1/4 in. All gages were Budd metalfilm strain gages that were temperature compensated when mounted on an aluminum structure and had a resistance of 120 ohms.

The radio telemetry equipment was set up as shown in Figures 27, 28 and 29. The equipment shown operates thus: A strain gage feeds through a balanced bridge and provides the modulation voltage of the subcarrier (54 mc). The subcarrier rides on the main frequency of approximately 103 mc. This, along with a battery for power, is mounted in the instrument ring on the rotating impeller shaft (Figure 27).

A receiving antenna picks up this signal and feeds it to an FM receiver. The output of the receiver is monitored by an electronic counter to insure the subcarrier operation. The electronic counter is also used to check and adjust the subcarrier frequency. The signal then is fed into a filter and discriminator which changes the signal from the strain gage into a DC signal. A zero voltage or centering control is incorporated in this instrument. A DC impedance matching amplifier connects the AC signal to the visicorder oscillograph. A scope in parallel with the recorded input is used to keep a check on hash and possible limiting of any previous circuit.

The signal from the strain gage is amplified and displayed as a wave on the oscilloscope and as a vibrating light beam on the oscillograph. This signal has no significance until it is calibrated, and the amplitude of the electronic beam deflection is correlated to the strain to which the gage is subjected.

Outline of Test Procedure

The test followed this procedure:

1. Strain gage locations were selected.
2. Strain gages were installed.
3. Calibration was checked.
4. Zero r.p.m. calibration mark was recorded.
5. Wheel was run up to 1,180 r.p.m. and stresses were recorded.
6. Zero r.p.m. calibration mark was recorded.

Calibration

The following three calibration techniques were used:

1. Synthetic Strain
2. Cantilever Beam
3. Eccentric Weight

While any of the above three techniques could be used to calibrate

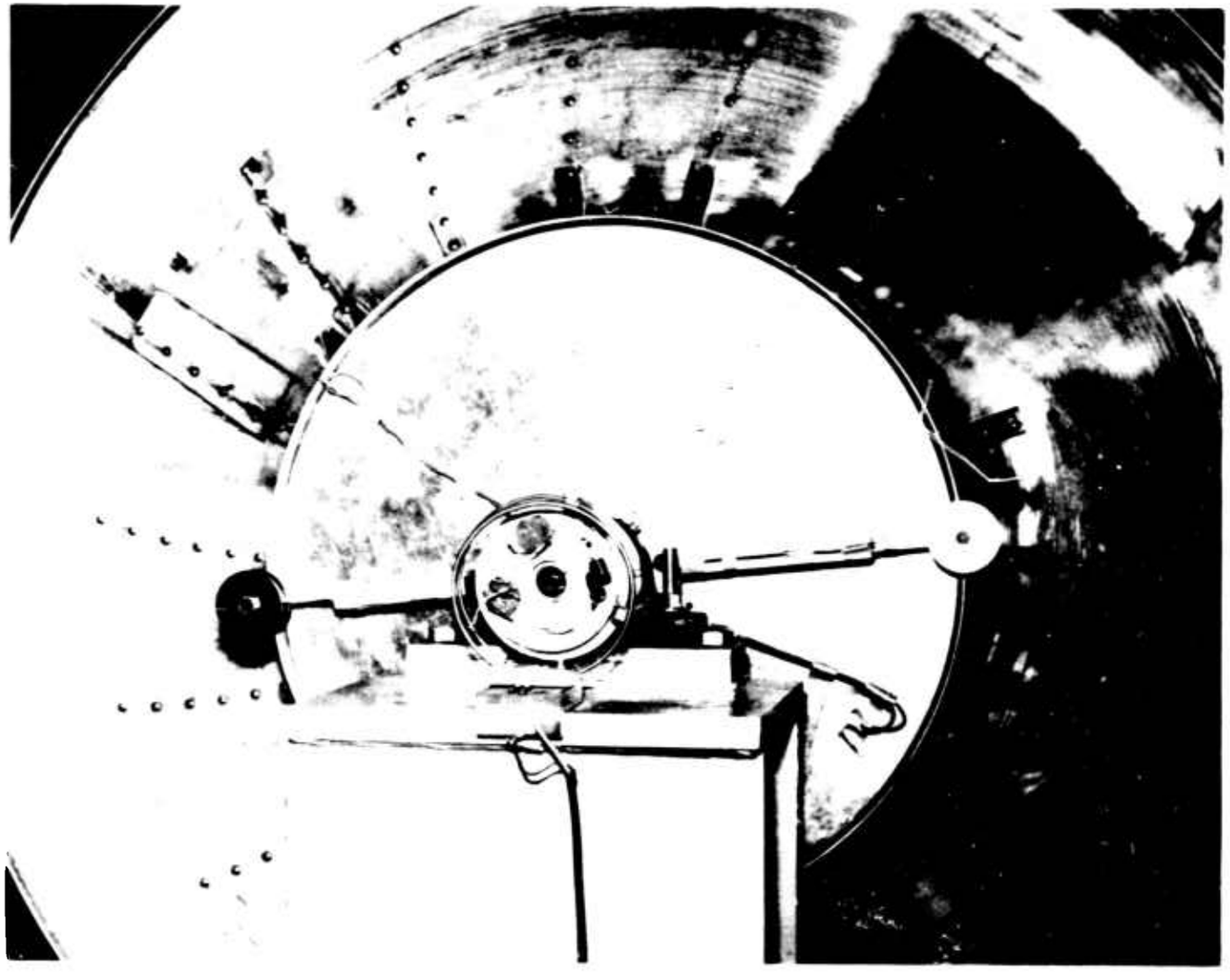

Figure 27. Telemetry Equipment and Eccentric Calibration Device.

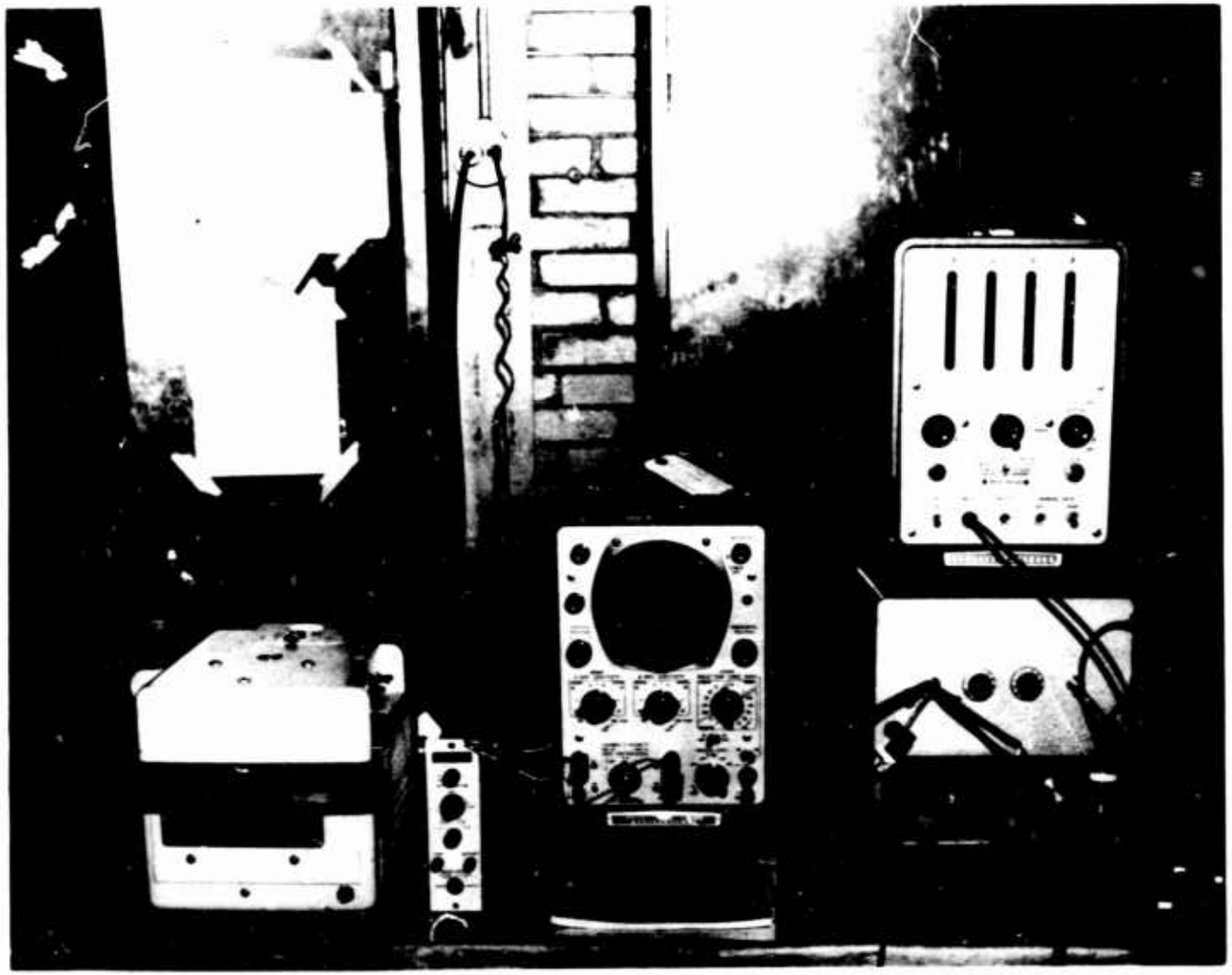

Figure 28. Radio Telemetry Receiving and Recording Equipment.

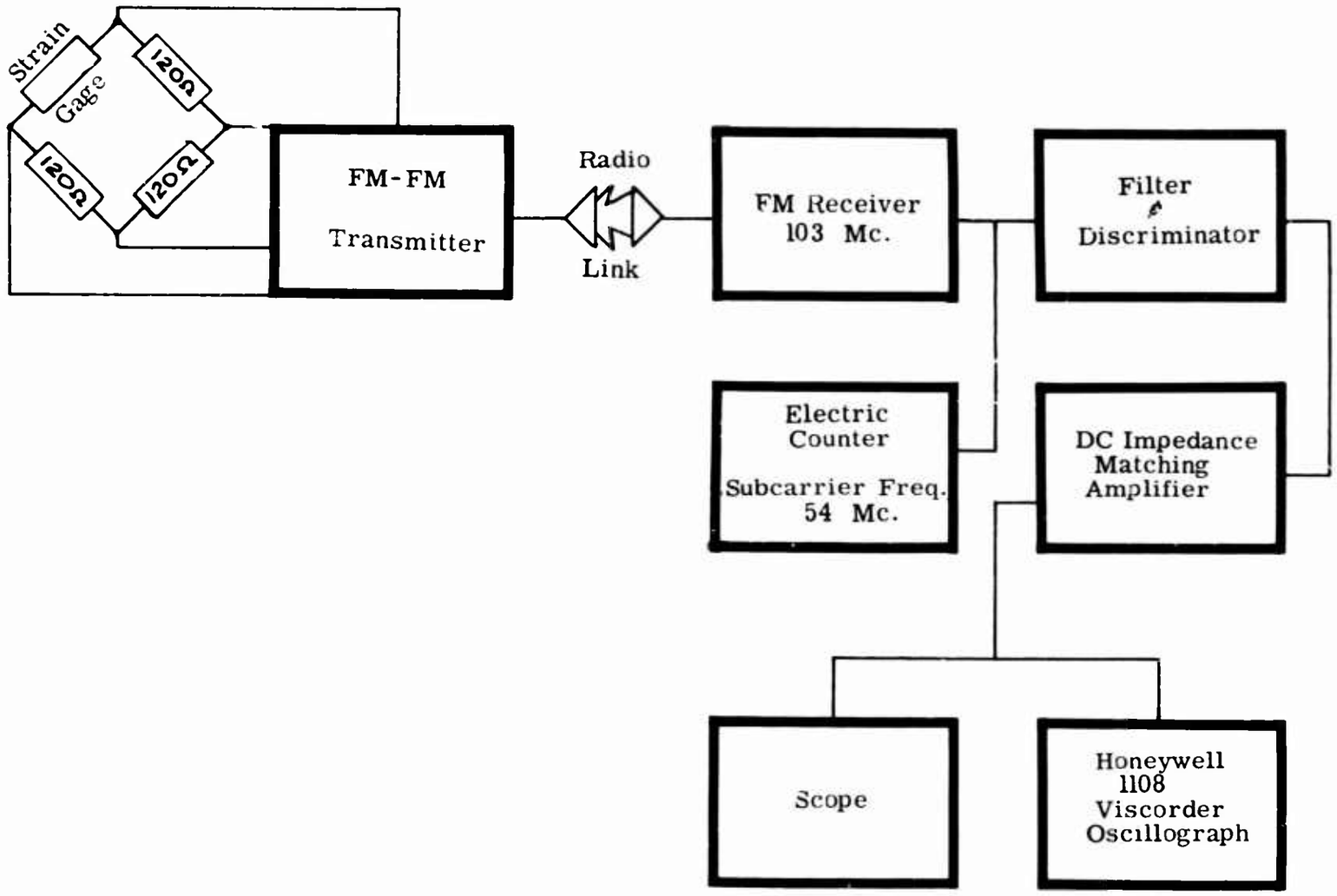

Figure 29. Schematic for Radio Telemetry System.

the strain signal, each technique was used for a specific function. Thus, the synthetic strain technique was used to calibrate the strain signal before the wheel was run. The cantilever beam technique was used to check the synthetic strain calibration and to check static operation of the telemetering equipment. The eccentric weight calibration technique was used to check the first two and also to check the operation of the telemetering equipment under actual operating conditions. Each of the calibration techniques will be described next.

The synthetic strain technique (Reference 8) is the electrical calibration method shown in Figure 30. The strain gage resistance in one leg of the Wheatstone bridge is shunted by an open-circuited resistor of much higher resistance. When this resistor circuit is closed, a bridge unbalance can be considered as a synthetic strain and, as such, will appear as deflection of electron beam on the oscillograph. The deflection of the beam from the synthetic or calibrating strain makes it possible to determine the calibration factor relating strain to the displacement of the oscilloscope electron beam.

The size of the calibration resistor Rc is selected so that the resistance change obtained by shunting the gage is equal to that produced by a particular strain.

The resistance Rc of the calibration resistor is found from the following relation:

$$Rc = \frac{Rg}{F\epsilon}$$

where

Rg = Gage resistance
F = Gage factor
ϵ = Strain (in./in.)

If the following are known,

Rc = 60,000 ohms
Rg = 120 ohms
F = 2.06,

the strain can be found thus:

$$\epsilon = \frac{Rg}{FRc}$$

$$= \frac{120}{2.06 \times 60,000}$$

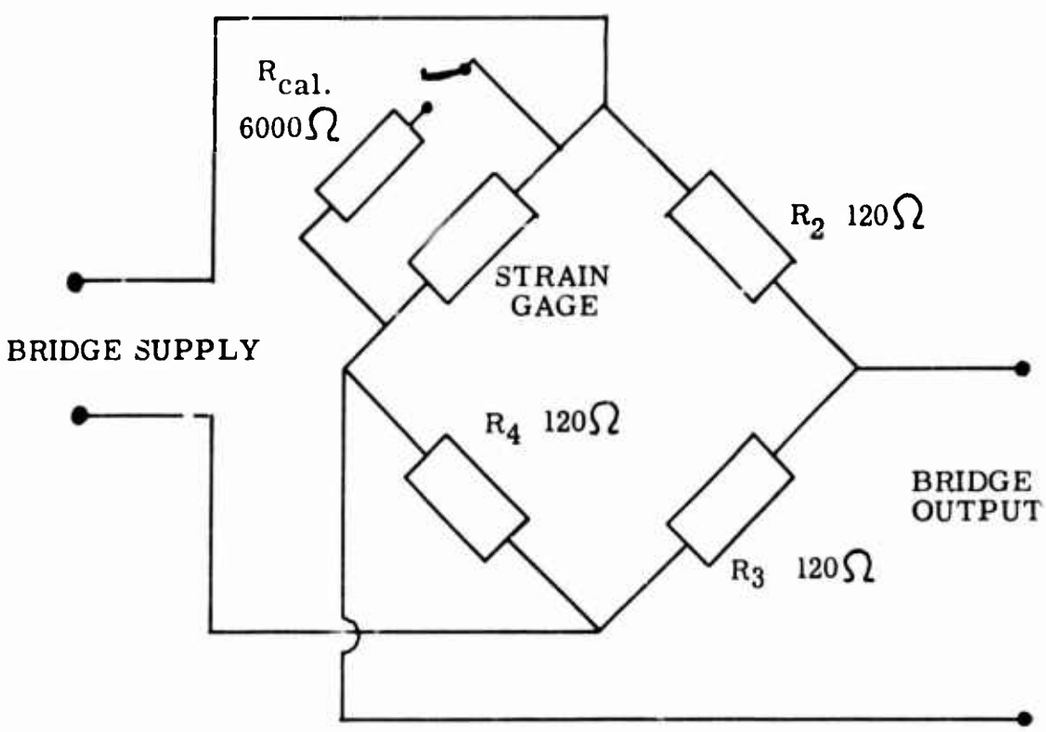

Figure 30. Synthetic Strain Calibration Technique.

$$\epsilon = 970.9 \times 10^{-6} \text{ in./in.}$$

If the electron deflection is 2.5 inches or 25 marks on the oscillograph scale, the strain for each mark is

$$\epsilon = \frac{970.9 \times 10^{-6}}{25}$$

$$= 38.84 \quad \text{per mark}$$

where

$$\mu = 1 \times 10^{-6} \text{ in.}$$

Since the stress σ is given by

$$\sigma = E \epsilon ,$$

then

$$\sigma = (10.3 \times 10^{6}) \times 38.84 \times 10^{-6}$$

$$= 400 \text{ p.s.i./mark}$$

where

E = Modulus of elasticity (10,300,000 p.s.i. for aluminum).

The cantilever beam calibration method is used by Joy Manufacturing Company in the following manner: stresscoat cantilever beam calibration device (as seen on the right edge of the table in Figure 28) is used to apply a known strain to a strain gage in the Wheatstone bridge and to observe the deflection of the oscillograph electron beam. Thus, a stresscoat calibrating bar is taken and placed in the calibrating scale, and the desired calibration strain, such as 1,000 μ in./in., is location marked on the beam. A small (1/8 in. x 1/8 in.) strain gage is then glued on the test bar with its centerline on the mark on the test bar. The calibration test bar is then placed on the calibrating device, and the strain gage is wired to the Wheatstone bridge. Then the cantilever beam is deflected a known amount (1,000 μ in./in.) by moving the handle on the calibrating device cam. The deflection of the oscillograph beams (2.5 inches) is then equal to this known strain. To check the electrical calibration device, the gage is shunted with a high resistance calibrating resistor and the oscillograph beam deflection (2.5 inches) is observed. If the calibrating devices and telemetering system operate properly, the beam deflection should be the same.

Thus, for the calibration used for strain gage testing, a 2.5-inch deflection is equal to 10,000 p.s.i., or 1 mark is equal to 400 p.s.i.

Thus, the deflection of the cantilever beam to produce a strain of 1,000 μ in./in. produced the same deflection (2.5 inches) on the oscillograph scale as the 6,000-ohm calibrating resistance. Since the stress can be found from

$$\sigma = E \epsilon,$$

$$\text{then } \sigma = 10^3 \times 10^6 \times 1{,}000 \times 10^{-6}$$

$$= 10{,}300 \text{ p.s.i.}$$

10,300 p.s.i. = 2.5-in. deflection.

Therefore, the cantilever beam method checked the synthetic strain method.

The eccentric weight calibration method is similar to the cantilever beam method. A known strain is applied on a strain gage and the deflection is observed. The strain, however, is applied by the centrifugal force of a weight at the end of a rotating bar. The device is shown in Figure 27, and consists of two weights at the ends of rods that have test sections of known area machined for the strain gages. The weight of the bar above the centerline was carefully calculated, and the weights were carefully weighed. Thus, for any r.p.m., the centrifugal force of the weight can be calculated, and stress can be found from

$$\sigma = \frac{F}{A}$$

where

F = Centrifugal force (lb.)

A = Area of test section (in.^{2}).

This method can be used to check the calibration of the other two methods and to check operation of the telemetry system under operating conditions.

The calculation procedure for eccentric weight calibration method is shown in Table IV. An example of the calculation is shown below.

The centrifugal force is given by

$$F = \frac{W}{g} \omega^2 r$$

where

W = Weight (lb.)

r = Radius to cg of weight (ft.)

TABLE IV
ECCENTRIC WEIGHT CALIBRATION TECHNIQUE DATA

N, r.p.m.	ω, 1.0472 N/10	$\omega^2 x10^4$	F, 3.61958 ω^2	Stress Cal. 16 F	Def. Mark	Calib., 400 p.s.i./mark	Stress Exp.	Dev. %	Notes
1175	123.05	1.5141	547.9	8766	21.5	400	8500	-1.89	Run 1
967	101.26	1.0254	371.2	5939	15.0	"	6000	+1.03	"
736	77.07	.5940	215.0	3440	8.5	"	3400	-1.16	"
507	53.09	.2818	102.0	1632	4.0	"	1600	-1.96	"
1170	122.52	1.5011	543.3	8693	21.2	400	8480	-2 45	Run 2
975	102.10	1.0424	377.3	6037	15.3	"	6120	+1.37	"
718	75.19	.5654	204.6	3273	8.7	"	3480	+6.32	"
508	53.20	.2830	102.4	1638	4.4	"	1760	+7.45	"

g = Constant of acceleration (32.2 ft./sec.^{2})

ω = Angular velocity (rad./sec.).

The angular velocity is given by:

$$\omega = \frac{2N\pi}{60}$$

$$= \frac{1.0472\,N}{10}$$

where

N = Rotating speed (r.p.m.).

Therefore, for the calibration device shown in Figure 27,

W = 0.999 lb.

r = 14 in.

$$F = \frac{0.999 \times 14}{32.2 \times 12}\,\omega^2.$$

The stress is given by

$$\sigma = \frac{F}{A}$$

$$= \frac{F}{1/16}$$

where

A - Area = 1/16 in.^{2}.

Therefore, for 1,175 r.p.m.,

$$\omega = \frac{1.0472\,N}{10}$$

$$= 1.0472 \times \frac{1,175}{10}$$

$$= 123.05 \text{ rad./sec.}$$

$$F = .0361958 \times \omega^2$$

$$= .0361958 \times 123.05^2$$

$$= 547.9 \text{ lb.}$$

$$\sigma = 16F$$

$$= 16 \times 547.9$$

$$= 8,766 \text{ p.s.i.}$$

The deviation is calculated from

$$\text{Percent deviation} = \frac{\text{Exp. Stress - Cal. Stress}}{\text{Cal. Stress}}$$

$$= \frac{8,600-8,766}{8,766}$$

$$= 1.89 \text{ percent.}$$

Data Reduction

Structural analyses are usually presented in terms of stresses. The stresses, however, are derived quantities; thus, the measured strain readings must be converted to computed stresses.

The uniaxial stresses can be obtained from measured strains by using Hooke's law ($\sigma = E\epsilon$) so long as the proportional limit is not exceeded. Thus, the uniaxial stresses were obtained directly from the strain graphs by using the calibration factor.

Typical strain gage data as recorded by oscillograph are shown in Figure 31. The middle trace in Figure 31, for gage number 16, shows (starting from left to right) the 0-r.p.m. calibration trace; a dip of calibration trace due to switching off of the paper feed; full-speed 1,184-r.p.m. trace; a dip due to switching off the paper feed; and another 0-r.p.m. calibration trace. The darker lines parallel to the trace are 0.5-inch lines and the lighter lines are 0.1-inch lines. The arrow shows that the strain is in tension, and the calibration is 2.5 inches, when the strain gage is shunted with a 60,000-ohm resistor. The calibration, as calculated in the calibration section, is 2.5 inches = 10,000 p.s.i. or 0.1 inch = 400 p.s.i.

Thus, if gage 16 represents uniaxial stress, the stress at 1,184 r.p.m. is

$$\text{Uniaxial Stress} = (\text{Number 0.1 in marks}) \times \frac{400 \text{ p.s.i.}}{\text{mark}}$$

$$= 2.6 \times 400$$

$$= 1,040 \text{ p.s.i.}$$

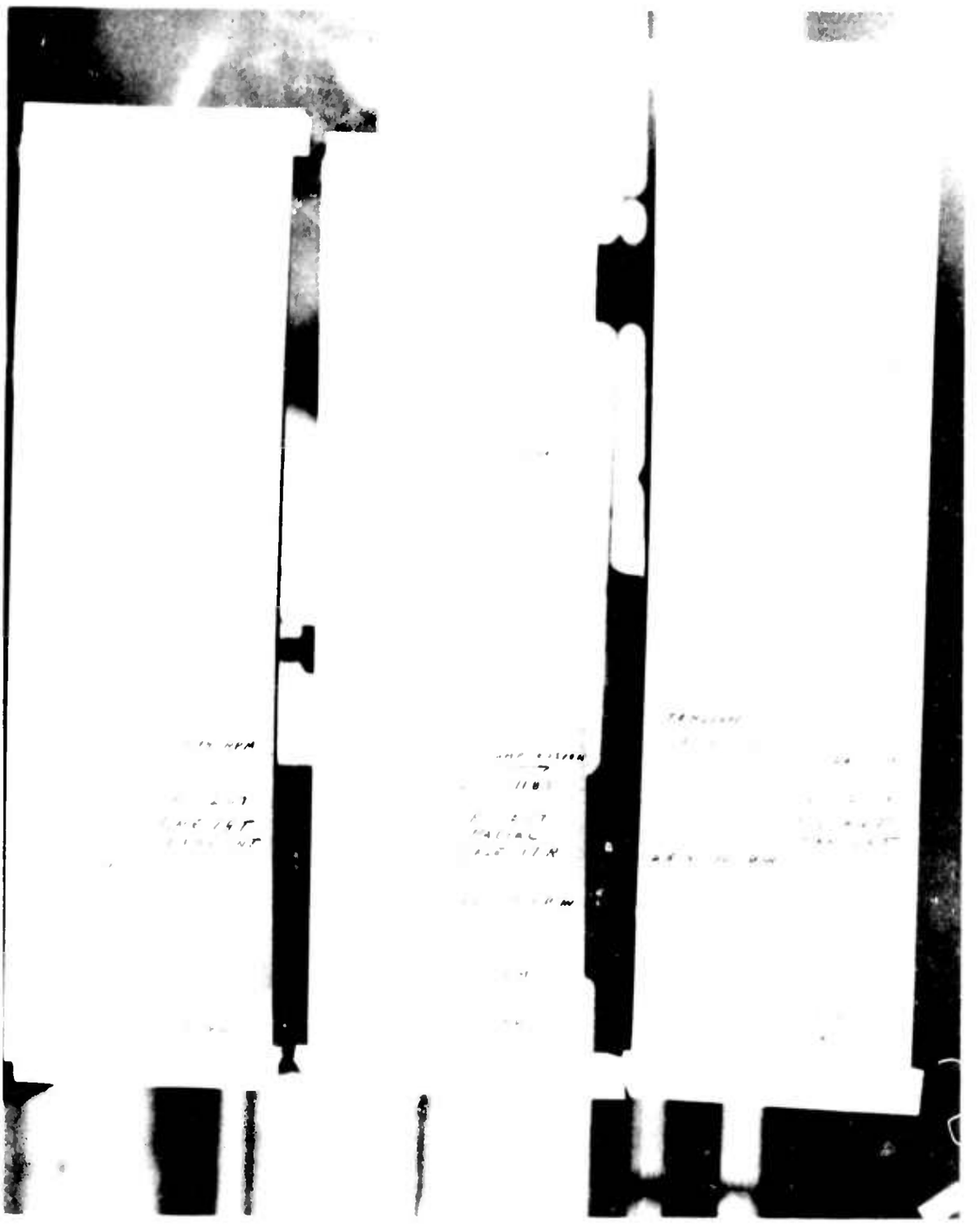

Figure 31. Typical Strain Gage Test Data.

The biaxial stresses, however, cannot be calculated using Hooke's law because of Poisson's effect -- strains unaccompanied by stresses (Reference 8). The calculation of stresses from the indicated strains is more complex, and at least two perpendicular strain gages are necessary to define the stress picture. In case of two perpendicular strain gages, the following equation (Reference 8) can be used to calculate the stresses in the direction of each gage (σ_1 in direction 1 and σ_2 in direction 2):

$$\sigma_1 = M\epsilon_1 + N\epsilon_2$$

$$\sigma_2 = M\epsilon_2 + N\epsilon_1$$

where

$$M = \frac{E}{1 - \nu^2}$$

$$N = \frac{E^2}{1 - \nu^2}.$$

When a number of perpendicular gages are used, the calculation of biaxial stresses is simplified if a computing table is made. Such a table (Tables V and VI), similar to that used by Battelle Memorial Institute for steel (Reference 4), was computed for aluminum (ν = .33 and E = 10,300,000 p.s.i.). An example of biaxial stress calculation for gages 17 (radial) and 18 (tangential) is given below. The photograph of recorded data for gages 17 and 18 is shown in Figure 31.

From Figure 31,

Gage 17 Strain = 6.4 marks
Gage 18 Strain = 3.4 marks

From the calibration procedure section,

Calibration for 0.1-in. mark on chart

$$= 400 \text{ p.s.i.}$$

$$= 38.8\ \mu\frac{\text{in.}}{\text{in.}}.$$

Actual strain of gage 17 in radial direction is

$$\epsilon_1 = -6.4 \times 38.8$$

$$= -248\ \mu\frac{\text{in.}}{\text{in.}}.$$

TABLE V
TABLE FOR COMPUTING BIAXIAL STRESS FOR ALUMINUM -
TABLE OF $M\epsilon$

Strain Index in./in. x 10^{-6}	in./in. x 10^{-6}									
	0	1	2	3	4	5	6	7	8	9
	Stress Index (pounds per square inch)									
0	0	12	23	35	46	58	69	81	92	103
10	116	127	139	150	162	173	185	196	208	220
20	231	243	254	266	277	289	300	312	324	335
30	347	358	370	381	393	405	416	428	439	450
40	462	474	485	497	509	520	532	543	555	566
50	580	589	601	613	624	636	647	659	670	682
60	694	705	717	728	740	751	763	774	786	797
70	809	821	832	844	855	867	878	880	902	913
80	925	936	948	959	971	982	994	1006	1017	1025
90	1030	1052	1063	1075	1086	1098	1110	1121	1133	1144

TABLE VI
TABLE FOR COMPUTING BIAXIAL STRESS FOR ALUMINUM -
TABLE OF $N\epsilon$

Strain Index in./in. $\times 10^{-6}$	in./in. $\times 10^{-6}$									
	0	1	2	3	4	5	6	7	8	9
	Stress Index (pounds per square inch)									
0	0	4	8	11	15	19	23	27	30	34
10	38	42	46	50	53	57	61	65	69	72
20	76	80	84	88	92	95	99	103	107	111
30	114	118	122	126	130	134	137	141	145	149
40	153	156	160	164	168	172	175	179	183	188
50	191	194	198	202	206	210	214	217	221	223
60	229	233	236	240	244	248	252	256	259	263
70	267	271	275	278	282	286	290	294	298	302
80	305	309	313	317	320	324	328	332	336	339
90	343	347	351	355	359	362	366	370	374	378

Actual strain of gage 18 in tangential direction is

$$\epsilon_2 = 3.4 \times 38.8$$

$$= 132\ \mu\ \frac{\text{in.}}{\text{in.}}.$$

From Tables V and VI (interpolated for the last digit),

for $\epsilon_1 = -248$

$\epsilon_2 = 132,$

one finds

$$M\epsilon_1 = -2870 \qquad M\epsilon_2 = 1520$$

$$N\epsilon_2 = 510 \qquad N\epsilon_1 = -940.$$

Actual biaxial stress in radial direction is

$$\sigma_1 = M\epsilon_1 + N\epsilon_2$$

$$= -2,870 + 510$$

$$= -2,360 \text{ p.s.i.}$$

Actual biaxial stress in tangential direction is

$$\sigma_2 = M\epsilon_2 + N\epsilon_1$$

$$= 1,520 - 940$$

$$= 580 \text{ p.s.i.}$$

The actual running speeds were 1,194 r.p.m. for gage 17 and 1,198 r.p.m. for gage 18. The above stresses were not corrected for exact speed of 1,180 because the difference is less than 3 percent and the strain traces cannot be read that accurately.

PROOF TESTING

After completion of the strain gage testing, the wheel was cleaned up and dynamically balanced. It was found, after cleaning the wheel, that full-speed 1,180-r.p.m. dynamic balancing was required since double amplitude of vibration was approximately 3 mils at 1,180 r.p.m. After

permanent weights were added, the wheel was run up and held at 1,468 r.p.m. for 3.5 minutes; it was then run up to 1,468 r.p.m. and a strain gage reading of gage 17 was taken. The uniaxial stress for this reading is given on the bottom of Table VII. After proof testing, the wheel was visually inspected and no damage was found.

SOUND-EXCITED VIBRATION TESTING

The equipment used in sound-excited vibration analysis is shown in Figure 32 and in a schematic drawing, Figure 33. The equipment shown in the above figures works as follows: A random noise generator (loudspeaker) beams a "Pink Noise" on the structure. The "Pink Noise" is a random noise with frequencies within a range of 35 to 10,000 cycles per second with equal sound power level per octave. This random frequency noise excitation causes the structure to vibrate in all of its possible modes of vibration. The vibration sensing element, shown attached to the diffuser in Figure 32, is an accelerometer, Endevco Series 2000, Model A 2213. The accelerometer transduces these vibrations into an electrical signal of complex wave form, which is amplified and analyzed on a wave analyzer and recorded on a graphic chart. The chart is nondimensional as to amplitude, and the inspection of this graphic chart indicates predominant peak frequencies. For more details about sound-excited vibration testing, see Reference 7.

Using the above equipment, graphic vibration recordings were made of different parts of the wheel. The recordings were taken with the accelerometer on different parts of the impeller blade inducer, the top of the blade, the inlet cylinder and the front and back diffusers. An attempt was also made to locate the nodal pattern of the front diffuser excited with an exciting frequency of 70 cycles per second. This was done in the following manner: A yardstick with the end taped with electrical tape was moved around the periphery of the diffuser, and the vibration trace was observed on the oscilloscope. Points at which the stick did not affect the oscilloscope trace were marked as nodes. These nodes are marked N with drafting tape and are shown in Figure 34.

Each of the parts of the impeller has its own resonant frequency. The frequencies of these parts are then forced on the other structural parts, which also have their own frequencies. Thus, a complicated structure, such as an RD-type impeller, has a large number of peak frequencies which are difficult to analyze. If the exciting frequencies to which the structure will be subjected are known, such as operating frequency and blade passing frequency, then each part of the structure can be excited with a random noise generator at these discrete frequencies. The part which has resonant frequency at the discrete frequencies used can thus be found, and its damping can be changed to alter its resonant frequency.

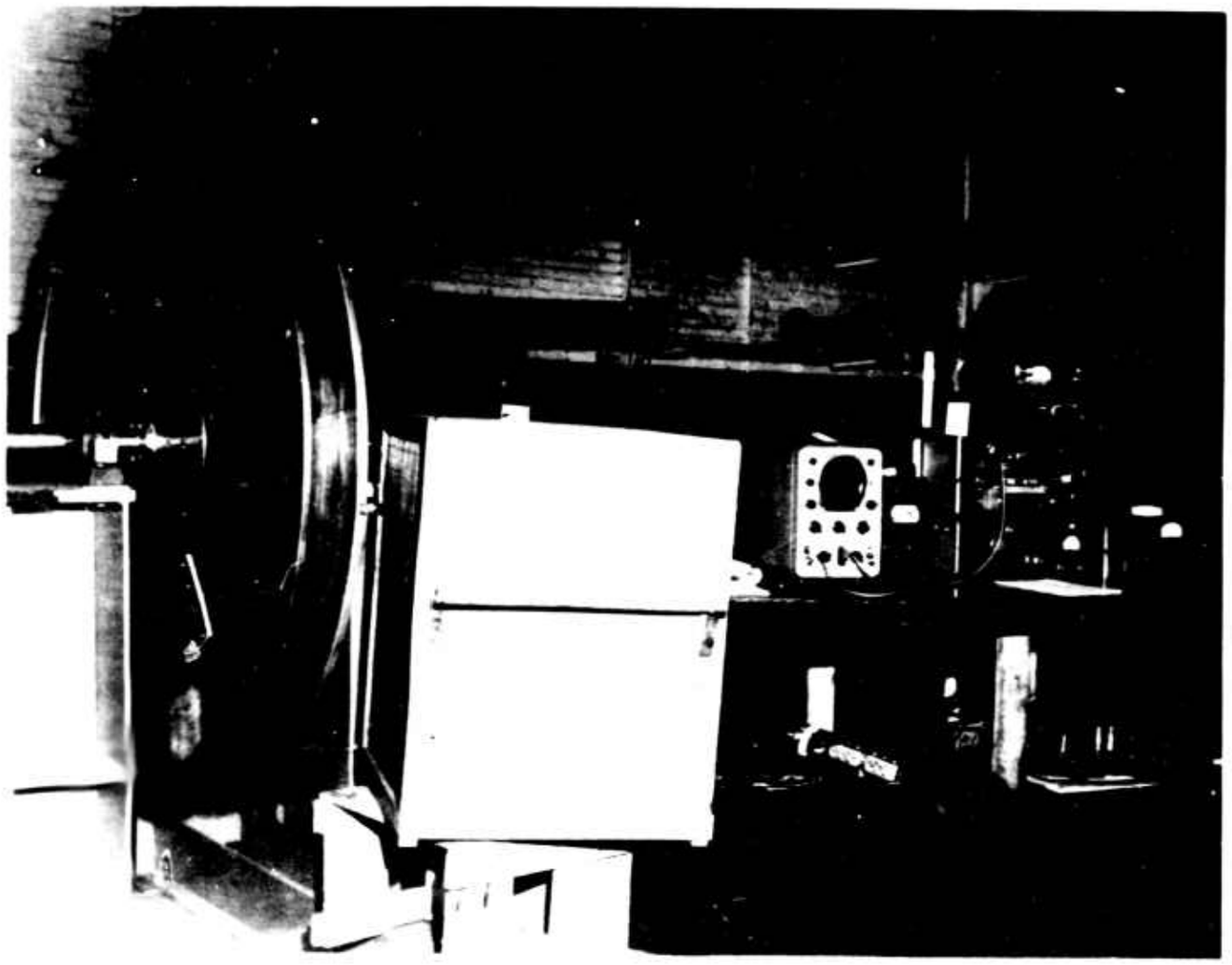

Figure 32. Sound-Excited Vibration Equipment.

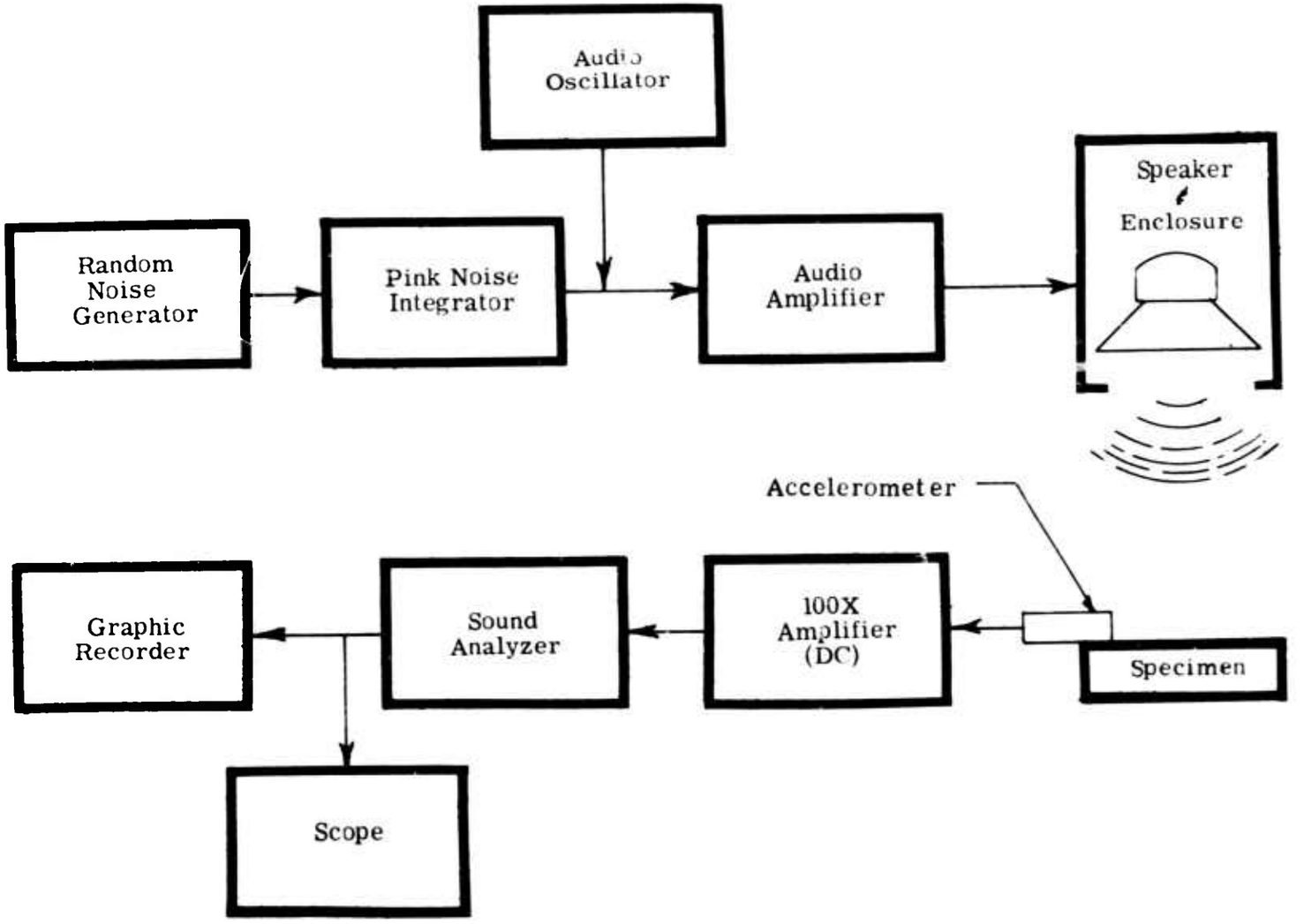

Figure 33. Schematic for Sound-Excited Vibration Analysis.

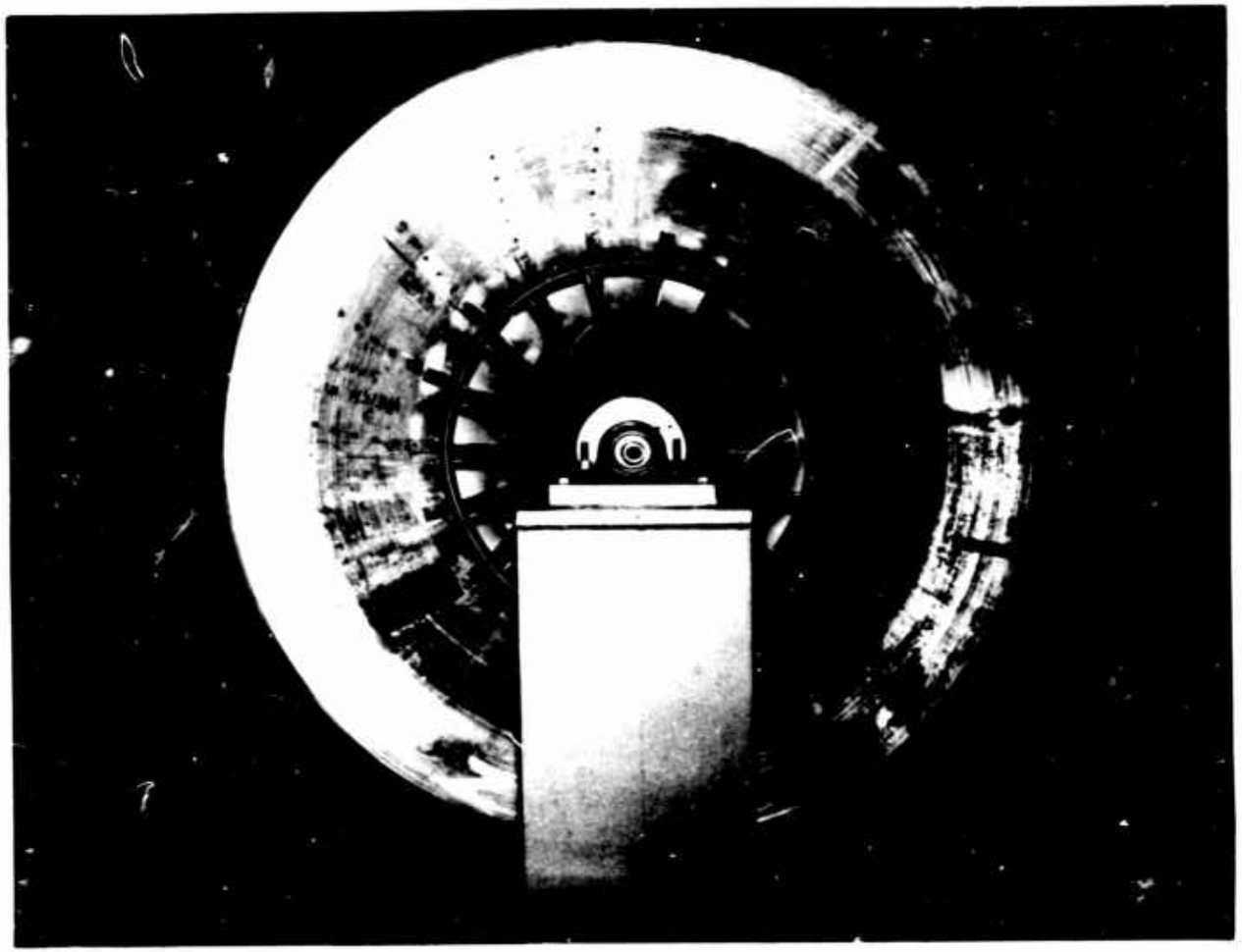

Figure 34. Nodal Pattern of Front Diffuser at 70-CPS Excitation.

RESULTS

The results for each type of test will be given next.

Balancing

Before the impeller was mounted on the shaft, it was statically balanced; 4 ounces of static weight were required. After the wheel was mounted on the dynamometer, it was dynamically balanced at 500 r.p.m. and checked at 700 r.p.m. The results are given in Table II. The impeller was finish balanced at 1,180 r.p.m. after completion of strain gage tests, and results are given in Table II.

Stresscoat Testing

From the calibration bars, the stresscoat sensitivity was found to be 9,000, 6,500 and 7,000 pounds per square inch for coatings 1204, 1205 and 1206, respectively. Sensitivity is defined as the minimum stress required to produce first crack in the coating. The impeller was run at seven speeds (300, 500, 700, 900, 1,150, 1,350 and 1,450 r.p.m.), and the impeller was checked for cracks after each run. Cracks were found at 500- and 700-r.p.m. runs on the edge of the inlet cylinder, the top screw of one blade and a balancing weight. These cracks did not propagate at higher speeds. No crack patterns were obtained on any of the three coatings at the proof speed of 1,450 r.p.m. The coatings were dy-checked after the 1,450-r.p.m. run to find closed-up cracks, but none were found.

Strain Gage Testing

The strain gage test results are given in Table VII, and strain gage locations are given in Figure 26. The eccentric weight technique calibration run results are given in Table IV. The air load results for gages 17 and 18 at 728 r.p.m. are given on the bottom of Table VI. The uniaxial stress for gage 17 at 1,486 r.p.m. is also given on the bottom of Table VI.

From Table VI, it is seen that the highest stress at 1,180 r.p.m. is the radial stress at the base of the back diffuser -- gage 19, 3,690 p.s.i. The highest tangential stress is near the rim of the front diffuser -- gage 21, 2,800 p.s.i. To calculate biaxial stress of gage 6, the tangential stress of gage 8 was used.

The calibration using the synthetic strain technique was 2.5 inches = 10,000 p.s.i. It was checked using cantilever beam method, which gave calibration of 2.5 inches = 10,300 p.s.i. The calibration using the eccentric weight technique deviated from actual stress from -2.45 to + 7.45 percent.

TABLE VII
IMPELLER STRESS LEVEL DATA
(POUNDS PER SQUARE INCH
AT 1,180 R. P. M.)

Gage No.	Radial (Meridional)	Tangential (Hoop)	Notes
1	0	-	-
2	-	810	-
3	640	-	-
4	-	1340	-
5	-	1400	Uniaxial
6	2980	-	-
7	2760	-	-
8	-	2310	-
9	480	-	Uniaxial
10	-	0 (Axial)	Uniaxial
11	-	1000	Uniaxial
12	1380	-	-
13	-	1720	-
14	2080	-	-
15	-	2040	-
16	-	1040	Uniaxial
17	-2360	-	-
18	-	580	-
19	3690	-	-
20	-	2210	-
21	-	2280	Uniaxial
17R	-4200	-	Uniaxial @ 1486 r.p.m.
17R	870	-	728 r.p.m.
18T	-	270	728 r.p.m.
17R	910 ± 310	-	Air Load 728 r.p.m.
18T	-	250 ± 110	Air Load 728 r.p.m.

Proof Testing

The impeller was run at a proof speed of 125 percent above operating speed for 3.5 minutes. Visual inspection of the impeller revealed no damage.

Sound-Excited Vibration Testing

The results of the vibration testing are given in graphic recordings which are not included in this report. There are two recordings for each diffuser, three for each blade inducer, one for the top of the blade and one for the inlet cylinder. The locations of the accelerometer for the above recordings are marked on each recording. The frequencies of the peaks of the graphic recordings are given in Tables VIII and IX. Tables VIII and IX are arranged to show the peak frequencies of graphic recordings as multiples of 32 and 36 cycles per second, respectively.

The nodal pattern of the front diffuser at 70-cycles-per-second excitation is shown in Figure 34. The nodes are marked N with drafting tape.

ANALYSIS OF RESULTS

The results will be analyzed following the same order as the results reported above.

Balancing

The good static balance (only 4 ounces required) indicates that the impeller is accurately made and that its center of gravity is close to the centerline of the impeller.

The final dynamic balance (see Table II) indicates that the impeller on its test setup is well balanced at 1,180 r.p.m. If the T. C. Rathbone curves, Figure 25, are used as criteria, then the final balance is "very smooth".

Stresscoat Testing

The cracks that appeared during the 500- and 700-r.p.m. runs can be attributed to stress concentrations, which were relieved by centrifugal load. These cracks failed to propagate at higher speeds and were not found in the same locations on symmetrical portions of the impeller. Cracks on the inlet cylinder edge were probably caused by putting on the inlet cover after the impeller was stresscoated. The run at 1,450 r.p.m. (the design proof speed of the impeller) showed that the stresses in stresscoated areas, with the exception of stress concentration areas, were below 6,500 p.s.i. The only good stress concentration area was near the top screw of one of the blades which

TABLE VIII
VIBRATION FREQUENCIES OF RD IMPELLER PARTS
(MULTIPLES OF 32)

	Freq. c.p.s.	Front Diff.	Front Diff. Over Blade	Back Diff.	Back Diff. Over Blade	Top of Blade	Inlet Cyl.	Top of Inducer	Bottom of Inducer	Middle of Inducer
1	32	31	32	-	31	-	-	-	31	-
2	64	-	-	64	66	-	-	-	-	-
3	96	100	96	84	100	-	-	-	-	-
4	128	120	125	128	130	-	130	130	130	130
5	160	-	-	-	-	150	-	-	-	-
6	192	-	-	195	195	-	-	-	-	-
7	224	-	210	-	-	-	-	-	-	-
8	256	-	-	266	-	-	-	-	-	-
9	288	275	-	-	-	-	-	-	-	-
10	320	-	305	-	325	-	325	320	320	320
11	352	-	-	340	-	340	-	-	-	-
12	384	-	-	-	-	-	-	-	-	-
13	416	-	-	-	-	-	-	-	-	-
14	448	-	440	-	-	-	440	-	440	-
15	480	490	-	-	-	-	-	490	-	-
16	512	-	-	-	-	-	-	-	-	-
17	544	-	-	-	-	-	540	-	-	-
18	576	-	-	-	-	-	-	-	-	-
19	608	610	-	-	605	-	-	-	-	-
20	640	-	640	-	-	-	-	-	640	-
21	672	-	-	-	-	-	-	-	-	-
22	704	-	-	-	-	-	-	-	-	-
23	736	-	740	-	-	-	-	-	-	-
24	763	-	-	-	-	-	-	-	-	-

TABLE IX
VIBRATION FREQUENCIES OF RD IMPELLER PARTS
(MULTIPLES OF 36)

	Freq. c.p.s.	Front Diff.	Front Diff. Over Blade	Back Diff.	Back Diff. Over Blade	Top of Blade	Inlet Cyl.	Top of Inducer	Bottom of Inducer	Middle of Inducer
1	36	36	36	36	36	-	-	-	36	38
2	72	70	68	74	74	-	-	71	-	-
3	108	-	-	-	-	-	-	-	-	-
4	144	150	-	-	-	150	-	-	-	-
5	180	-	-	-	-	-	-	-	-	-
6	216	210	210	-	-	-	-	-	-	-
7	252	-	-	-	-	-	-	-	-	-
8	288	275	-	-	-	-	-	-	-	-
9	324	-	-	-	325	-	325	320	320	330
10	360	-	-	-	-	-	-	-	-	-
11	396	-	-	-	400	-	-	-	-	400
12	432	-	-	440	-	-	440	-	-	-
13	468	-	-	-	-	-	-	-	-	-
14	504	-	-	500	-	-	-	-	500	-
15	540	-	-	-	-	-	540	-	-	-
16	576	-	-	-	-	-	-	-	-	-
16	612	610	-	-	610	-	-	-	-	-
18	648	-	-	-	-	-	-	-	640	-
19	684	-	-	-	-	-	-	-	-	-
20	720	-	-	-	-	-	-	-	-	-
21	756	-	-	-	-	-	-	-	-	-
22	792	-	-	-	-	-	-	-	-	780
23	828	-	-	-	-	-	-	-	-	-
24	864	-	-	-	-	870	-	-	-	-

stress-relieved itself after the 700-r.p.m. run. The main purpose of the stresscoat testing was to find stress concentration areas in which to locate strain gages. The stresscoat results at 1,450 r.p.m., however, were not sufficient to locate the strain gages properly.

Strain Gage Testing

The strain gage tests gave the stress levels (Table VII) of different impeller locations (Figure 25) where the stress levels were highest.

The results indicate that the highest stress levels in the wheel are at the diffuser base. The back diffuser had higher stress levels, 3,690 p.s.i. radial and 2,210 p.s.i. tangential, than the front diffuser, 2,980 p.s.i. radial and 2,310 p.s.i. tangential. Since, from experience, the industrial RD impellers have highest stress levels at the front diffuser base, the lightweight RD wheel should also have highest stress levels at the front diffuser base. The difference in stress levels is probably due to a failure to locate the strain gages at the exact point of maximum curvature of the front diffuser base. The tangential stress of 2,800 p.s.i. near the diffuser rim is much higher than expected and is probably due to the formed cylindrical flange on the top of the diffuser. The stress levels of the impeller are well below the yield strength of 40,000 p.s.i. and the fatigue strength of 14,000 p.s.i. of the 6061 T-6 aluminum alloy from which most of the wheel was fabricated (Reference 3). The material property of primary interest in rotating structures is the fatigue strength of the material, since some parts of the wheel are subjected to stress reversals. Since the stress levels at all tested locations are well below the fatigue limit of the material, the impeller is adequate from a stress standpoint.

The expected accuracy of the above strain gage results should be within ± 7 percent, since the maximum deviation using eccentric weight calibration technique was -2.45 to + 7.45 percent. The higher stress level values should be more accurate, as can be seen from the calibration data in Table IV.

Proof Testing

Since there were no structural failures during proof testing of the impeller for 3.5 minutes at 1,468 r.p.m., or at 125 percent overspeed, the impeller is adequate for operation at 1,180 r.p.m.

Sound-Excited Vibration Testing

From Table VIII and the graphic plots, it is seen that the peak frequencies common to most parts of the impeller are 128 and 320 cycles per second. Therefore, the impeller should not be subjected to continuous excitation at the above frequencies. The front diffuser is

probably the most sensitive part of the impeller, as far as vibration is concerned, and an attempt should be made not to excite the diffuser with any of the peak frequencies on the front diffuser graphic plot. If the number of front diffuser peak frequencies of the lightweight RD impeller is compared with the industrial RD impeller with thicker structural parts, such as the Steel RD 56-50, it is seen that the lightweight impeller has a larger number of peak frequencies in the low frequency range (30 to 250 cycles per second). Typical peak frequency comparison would be 160, 290, and 780 cycles per second for the RD 56-50 impeller and 32, 68, 96, 125, 210, 305, and 560 cycles per second for the lightweight RD impeller. Thus, it appears that reduction in section modulus of the wheel structural parts increases peak resonant frequencies, and thus vibration problems.

From Table VIII, it can be seen that most of the peak frequencies are multiples of either 32 or 36 cycles per second. A good explanation for this occurrence is not apparent.

From the analyses of the above tests, it can be concluded that the wheel tested is adequate for operation at its design speed of 1,180 r.p.m., provided it is not subjected to exciting frequencies which coincide with resonant frequencies of its parts. Particular care should be taken not to excite diffusers and blade inducers at their resonant frequencies.

A standard practice for industrial RD impellers is to vibration test them to obtain graphic plots and then to stiffen them if any of the predominant peak frequencies fall close to operating and blade passing frequencies.

SECTION V

COMPARISON OF CALCULATED AND MEASURED STRESS LEVELS

PRESENTATION OF DATA

Calculated stresses obtained from the computer analysis discussed in Section I of this report for fan RD 51-.50-1.3-75°, shown in Figures 6, 7, and 8, are tabulated in Appendix V for Run 44 and Appendix VI for Run 41. As discussed in Section III, Run 44 better represents the fan configuration which was built and tested than Run 41. In this section, the results of Run 44 (Appendix V) will be used, except as noted. The reader is also reminded that the ray or station locations for Run 44 are shown on Figure 8, page 33. Figure 8 is a scaled reduction of the corresponding full-scale drawing and the scale factor is 1 : 3.195. The ray locations for Run 41 can be laid out from the values of the angle θ given in Appendix VI.

Measured stresses, obtained by means of dynamic strain gage readings on the same RD 51-.50-1.3-75° fan, are discussed in Section IV. The location of the 21 strain gages is shown both in Table II and in Figure 26. It is better not to scale Figure 26, but to use the dimensions shown in Table II to locate the strain gages. The measured stresses for the 21 strain gages are tabulated in Table VI.

Consideration was given to a graphical presentation of the results, plotting radial and tangential stresses against radius for both hub and shroud, as well as plotting tensile and shear stresses against radius for the blades. This can be done very simply, since these stresses are tabulated against the radius in Appendixes V and VI. It was felt, however, that a discussion based on tabulated data would be clearer. These data are presented in Table X. Results from the 21 strain gage readings will be discussed successively, in three categories: first, those for which perfect agreement between theory and experiment was found; second, those for which a disagreement was found but an obvious explanation can be offered; third, those for which there is poor agreement, which may reflect on the validity of the analysis.

TABLE X
COMPARISON OF CALCULATED AND
MEASURED STRESS LEVELS (RAW DATA)

Gage Number (Figure 26 and Table III)	Measured Value, pounds (Table VII, p. 88)	Calculated Value, pounds (Appendix V)	
		Run 44	Run 41
1	0	0	
2	810	818	
3	640 (radial component is 218)	96	
4	1340	1624	
5	1400	1818	
6	2980		
7	2760	1392	3889
8	2310	1490	1509
9	480	1024	
10	0	255	
11	1000	2771	
12	1380	1400	
13	1720	1700	
14	2080	2135	
15	2040	1400	
16	1040	818	
17	- 2360	- 1392	- 3889
18	580	Not available	
19	3690	2135	2343
20	2210	1452	1491
21	2280	1200	1200

COMPARISON OF DATA (TABLE X)

Perfect Agreement

Gage 1: The theory assumes no axial stress. This is the cylindrical part of the shroud, where one would expect this hypothesis to be well verified. Indeed, one finds that the stress reading is zero.

Gage 2: The tangential (hoop) stress is calculated to be 818 p.s.i. (Station 3 for the shroud) and is measured to be 810 p.s.i., showing excellent agreement.

Gage 16: The theory on which the computer program is based (the original Stodola method) predicts a sharp increase in hoop stress at the shroud inlet as one moves from the outside to the inside of the shroud (see in Appendix V that the tangential stress at Station 3 of the shroud, which corresponds to a radius of 13.591 inches, is 818 p.s.i., while the tangential stress at Station 2, which corresponds to a radius of 13.590 inches, is 3,050 p.s.i.). It is well shown that this stress rise is due to an idiosyncrasy of the analysis, but does not really take place. In order to verify this, gage 16 was placed at the same station as gage 2, inside rather than outside the shroud. A reading of 1,040 p.s.i. confirms that the stress rise of the program does not take place in reality.

Gages 12 and 13: Gages 12 and 13 are the most significant gages for the whole stress correlation program, since they correspond to a condition in which the meridional stress is radial, the axial stress is zero as postulated in the analysis and the hub cross section is uniform. As shown in Table X, the measured radial stress (gage 12) is 1,380 p.s.i., and the calculated one is 1,400 p.s.i.; the measured hoop stress is 1,700 p.s.i., and the calculated one is 1,000 p.s.i.

In view of the fact that hub and shroud stresses are interdependent in the analysis of Section I, one is led to conclude from the agreement between calculated and measured stresses both on the hub and the shroud at more than one station that the analytical method is essentially quantitatively correct. Such agreement as shown above cannot be coincidental.

Qualified Agreement

Gages 3, 4 and 5: Gages 3, 4 and 5 were placed on the outside of the shroud, in regions where the shroud meridional curvature (making it a conical rather than a cylindrical surface) is quite pronounced. Gage 3 is a meridional gage. Therefore, it has both an axial and a radial component. It is not possible physically to measure the radial component alone; actually, that component is quite small, being calculated in Appendix V to be 96 p.s.i. To satisfy the assumptions of the analysis

of no axial stress, the measured meridional stress should be zero. It is seen in Table X that its value is 640 p.s.i. Therefore, the Deutsch analysis does not strictly hold in regions of large shroud curvature change. This is a relatively secondary effect, as can be seen from the fact that the measured hoop stresses for gages 4 and 5 (1,340 p.s.i. and 1,400 p.s.i.) do not differ by more than 20 to 25 percent from the calculated ones (1,624 p.s.i. and 1,818 p.s.i., respectively). However, an shown later, these three-dimensional effects can be accounted for in an extension of the Deutsch theory.

Gage 11: What appears to be a large discrepancy (1,000 p.s.i. measured hoop stress against 2,771 p.s.i. calculated stress) can be explained very simply. First, the reason that a gage had been placed there was the existence of local stress concentrations shown at low r.p.m. with the stresscoat paint (as explained in Section IV, these stress concentrations relieved themselves at design r.p.m.). This is a very unlikely location for a strain gage, since the strain gage was mounted on the machined hub disc, not on the backplate, to which there was no access after the fan had been assembled. What happened obviously was that the centrifugal load chose to travel through the backplate rather than through the hub disc. Thus, the stress distribution through a hub cross section at the gage-11 location must have been very nonuniform. This could be verified by glueing a strain gage on the inside of the backplate. This was not done, since it would have necessitated a complete disassembly of the fan in the shop.

Disagreement

Gages 9 and 10: After the test program was under way, it was realized belatedly that it was a mistake to install the strain gages after fan assembly. It would have been much easier to install them on the fan components, for example the blades, before the assembly. In particular, it turned out to be practically impossible to instrument the upper part of the hub and the blades. A total of only two strain gages was put on the blades, as shown on Figure 26, and even those were hard to install. The results of Table X show a discrepancy between measured value (480 p.s.i.) and calculated value (1,024 p.s.i.) of tensile stress of the order of a factor of two. As to shear stresses, they are 0 and 255 p.s.i., respectively. This means that the blades carry less load than calculated. This is certainly conservative, but no explanation for it will be advanced, as it is futile to try to speculate from such a small number of measurements.

Gages 6, 7, 8, 14, 15, 17, 18, 19 and 20: Except for the general validation of the Deutsch analysis, the most important results of the experimental stress determination were concerned with a determination of the stresses at the base of the diffuser (Station 13); at that particular point the Deutsch analysis, as applied in Run 44, was found to be faulty. Therefore, this deserves to be discussed at some length.

It was recognized in Section I (page 7) that the basic Deutsch centrifugal analysis did not account for the bending stress imposed upon both shroud

and hub discs because of the conical shape of the diffuser (β = 4.24 degrees for the present fan). It was proposed to represent this effect by considering the diffuser section of the wheel as a circular plate with a hole of uniform radial and axial thickness having its inner edge fixed and having a uniformly distributed load applied. The corresponding radial bending stress, to be added to the radial bending stress found in the normal Deutsch analysis, is given on page 7. It is assumed that the additional tangential stress due to this effect is zero.

During the first series of stress runs, in December 1965, gages 6, 7, 8, 14 and 15 were installed. All were nominally at Station 13. The first results were inconsistent; this was attributed to errors on the strain gage locations and errors in readings. Finally, the radial stress for gage 6 was found to be 2,980 p.s.i. and that for gage 7, 2,760 p.s.i. Gage 6 was near a blade; gage 7 was halfway between blades. It made sense that the stress near the blade should be larger than the other, because of blade restraint. Now, the results of the readings of gages 7 (radial stress) and 8 (hoop stress) did not agree well with the calculated results of Run 44: 2,760 p.s.i. against 1,392 p.s.i. (radial); 2,310 p.s.i. against 1,490 p.s.i. (hoop). What was still more surprising was that the results of Run 41 were far different from those of Run 44 for radial stresses: 3,889 p.s.i. against 1,390 p.s.i. The measured radial stress was just halfway between the calculated stresses for Runs 41 and 44. This definitely must be considered coincidental. Hoop stresses for Runs 41 and 44 were the same: 1,509 p.s.i. against 1,490 p.s.i. Thus, for shroud stresses at Station 13, the base of the diffuser, two facts were apparent: first, the calculated additional radial stress was much too low (according to run 44) or much too high (according to run 41); second, there was a definite additional tangential stress due to conicity which was not accounted for in the theory.

Gages 14 and 15 gave the corresponding values for radial and hoop stresses at Station 13 for the hub. The measured value for radial stress was 2,080 p.s.i., against 2,135 p.s.i. calculated; for hoop stress, it was 2,040 p.s.i. against 1,400 p.s.i. From this, one can draw three conclusions. First, there is reasonable agreement between theory and experiment for radial stress; however, this turned out to be coincidental, since gages 14 and 15 had mistakenly been placed between Stations 13 and 14, rather than exactly at Station 13. Second, calculated hoop stresses are too low, as in the case of the shroud. Third, hub stresses at Station 13 are lower than shroud stresses, this being explained by the fact that the inner shroud disc exerts more restraint on the diffuser section than the inner hub disc. Unfortunately, this was disproved by further testing.

After these results were obtained, it was decided to use the remaining strain gages around Station 13 in an attempt to clarify the situation described above. Additional gages 17, 18, 19 and 20 were therefore

installed. Gages 17 and 18 were installed on the inside of the shroud, and it was confirmed that the tensile radial stress changed into a compression stress. Gages 19 and 20 were installed on the outside of the hub, exactly at Station 13. A radial stress of 3,690 p.s.i. and a hoop stress of 2,210 p.s.i. were found, thus confirming that the analysis definitely underestimated both radial and hoop stresses at the diffuser base.

Etablissements Neu, of Lille, Franch, has over the years established empirical formulas to calculate the additional stresses at the base of the diffuser due to diffuser conicity. These formulas were applied in the above case, but failed to provide satisfactory agreement (they also underestimated the magnitude of the additional stress). At least, these formulas recognize qualitatively the need for an additional hoop stress, as well as a radial one.

As the matter stood in January 1966, additional tests would have been required. They were not possible because of a lack of time and a shortage of strain gages. If a fan configuration similar to that tested in the present program is used, the stress levels of Table X can be used with great confidence. Pending a better analytical determination of the stresses at the base of the diffuser, each new fan of different design should be tested and strain gages should be monitored at the base of the diffuser, the stresses elsewhere being safely determined on the basis of the Deutsch theory.

Gage 21: The last gage was placed, in the tangential direction, as far out on the shroud diffuser as possible (where the radial stress is zero). As can be seen in Table X, the measured stress is 2,280 p.s.i. and the calculated one is 1,200 p.s.i. The reason for this discrepancy was understood, as a result of the investigations reported above. The difference is about 1,000 p.s.i., which is the magnitude of the hoop stress increment due to diffuser conicity; this hoop stress increment, in the present case, is approximately constant between Stations 13 and 15 (while the additional radial stress is expected to decrease linearly from its maximum value at Station 13 to zero at Station 15).

EVALUATION OF THE RESULTS

The analyses of this report, including the theoretical stress analysis, the design analysis, and the experimental stress determination, are of a pioneering nature, and the results are felt to be both encouraging and rewarding. The program had a double objective. First, the computer program was used as an analytical tool, a design guide, for "proportioning" a minimum-weight structure, as was explained in Section III. Second, it was meant to provide a quantitative assessment of the stress levels within the fan. The first objective was fully achieved. As was shown in the previous paragraph, the second objective was accomplished in general, except at the base of the diffuser.

Quantitative agreement was not perfect, and this was due to many factors which are worth recalling briefly. First, there were some

incertitudes about stress readings and the exact location of the strain gages (as pointed out in Section IV). Though the repeatability and reliability of these dynamic readings is remarkable, still better results could have been obtained with more time and more strain gages (about 40 more strain gages would have made possible a thorough job). Also, strain gages should be installed at the time of the fan assembly, not when the fan is mounted on the dynamometer; the strain gages should be electrically connected to a collector ring, and the wires should be imbedded within the structure.

Second, the Deutsch analysis can be improved in two respects. On the one hand, the additional stresses due to diffuser conicity must be represented better than they are now. On the other hand, in the regions where shroud curvature (of a meridional section) is appreciable, the assumption that the axial stress is zero does not hold well and can be removed as follows: consider station n-1, n and n + 1 and the corresponding mass elements. Consider the equilibrium of element n to which are applied the radial stresses of the neighboring elements, $\sigma_{r_{i-1}}$ and $\sigma_{r_{i+1}}$, respectively. Since in general $\sigma_{r_{i-1}}$ is different from $\sigma_{r_{i+1}}$, there results a net torque on element n, which can be represented as an annular disc. Known formulas allow one to calculate the axial stress σ_a needed to be applied on element n to balance this torque. One can thus find for each element an axial stress σ_a, which can be superimposed to the other stresses of the Deutsch analysis. This can easily be incorporated in the computer analysis.

In conclusion, the present results are quite encouraging, and there are no obstacles, with modest amounts of theoretical and experimental work, to a complete understanding of the stresses of RD fans.

SECTION VI

WEIGHT OF LIGHTWEIGHT RD IMPELLERS

GEM DESIGN STUDIES

The contract specified that at the end of the program two design studies would be made, with a view toward a determination of the weight per horsepower of RD fans installed as lift fans for air cushion vehicles. The configurations which were chosen for this exercise were a modified Navy/Bell Aerosystems SK-5 air cushion vehicle and a Navy landing craft air cushion vehicle. The main ground rules of the design studies will first be described. Fan weight estimates will be discussed in the next paragraph.

Modified Bell SK-5 ACV With RD Fan

The purpose of the exercise was to see if the Bell SK-5 vehicle could be retrofitted, with minimum changes, with an RD fan and what the advantages of the RD fan over the existing radial fan would be. The design criterion furnished to Aerophysics by Bell Aerosystems came from Table 1 of Section 04.09 of Saunders-Roe Division of Westland Aircraft Ltd. Report No. Structure N5/53 for the static hover condition. That condition called for 703 horsepower for the radial lift fan at 950 r.p.m. and 150 horsepower for the propeller fan at 1,998 r.p.m. Bell also gave Aerophysics a pressure-capacity curve for the radial fan at 900 r.p.m. The pressure-capacity curve at 950 r.p.m. was thus easily obtained, and an RD fan was designed to match the above condition. This resulted in the selection of fan RD 79-.84-1.3-75^{0}. This fan is slightly more bulky than the radial fan, 103 inches overall diameter against 83 inches, but it turns slower, 780 r.p.m. against 950 r.p.m. A drawing of the fan installed in the Bell SK-5 vehicle is shown in Figure 35. The RD fan can be installed with only very minor changes to the structure of the vehicle and a partial relocation of one of the fuel tanks.

Initially, some thought had been given to the redesign of the SK-5 entire duct system to optimize it in conjunction with the use of the RD fan. This was abandoned as being unpractical, since it would have involved drastic changes to the SK-5 vehicle.

It is interesting to note that there are great resemblances between the RD fan of the 84 series chosen here and the radial fan, but there are differences in size and r.p.m. as noted above. The efficiencies are nearly the same (the radial fan being slightly more efficient, with an efficiency of 84 percent at design point). As will be seen in the next paragraph, the weights are nearly the same. One worthwhile difference is that the RD fan is shown equipped with adjustable inlet vanes which permit a modulation of the flow which is not possible with the radial fan. To use the reduced space available, 24 vanes are shown. Their total weight is estimated to be around 75 pounds.

As the SK-5 ACV starts operating in an overloaded condition, the RD fan shows increased advantages over the radial fan. The radial fan operates best at cushion pressures under 50 p.s.f. The RD fan shows to advantage at cushion pressures above 50 p.s.f.

Landing Craft ACV With RD Fan

Starting from the thought that the RD fan would show well for ACV's with high cushion pressures (70 to 100 p.s.f.), design studies were made of a family of landing craft air cushion vehicles. High cushion pressures are required because of the need for efficient stowage aboard LSD's (Landing Ship Dock). Vehicles of several sizes were studied. A typical configuration is shown in Figure 36. This particular vehicle was sized so as to have approximately the same lift-propulsion system as the SK-5 vehicle. In other terms, what was investigaged here was a Skimmer 5 with the same gas turbine-lift fan-propeller configuration, a reduced planform area (and a corresponding increased cushion pressure), and a full plenum chamber configuration.

It turns out that this configuration is very attractive in general, but not in the size shown in Figure 36. The cushion area is 285 square feet; assuming a cushion pressure of 100 p.s.f., this means a lifting capability of 28,500 pounds and hence, a payload of the order of 15,000 pounds. With a cargo well of 7-x-14-ft. size, there is no space to accommodate a payload. The design of Figure 36 should therefore be looked upon as a concept, not a practical vehicle. This particular design would become practical again by reducing the cushion pressure and the power plant size to match a 14,000-pound gross weight.

A few words may be said about the fan installation of the vehicle of Figure 36, which is matched to a plenum chamber configuration. The plenum chamber is contained by a fully peripheral flexible skirt. The plenum pressure bubble is fed through two transverse horizontal air delivery ducts located in the stern section where the RD fan is. A system of circumferential cut-off vanes around the RD fan, not shown, directs the air to the right and left through these ducts and into the plenum. Inlet air is drawn into the inverted RD fan through a large bulkhead, with an opening facing the cargo hold area, thus minimizing ingestion of water spray. The skirted plenum chamber flexible walls extend high up the side of the craft to the level of the fan discharge area. The hard structural body of the craft is well down within the plenum chamber, yet not so low as to be near the depressed water surface under the pressure bubble. The nominal gap between the skirt and the water is assumed to be 1 inch. This prescribes the use of an RD fan of the 70 series (such as the one shown on Figure 9, page 35).

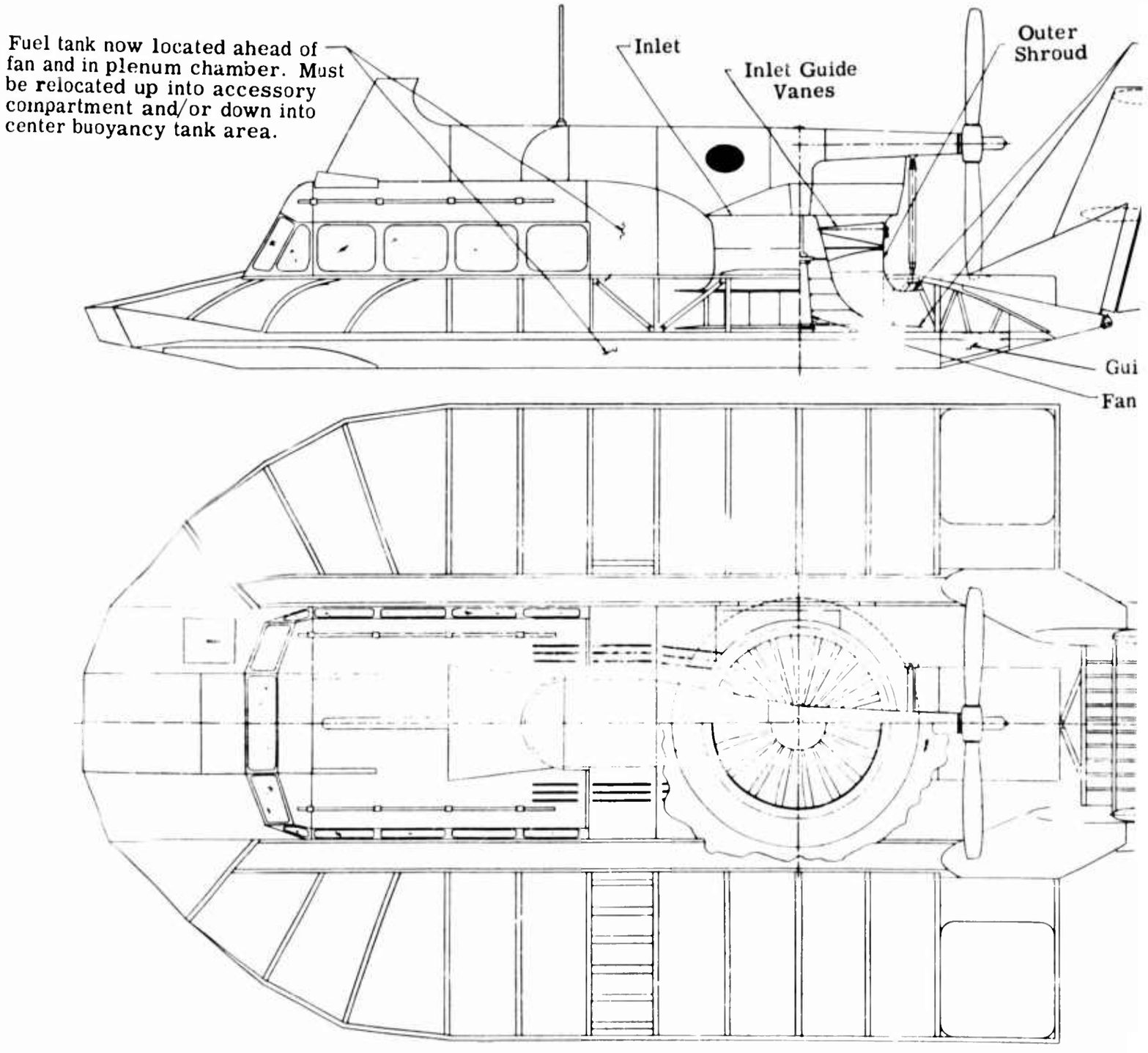

Figure 35. Design Study of Bell SK-5 Air Cushion Vehicle With RD Fan.

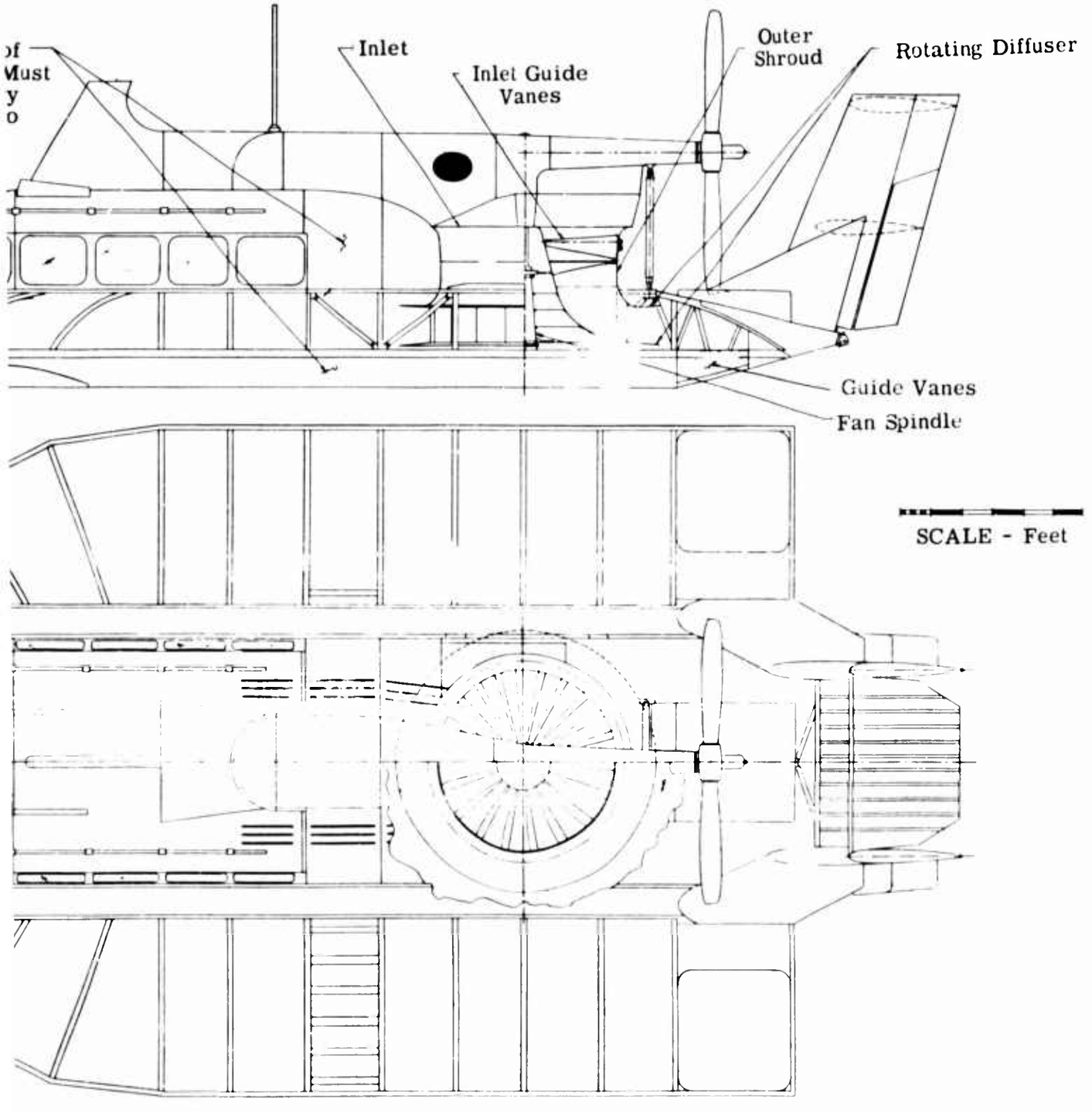

Figure 35. Design Study of Bell SK-5 Air Cushion Vehicle With RD Fan.

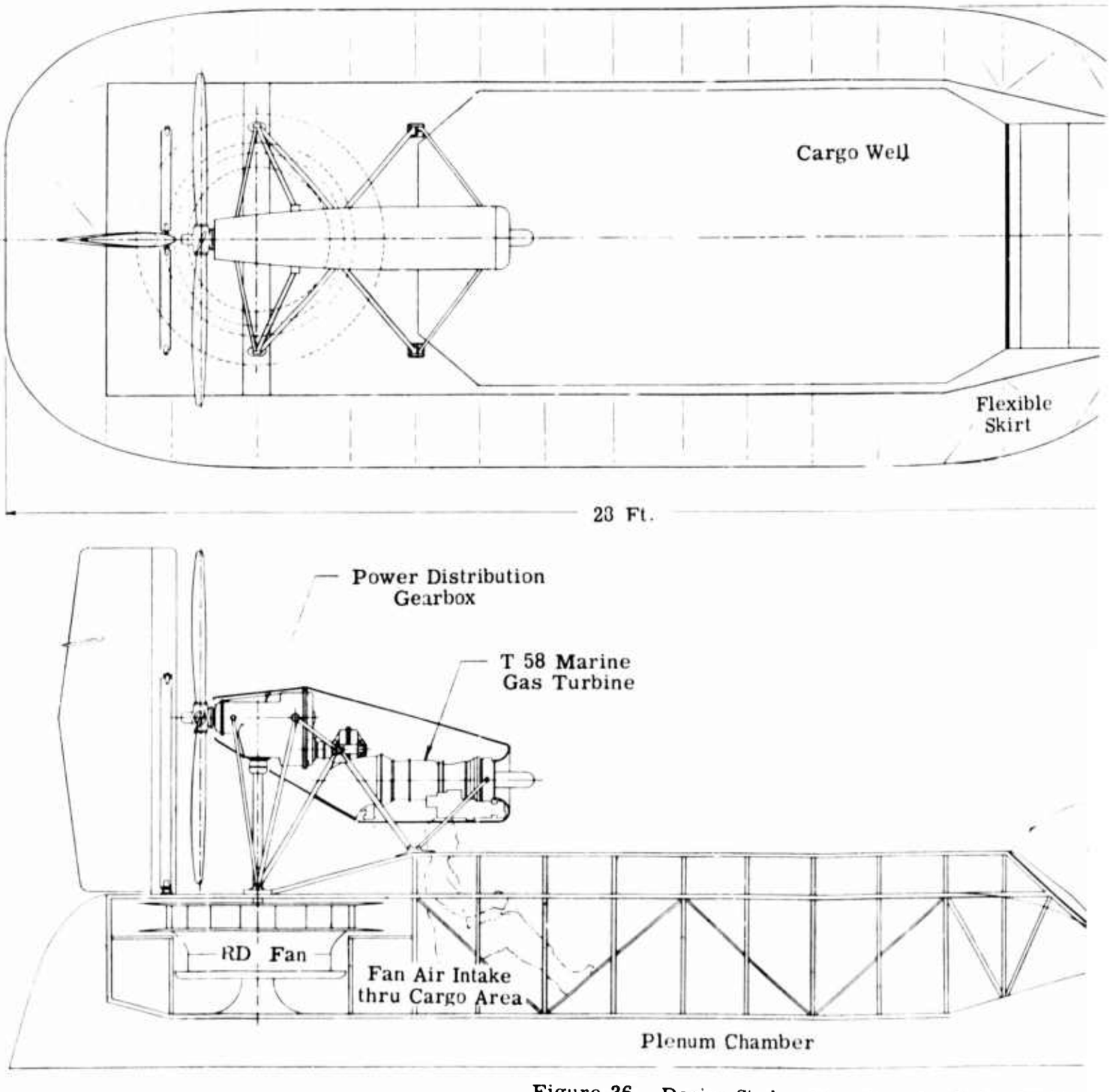

Figure 36. Design Study of Landing Craft Air Cushio

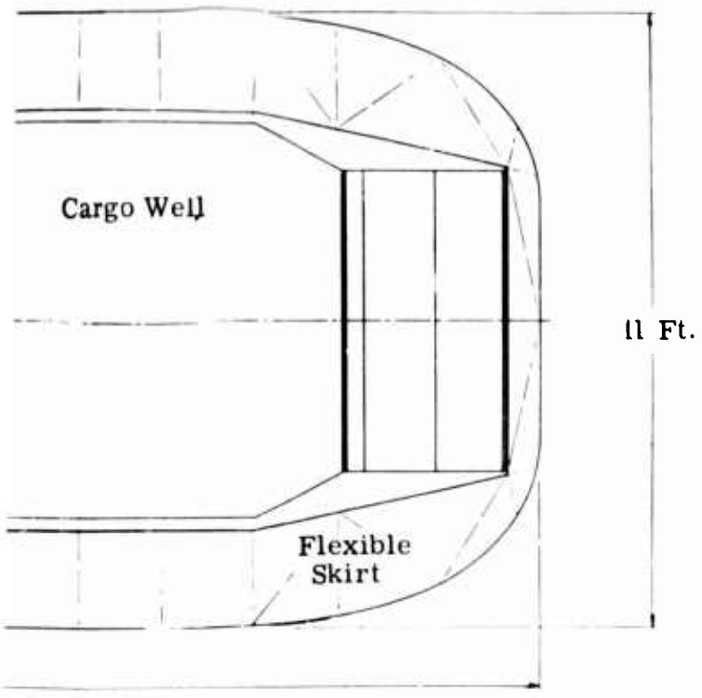

SCALE - Feet

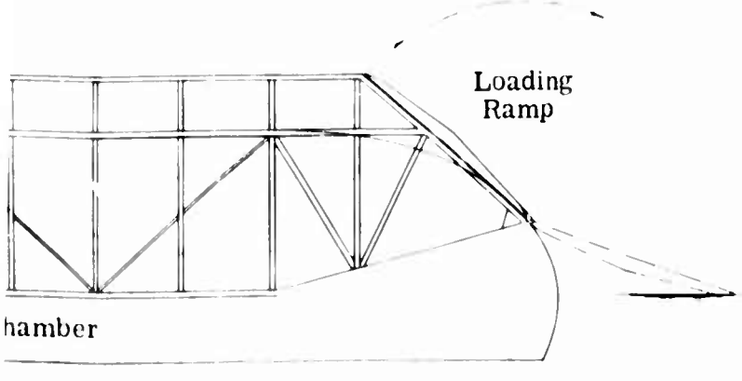

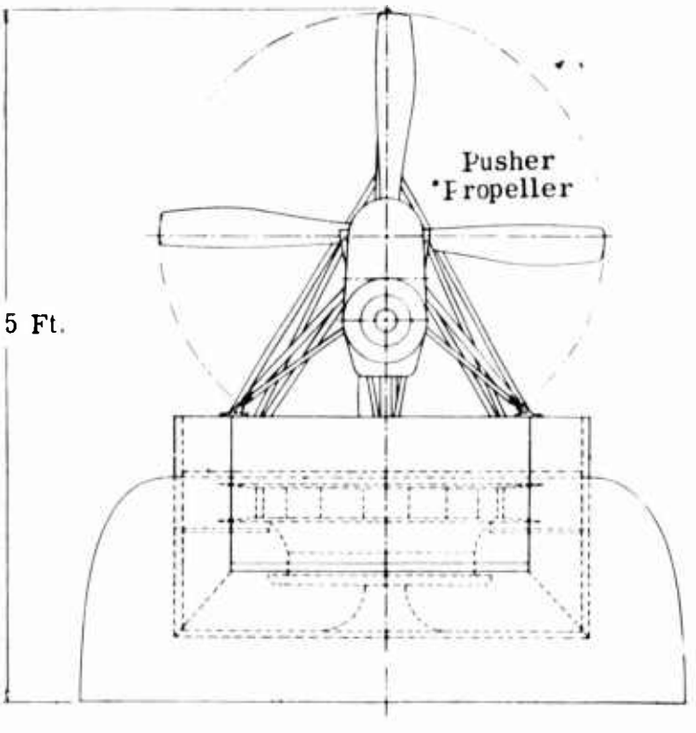

Study of Landing Craft Air Cushion Vehicle With RD Fan.

CONCLUSIONS CONCERNING WEIGHT OF RD IMPELLERS

The first conclusions to be drawn about the weight of RD impellers must logically concern the fan which was built under the contract: fan RD 51-.50-1.3-75°. A weight per horsepower depends critically upon which reference horsepower is being used. For the structural analysis of the fan as well as for the tests, the design r.p.m. was arbitrarily chosen as 1,180 r.p.m. Under these conditions, the strain gage results shown in Table X indicate that the maximum stress within the fan was a radial stress of 3,690 p.s.i. (gage 19). On the other hand, the maximum tensile yield stress for 6061-T4 aluminum sheet is 16,000 p.s.i. (see page 50). Even after assuming the ultimate stress to be 1.5 times the limit stress and designing conservatively for 125-percent overspeed, the margin of safety is nearly 1. This means that, at 1,180 r.p.m., the fan is designed overconservatively. Actually, the margin of safety is still positive at a design r.p.m. of 1,600. The radial stress of 3,690 p.s.i. now becomes 6,825 p.s.i., which is obviously conservative in comparison with a 16,000 p.s.i. allowable.

The design horsepower at 1,180 r.p.m. is 110 horsepower (Figure 4). Thus, at 1,600 r.p.m., it is $110 \times 1.36^3 = 277$ horsepower. The fan weight was found to be 137 pounds (Table I, page 55). The corresponding weight-to-horsepower ratio is therefore 0.5 pound per horsepower. This figure holds only if the fan is operated at a design speed of 1,600 r.p.m.; i.e., at a design fan pressure of 37-inch H_2O.

Such a fan pressure is higher than needed for most of today's air cushion vehicles. It is therefore of interest to calculate the weight per horsepower for RD fans operating at lower heads.

The calculations made for the RD 51-.50-1.3-75° fan were therefore repeated for the RD 51-.70-1.3-75° fan. This is a fan of the same overall diameter as the one which was built, but with a larger inlet area. It will be recalled that, originally, it had been a toss-up to choose which one of the two fans to build. The aerodynamic characteristics of fan RD 51-.70-1.3-75° are shown in Figure 5. The fan was laid out and stress analyzed (the input layout is shown in Figure 9), and the components were weighed. It was found that the weight per horsepower was again in the neighborhood of 0.5 pound per horsepower, but this time at a design r.p.m. of 1,400.

It is concluded that with the methods of fabrication described in this report, aluminum construction and hand fitting, an RD impeller can be built in the sizes corresponding to pressure rises between 15- and 30-inch H_2O and horsepower ratings between 100 and 1,000 for a weight of 0.5 pound per horsepower.

For example, the fan installed on the redesigned SK-5 of Figure 35 would weight 350 pounds (700 horsepower installed power). This is within 10

percent the same weight as that of the persent radial fan. The RD system is actually heavier because of the 75 pounds of inlet vanes. However, these permit a very nice flow control job, which is impossible with the radial fan.

It does not appear worthwhile to speculate about the weight of the ducting that goes along with a given air mover, for example, an RD fan. The advent of trunks has transformed most ACV's today into partial or total plenum chamber types. Even with most pure annular jet types, the trunk itself is an appreciable part of the ducting. It appears necessary to compare only the fans with one another.

CONCLUSIONS

1. A numerical method for the stress analysis of an indeterminate rotating diffuser fan structure was reduced to practice. The analysis was programmed for the IBM 1620 computer and could be run in a few minutes. This method was used as a tool for the analytical design of a minimum-weight RD fan. The fan thus designed was built and tested. The stress levels were established experimentally, using the strain gage technique.

This experiment in analytical design turned out very successfully: the fan which was built was both light and strong. No structural problems were encountered during the testing. A backup fan was built and did not have to be tested. No structural improvements to the fan need to be recommended.

2. A comparison of calculated and measured stress levels within the RD wheel indicates that the present analytical method gives satisfactory results, except at the base of the rotating diffuser and in the regions of large shroud curvature. An extension of the analysis to account for three-dimensional effects can be accomplished in a relatively straightforward fashion. Additional strain gage investigations, using more gages than were available for the present program, are desirable. The strain gages should be installed before fan assembly.

3. The method of fan fabrication used in this program is relatively expensive and time-consuming. It was determined that plastic fabrication of RD fans was both possible and practical, with approximately the same weight and strength characteristics as the aluminum fans, but with significant cost reduction. An R and D program of plastic fabrication techniques for large RD fans is strongly recommended.

REFERENCES

1. Advanced Balancing Techniques, International Research and Development Company, Worthington, Ohio, 1962, p. 7

2. Aerophysics Company, A Study of Radial-Flow Fans for GEM Propulsion System Applications, TRECOM Technical Report 64-33, U.S. Army Aviation Materiel Laboratories, Fort Eustis, Virginia, July 1964.

3. Alcoa Aluminum Handbook, published by Aluminum Company of America, Pittsburgh, Pennsylvania, 1962 Edition.

4. Crites, Nelson A., "Today's Strain Gages", Product Engineering, March 19, 1962.

5. Deutsch, E. J., "A Method of Stress Analysis for Shrouded Discs", Aerospace Engineering, Volume 21, Number 3, March 1962, pp. 24-30.

6. Joy Report X-327, Joy Manufacturing Company, New Philadelphia, Ohio, 1965.

7. Joy Report X-329, Joy Manufacturing Company, New Philadelphia, Ohio, 1965.

8. Perry, C. C., and Lissner, H. R., The Strain Gage Primer, Second Edition, McGraw-Hill Book Company, New York, 1962.

9. Roark, R. J., Formulas for Stress and Strain, McGraw-Hill Book Company, Inc., New York, 1954.

10. Smith, J.O. and Seely, F.B. Advanced Mechanics of Materials, 2d ed. John Wiley and Sons, Inc., New York, 1952.

APPENDIX I

FORTRAN LISTING, STRESS COMPUTER PROGRAM, SOURCE DECK I

```
      COMMON    C01(15),C02(15),C03(15),C04(15),C05(15),C06(15),C07(15)
      COMMON    C08(15),C09(15),C010(15),C011(15),C012(15),C013(15)
      COMMON    C014(15),C015(15),C016(15),C017(15),C018(15),C019(15)
      COMMON    C020(15),C021(15),C022(15),C023(15),C024(15),C025(15)
      COMMON    C026(15),C027(15),C028(15),C029(15),C030(15),C031(15)
      COMMON    C032(15),C033(15),C034(15),C035(15),C036(15),C038(15)
      COMMON    C039(15),C041(15),C043(15),C046(15),C049(15),C061(15)
      COMMON    C062(15),C063(15),C064(15),C065(15),C066(15),C067(15)
      COMMON    C068(15),C082(15),C083(15),C086(15),C087(15),C096(15)
      COMMON    C097(15),C099(15),C100(15),C103(15),C104(15)
      COMMON    C105(15),C108(15),C0561(15),DM2(15),DM3(15),DM4(15)
      COMMON    R00(15),R01(15),R02(15),R03(15),R04(15),R05(15)
      COMMON    R06(15),R07(15),R08(15),R09(15),R31(15),R32(15)
      COMMON    R33(15),R10(15),C058(15),C0311(15),C0331(15)
      COMMON    C060(15),C084(15),C085(15),C0601(15)
      COMMON    C0151(15),C0152(15)
  827 FORMAT (I3,2X,F6.2,2X,F6.2,2X,I3,4X,F4.0)
  828 FORMAT (F6.2,F6.2,F6.3,F6.2,F5.1)
  830 FORMAT (5X,F6.3,F6.3)
  282 READ 800
  800 FORMAT (40H                                          )
      READ 801
  801 FORMAT (40H                                          )
      READ 802
  802 FORMAT (40H                                          )
      READ 803,K0198,C0199,C0196,C0195,C0197
  803 FORMAT (I3,1X,F8.0,F7.0,4X,F5.2,5X,F3.0)
      READ 827,K0200,C0201,C0202,K0203,C0204
      READ 828,C0205,C0206,C0207,C0208,C0209
      DO 860 N=1, K0198
  860 READ 804,C07(N),C09(N),C05(N),C010(N),C011(N)
  804 FORMAT (5X,F7.3,F8.3,F8.3,F8.3,F6.3)
      DO 861 N=1,K0198
  861 READ 805,C06(N),C03(N),C02(N),C01(N),C08(N)
  805 FORMAT (5X,F7.3,F8.3,F8.3,F8.3,F6.0)
      DO 862 N=1,K0198
  862 READ 806,C04(N),C014(N),C017(N),C012(N),C013(N),C016(N),C015(N)
  806 FORMAT (5X,F4.0,F5.1,F6.1,F6.2,F6.2,F5.3,F6.3)
      DO 829 N=1,K0198
  829 READ 830,C0151(N),C0152(N)
      DO 526 N=1, K0198
      IF(C08(N))400,400,525
  400 IF(N-K0203)524,401,524
  401 C0220=C0204*C0205*C0207*(C0206+(C0208*C0209/57.296))*C0152(N)
      C0222=C0220/(6.283*C07(N)*C09(N)*(C07(N)-C07(N-1))*C015(N))
      C0223=C0220/(6.283*C05(N)*C010(N)*(C05(N)-C05(N-1))*C0151(N))
      C021(N)=C015(N)*(1.+C0222)
      C022(N)=C0151(N)*(1.+C0223)
      C063(N)=C021(N)
      C064(N)=C022(N)
```

```
      GO TO 526
  524 CO21(N)=CO15(N)
      CO22(N)=CO151(N)
      CO63(N)=CO21(N)
      CO64(N)=CO22(N)
      GO TO 526
  525 CO18(N)=CO8(N)*CO1(N)*CO3(N)
      CO19(N)=6.2832*CO7(N)*CO9(N)
      CO21(N)=CO15(N)+CO152(N)*CO18(N)/CO19(N)
      CO191=6.2832*CO3(N)*CO10(N)
      CO221=1.+(CO8(N)*CO1(N)*CO3(N)/CO191)*CO152(N)/CO151(N)
      CO22(N)=CO151(N)*CO221
  526 CONTINUE
      DO 865 N=1, KO198
      DM2(N)=CO7(N)
      DM3(N)=CO9(N)
  865 DM4(N)=CO15(N)
      DO 502 N=1,15
      IF(CO7(N)) 502,502,503
  502 CONTINUE
  503 DM1=N
      L=1
      RO197=CO197
      GO TO 511
  506 DO 534 N=1,KO198
      CO23(N)=R32(N)
      CO24(N)=R33(N)
      R32(N) = 0
      R33(N) = 0
      IF (SENSE SWITCH 1) 512,534
  512 PRINT737,CO23(N),CO24(N)
  737 FORMAT(15H 1ST HUB STRESS,F10.3,F10.3)
  534 CONTINUE
      DO 866 N=1,KO198
  866 DM4(N)=CO21(N)
      DO 533 N=1,KO198
      IF(CO7(N))533,533,513
  533 CONTINUE
  513 DM1=N
      L=2
      GO TO 511
  514 DO 516 N=1,KO198
      CO27(N)=R32(N)
      CO28(N)=R33(N)
      R32(N) = 0
      R33(N)=0
      IF (SENSE SWITCH 1) 515,516
  515 PRINT738,CO27(N),CO28(N)
  738 FORMAT(21H 1ST HUB+BLADE STRESS,F10.3,F10.3)
  516 CONTINUE
```

```
      DO 867 N=1,KO198
      DM2(N)=CO5(N)
      DM3(N)=CO10(N)
  867 DM4(N)=CO151(N)
      DO 509 N=1,15
      IF(CO5(N1) 509,509,510
  509 CONTINUE
  510 DM1=N
      RO197=0.
      L=3
      GO TO 511
  517 DO 535 N=1,KO198
      CO25(N)=R32(N)
      CO26(N)=R33(N)
      R32(N) = 0
      R33(N) = 0
      IF (SENSE SWITCH 1) 518,535
  518 PRINT739,CO25(N),CO26(N)
  739 FORMAT(18H 1ST SHROUD STRESS,F10.3,F10.3)
  535 CONTINUE
      DO 868 N=1,KO198
  868 DM4(N)=CO22(N)
      DO 537 N=1,15
      IF (CO5(N))537,537,519
  537 CONTINUE
  519 DM1=N
      L=4
      GO TO 511
  520 DO 869 N=1,KO198
      CO29(N)=R32(N)
      CO30(N)=R33(N)
      R32(N) = 0
      R33(N) = 0
      IF (SENSE SWITCH 1) 521,869
  521 PRINT740,CO29(N),CO30(N)
  740 FORMAT(24H 1ST SHROUD+BLADE STRESS,F10.3,F10.3)
  869 CONTINUE
      GO TO 522
  511 RO0(N)=DM2(N)*DM3(N)
      RO1(N)=RO0(N)*DM2(N)*DM4(N)*CO199*CO199*.00002839
      RO2(N)=1.0/(CO12(N)*1000000.0)
      RO3(N)=CO16(N)*RO2(N)
      RO4(N)=(1.0+CO16(N))*RO2(N)/DM2(N)
      RO5(N)=(CO14(N)/1000000.0)*CO17(N)
      RO6(N)=RO197
      RO7(N)= 1.0
      RO8(N)= 0.0
      RO9(N)= 0.0
      M = N+1
      DO 504 N=M,KO198
```

```
      R00(N)=DM2(N)*DM3(N)
      R11=(DM2(N)-DM2(N-1))/2.0
      R12=DM3(N)*R11
      R13=DM3(N-1)*R11
      R01(N)=R00(N)*DM2(N)*DM4(N)*C0199*C0199*.00002839
      R14=R01(N)+R01(N-1)
      R15=R11*R14
      R02(N)=1.0/(C012(N)*1000000.0)
      R03(N)=C016(N)*R02(N)
      R04(N)=(1.0+C016(N))*R02(N)/DM2(N)
      R16 = R04(N)*R11
      R17 = R04(N-1)*R11
      R18=R03(N)+R16
      R19=R02(N)+R16
      R20=R03(N-1)-R17
      R21=R02(N-1)-R17
      R05(N)=(C014(N)/1000000.0)*C017(N)
      R22=R05(N)-R05(N-1)
      R23=(R18*R12)-(R00(N)*R19)
      R24=((R20*R12)-(R00(N-1)*R19))/R23
      R25=((R21*R12)+(R13*R19))/(-R23)
      R26=((R00(N)*R20)-(R18*R00(N-1)))/R23
      R27=((R18*R13)+(R00(N)*R21))/(-R23)
      R28=((R22*R12)+(R15*R19))/R23
      R29=((R18*R15)+(R00(N)*R22))/R23
      R06(N)=(R24*R06(N-1))+(R25*R07(N-1))
      R07(N)=(R26*R06(N-1))+(R27*R07(N-1))
      R08(N)=((R24*R08(N-1))+(R25*R09(N-1)))+R28
  504 R09(N)=((R26*R08(N-1))+(R27*R09(N-1)))+R29
      R30=(C0195-R08(K0198))/R06(K0198)
      NN = DM1
      DO 505 N= NN,K0198
      R32(N)=(R06(N)*R30)+R08(N)
  505 R33(N)=(R07(N)*R30)+R09(N)
      GO TO (506,514,517,520,542,548),L
  522 DO 527 N=1,K0198
      IF(C08(N))527,527,528
  528 C031(N)=(C07(N)*(C024(N)-(C016(N)*C023(N))))/(C012(N)*1000000.0)
      C0311(N)=(C014(N)*C017(N)*C07(N))/1000000.0
      C032(N)=(C07(N)*(C028(N)-(C016(N)*C027(N))))/(C012(N)*1000000.0)
      C033(N)=(C05(N)*(C026(N)-(C016(N)*C025(N))))/(C012(N)*1000000.0)
      C0331(N)=(C014(N)*C017(N)*C05(N))/1000000.0
      C034(N)=(C05(N)*(C030(N)-(C016(N)*C029(N))))/(C012(N)*1000000.0)
      C036(N)=C0199*C0199*.00002839*C01(N)*C02(N)*C03(N)*C06(N)*C0152(N)
      C037=C036(N)*C08(N)/(C032(N)-C031(N))
      C038(N)=C036(N)*C08(N)/(C034(N)-C033(N))
      C039(N)=(C014(N)*C017(N)*(C05(N)-C07(N)))/1000000.0
      C040=(C033(N)-C032(N))-C039(N)
      C041(N)=C040*C038(N)/C08(N)
      IF (SENSE SWITCH 2) 530,531
```

```
530 PRINT741,C041(N)
741 FORMAT (17H 1ST BLADE FORCE,F10.3)
531 C042=C041(N)*C03(N)/C01(N)
    C0422=(SIN(C04(N)/57.296)*SIN(C04(N)/57.296))/(C012(N)*1000000.0)
    C0423=(COS(C04(N)/57.296)*COS(C04(N)/57.296))/(C013(N)*1000000.0)
    C0421=C0422+C0423
    C043(N)=C0421*C042
    C044=(C038(N)*(C033(N)-C0331(N))*(C033(N)-C0331(N)))/2.0
    C045=(C037*(C032(N)-C0311(N))*(C032(N)-C0311(N)))/2.0
    C046(N)=C044+C045
    C047=C08(N)*C041(N)*C043(N)/2.0
    C048=C046(N)-C047
    C049(N)=C037+C038(N)
    C050=C043(N)*C038(N)
    C051=C043(N)*C050
    C052=C051-(2.0*C048)
    C053=C049(N)*C052
    C054=(C050*C050)-C053
    C0541 ABSF(C054)
    C055=SQRT(C0541)
    C056=((C055-C050)/C049(N))+C0311(N)
    C057=C043(N)+C056+C039(N)
    C0581=((C033(N)-C057)*C038(N))/C08(N)
    C058(N)=ABSF(C0581)
    C059=C041(N)-C058(N)
    C060(N)=C059/C058(N)
    IF(SENSE SWITCH 3) 745,561
745 PRINT746,N,C060(N)
746 FORMAT(17HERROR RATIO STA. I3,F10.5)
561 C0601(N)=(C060(N)*C060(N))-.01
    IF(C0601(N)) 562,562,563
563 C041(N)=C058(N)
    GO TO 531
562 C061(N)=C056/C032(N)
    C062(N)=C057/C033(N)
    C063(N)=C021(N)*C061(N)
    C064(N)=C0151(N)*C062(N)
    C058(N)=C0581
527 CONTINUE
    DO 870 N=1,K0198
    DM2(N)=C07(N)
    DM3(N)=C09(N)
870 DM4(N)=C063(N)
    DO 540 N=1,15
    IF(C07(N))540,540,541
540 CONTINUE
541 DM1=N
    R0197=C0197
    L=5
    GO TO 511
```

```
  542 DO 544 N=1,KO198
      CO65(N)=R32(N)
      CO66(N)=R33(N)
      R32(N) = 0
      R33(N) = 0
      IF (SENSE SWITCH 1) 543, 544
  543 PRINT742,N,CO65(N),CO66(N)
  742 FORMAT(25H REVISED HUB STRESS STA ,I3,F10.3,F10.3)
  544 CONTINUE
      DO 871 N=1,KO198
      DM2(N)=CO5(N)
      DM3(N)=CO10(N)
  871 DM4(N)=CO64(N)
      DO 799 N=1,KO198
      IF (CO5(N)) 799,799,547
  799 CONTINUE
  547 DM1=N
      RO197=0.
      L=6
      GO TO 511
  548 DO 560 N=1,KO198
      CO67(N)=R32(N)
      CO68(N)=R33(N)
      R32(N) = 0
      R33(N) = 0
      IF (SENSE SWITCH 1) 549,560
  549 PRINT743,N,CO67(N),CO68(N)
  743 FORMAT(27H REVISED SHROUD STRESS STA I3,F10.3,F10.3)
  560 CONTINUE
      DO 565 N=1,KO198
      CO69=(CO66(N)-(CO16(N)*CO65(N)))*CO7(N)/(CO12(N)*1000000.0)
      CO70=(CO68(N)-(CO16(N)*CO67(N)))*CO5(N)/(CO12(N)*1000000.0)
      IF(CO8(N))566,566,567
  566 CO82(N)=CO69
      CO83(N)=CO70
      CO64(N)=0
      CO103(N)=CO65(N)
      CO104(N)=CO66(N)
      CO105(N)=CO67(N)
      CO108(N)=CO68(N)
      GO TO 568
  567 CO71=(CO70-CO69)-CO39(N)
      CO72=CO58(N)+((CO71*CO38(N))/CO8(N))
      CO73=(CO72*CO43(N))/CO41(N)
      CO74=(CO8(N)*CO72*CO73)/2.0
      CO75=CO46(N)-CO74
      CO76=CO38(N)*CO73
      CO77=CO73*CO76
      CO78=CO77-(2.0*CO75)
      CO79=CO49(N)*CO78
```

```
      CO80=(CO76*CO76)-CO79
      CO801=ABSF(CO80)
      CO81=SQRT(CO801)
      CO82(N)=((CO81-CO76)/CO49(N))+CO311(N)
      CO83(N)=CO73+CO82(N)+CO39(N)
      CO84(N)=((CO33(N)-CO331(N)-CO83(N))*CO38(N))/CO8(N)
  568 IF (SENSE SWITCH 3) 875,300
  875 PRINT744,N,CO82(N),CO83(N),CO84(N)
  300 CONTINUE
  744 FORMAT (26H MOD,SHO DEF, BLD LOAD STAI3,F10.8,F10.8,F10.3)
      IF(CO1(N))886,886,569
  886 CO85(N)=0
      GO TO 887
  569 CO85(N)=CO84(N)/(CO1(N)*CO2(N))
  887 CO86(N)=CO85(N)*SIN(CO4(N)/57.296)
      CO87(N)=CO85(N)*COS(CO4(N)/57.296)
      IF(N-K0198)571,570,571
  570 CO88=CO4(N)
      GO TO 572
  571 CO88=CO4(N+1)
  572 IF(N-1)573,573,574
  573 CO89=CO4(N)
      GO TO 876
  574 CO89=CO4(N-1)
  876 CO90=(CO89-CO4(N))/114.59
      CO91=(CO4(N)-CO88)/114.59
      CO92=SIN(CO90)
      CO93=SIN(CO91)
      CO941=1.0-(CO92+CO93)
      IF(CO941)889,888,889
  888 CO94=1.0
      GO TO 890
  889 CO94=1.0/CO941
  890 CO951=1.0+(CO92+CO93)
      IF(CO951)892,891,892
  891 CO95=1.0
      GO TO 893
  892 CO95=1.0/CO951
  893 IF (CO195) 575,575,576
  575 CO96(N)=1.35*CO86(N)*CO95
      CO97(N)=1.35*CO87(N)*CO95
      IF(CO1(N))879,879,877
  879 CO98=0
      GO TO 577
  877 CO98=((1.35*CO94)*(CO36(N)+CO84(N)))/(CO1(N)*CO2(N))
      GO TO 577
  576 CO96(N)=CO195*CO86(N)*CO95
      CO97(N)=CO195*CO87(N)*CO95
      IF(CO1(N))879,879,878
  878 CO98=((CO195*CO94)*(CO36(N)+CO84(N)))/(CO1(N)*CO2(N))
```

```
    577 C099(N)=C098*SIN(C04(N)/57.296)
        C0100(N)=C098*COS(C04(N)/57.296)
        IF(C065(N))895,894,895
    840 C0104(N)=0
        C0103(N)=0
        GO TO 896
    894 C0103(N)=0
        C0104(N)=C066(N)
        GO TO 896
    895 C0101=C066(N)/C065(N)
        IF (C07(N))880,880,881
    681 C0103(N)=(C012(N)*C082(N)*1000000.0)/(C07(N)*(C0101-C016(N)))
        C0104(N)=C0101*C0103(N)
    896 IF(C067(N))898,883,898
    883 C0105(N)=0.
        C0108(N)=C068(N)
        GO TO 903
    898 C0102=C068(N)/C067(N)
        IF (C05(N))883,883,884
    884 C0105(N)=(C012(N)*C083(N)*1000000.0)/(C05(N)*(C0102-C016(N)))
        IF(C011(N))897,897,885
    897 C0107=0.0
        GO TO 498
    885 IF(C08(N))897,897,904
    904 C0106=C08(N)*C011(N)*C011(N)*4.0*C010(N)
        C0107=(3.14159*C084(N)*C05(N))/C0106
    498 CONTINUE
        C0108(N)=(C0102*C0105(N))+(C0107*SIN(C04(N)/57.296))
    850 FORMAT (2XF9.0,F9.0,F9.0,F9.0,F9.0)
    903 IF (C08(N))901,902,901
    902 C086(N)=0.
        C087(N)=0.
        C096(N)=0.
        C097(N)=0.
        C099(N)=0.
        C0100(N)=0.
    901 CONTINUE
        PUNCH 850,C086(N),C087(N),C096(N),C097(N),C099(N)
    900 FORMAT(2X,F9.3,F9.5,F9.5)
        PUNCH 900,C021(N),C082(N),C083(N)
    565 PUNCH 850,C0100(N),C0103(N),C0104(N),C0105(N),C0108(N)
        PRINT863
    863 FORMAT (47HPUT OUTPUT CARDS AFTER INPUT CARDS,RUN DECK TWO)
        PAUSE
        GO TO 282
        END
```

APPENDIX II

FORTRAN LISTING, STRESS COMPUTER PROGRAM, SOURCE DECK II

```
      COMMON    C01(15),C02(15),C03(15),C04(15),C05(15),C06(15),C07(15)
      COMMON    C08(15),C09(15),C010(15),C011(15),C012(15),C013(15)
      COMMON    C014(15),C015(15),C016(15),C017(15),C018(15),C019(15)
      COMMON    C020(15),C021(15),C022(15),C023(15),C024(15),C025(15)
      COMMON    C026(15),C027(15),C028(15),C029(15),C030(15),C031(15)
      COMMON    C032(15),C033(15),C034(15),C035(15),C036(15),C038(15)
      COMMON    C039(15),C041(15),C043(15),C046(15),C049(15),C061(15)
      COMMON    C062(15),C063(15),C064(15),C065(15),C066(15),C067(15)
      COMMON    C068(15),C082(15),C083(15),C086(15),C087(15),C096(15)
      COMMON    C097(15),C099(15),C0100(15),C0103(15),C0104(15)
      COMMON    C0105(15),C0108(15),C0561(15),DM2(15),DM3(15),DM4(15)
      COMMON    R00(15),R01(15),R02(15),R03(15),R04(15),R05(15)
      COMMON    R06(15),R07(15),R08(15),R09(15),R31(15),R32(15)
      COMMON    R33(15),R10(15),C058(15),C0311(15),C0331(15)
      COMMON    C060(15),C084(15),C085(15),C0601(15)
      COMMON    C0151(15),C0152(15)
  827 FORMAT (I3,2X,F6.2,2X,F6.2,2X,I3,4X,F4.0)
  828 FORMAT (F6.2,F6.2,F6.3,F7.2,F5.1)
  830 FORMAT (5X,F6.3,F6.3)
  834 FORMAT (19X,19HDIFFUSER DIMENSIONS)
  835 FORMAT (42H   INNER RADIUS   SHROUD ANGLE   HUB ANGLE,8HDIAMETER)
  836 FORMAT (8X,2HIN,13X,3HDEG,10X,3HDEG,8X,5HRATIO)
  837 FORMAT (5X,F7.3,9X,F6.2,7X,F6.2,6X,F6.3)
  838 FORMAT (18X,21HDIFFUSER HAS NO VANES)
  840 FORMAT (16X,24HDIFFUSER VANE DIMENSIONS)
  841 FORMAT (4X,43HRADIAL   NO   WIDTH   FLAT   THICKNESS   BEND ,4HBEND)
  842 FORMAT (3X,12HLOCATION  OF,10X,6HLENGTH,11X,13HRADIUS  ANGLE)
  843 FORMAT (6X,2HIN,5X,9HVANES  IN,6X,2HIN,6X,2HIN,7X,2HIN,6X,2HIN)
  844 FORMAT (3X,F7.3,1X,F4.0,2X,F6.2,1XF6.2,3X,F5.3,3X,F6.2,2X,F6.2)
  823 FORMAT (48H STA  YOUNGS      SHEAR   POISSONS          DENSITY)
  824 FORMAT (32H NO.  MODULUS   MODULUS    RATIO)
  825 FORMAT (6X,7HMEGAPSI,3X,7HMEGAPSI,14X,18HHUB  SHROUD  BLADE)
  826 FORMAT (I4,3X,F5.1,5X,F5.1,5X,F5.3,3X,F5.3,2X,F5.3,2X,F5.3)
  800 FORMAT (40H                                              )
  801 FORMAT (40H                                              )
  802 FORMAT (40H                                              )
  803 FORMAT (I3,1X,F8.0,F7.0,4X,F5.2,5X,F3.0)
  804 FORMAT (5X,F7.3,F8.3,F8.3,F8.3,F6.3)
  805 FORMAT (5X,F7.3,F8.3,F8.3,F8.3,F6.0)
  806 FORMAT (5X,F4.0,F5.1,F6.1,F6.2,F6.2,F5.3,F6.3)
  850 FORMAT(2X,F9.0,F9.0,F9.0,F9.0,F9.0)
  900 FORMAT(2X,F9.3,F9.0,F9.0)
  703 FORMAT(1H )
  704 FORMAT(34H CALCULATED VALUES OF HUB STRESSES  )
  705 FORMAT(16H STATION  RADIUS6X10HTANGENTIAL2X6HRADIAL6X6HRADIAL)
  706 FORMAT(22X30HSTRESS       STRESS       GROWTH)
  707 FORMAT(12X2HIN9X3HPSI9X3HPSI10X2HIN)
  709 FORMAT (5X,I3,3X,F7.3,4X,F8.0,4X,F8.0,5X,F7.5)
  710 FORMAT(34H CALCULATED VALUES OF SHROUD STRESSES  )
  711 FORMAT(16H STATION  RADIUS6X6HRADIAL4X10HTANGENTIAL4X6HRADIAL)
```

```
712 FORMAT(5H    NO17X6HSTRESS6X6HSTRESS6X6HGROWTH)
713 FORMAT(12X2HIN10X3HPSI8X3HPSI10X2HIN)
715 FORMAT (4X,I3,3X,F8.3,3X,F8.0,4X,F8.0,5X,F7.5)
716 FORMAT (1H2)
717 FORMAT (36H CALCULATED VALUES OF BLADE STRESSES)
720 FORMAT (49H BLADE STRESS CONCENTRATION FACTOR = 1.35          )
721 FORMAT(36H BLADE STRESS CONCENTRATION FACTOR = F5.2)
723 FORMAT (18X,8HHUB SIDE,20X,11HSHROUD SIDE)
724 FORMAT (18X,8HOF BLADE,21X,9HOF  BLADE)
725 FORMAT (22X,10HSTRESS PSI,20X,10HSTRESS PSI)
726 FORMAT (4H STA,15X,5HSHEAR,4X,7HTENSILE,14X,5HSHEAR,4X,7HTENSILE)
727 FORMAT (4H NO.,5X,6HRADIUS,24X,6HRADIUS)
728 FORMAT (11X,2HIN,7X,3HPSI,7X,3HPSI,8X,2HIN,7X,3HPSI,7X,3HPSI)
730 FORMAT (I4,4X,F7.3,F10.0,F10.0,F10.3,F10.0,F10.0)
731 FORMAT (13X,10HMEAN BLADE)
732 FORMAT (49H STA      RADIUS      SHEAR     TENSILE                  )
733 FORMAT (49H NO.                  STRESS     STRESS                  )
734 FORMAT (49H            IN        PSI        PSI                     )
736 FORMAT (I4,F10.3,F10.0,F10.0)
737 FORMAT (43H SHROUD BENDING BETWEEN BLADES NOT INCLUDED)
738 FORMAT (39H SHROUD BENDING BETWEEN BLADES INCLUDED)
801 FORMAT (12H INPUT DATA )
810 FORMAT(7H    RPM=F8.0,11H  RIM LOAD=F7.0,20H WHEEL HAS CENT.HOLE)
803 FORMAT(7H    RPM=F8.0,11H  RIM LOAD=F7.0,22HWHEEL HAS NO CENT.HOLE)
812 FORMAT (17X,3HHUB,22X,6HSHROUD,16X,3HRAY)
813 FORMAT(30X33X5HANGLE)
814 FORMAT (4H STA,8X,14HRADIUS  LENGTH,8X,21HRADIUS  LENGTH  DEPTH)
815 FORMAT(4H NO.10X,2HIN6X,2HIN12X,2HIN6X,2HIN5X,2HIN11X,3HDEG)
816 FORMAT(I4,7X,F7.3,F8.3,7X,F7.3,F8.3,F7.3,8X,F4.0)
817 FORMAT (20X,6HBLADES,25X,7HCOEF.OF,5X,5HDELTA)
818 FORMAT(30X20X9HEXPANSION6X  1HT)
819 FORMAT(4H STA4X3OHRADIUS  LENGTH  WIDTH  THICK   NO OF)
820 FORMAT(4H NO.6X2HIN6X2HIN5X2HIN5X2HIN5X6HBLADES3X11HMICROIN/IN )
821 FORMAT(30X21X16HDEG.F      DEG.F)
822 FORMAT(I4,F10.3,F8.3,F7.3,F7.3,F7.0,8X,F5.1,5X,F6.0)
600 READ 600
    READ 601
    READ 802
    READ 603,KO198,CO199,CO196,CO195,CO197
    READ 827,KO200,CO201,CO202,KO203,CO204
    READ 828,CO205,CO206,CO207,CO208,CO209
    DO 860 N=1, KO198
860 READ 804,CO7(N),CO9(N),CO5(N),CO10(N),CO11(N)
    DO 861 N=1,KO198
861 READ 805,CO6(N),CO3(N),CO2(N),CO1(N),CO8(N)
    DO 862 N=1,KO198
862 READ 806,CO4(N),CO14(N),CO17(N),CO12(N),CO13(N),CO16(N),CO15(N)
    DO 829 N=1,KO198
829 READ 830,CO151(N),CO152(N)
    DO 851 N=1, KO198
```

```
      READ  850,CO86(N),CO87(N),CO96(N),CO97(N),CO99(N)
      READ  900,CO21(N),CO82(N),CO83(N)
  851 READ  850,CO100(N),CO103(N),CO104(N),CO105(N),CO108(N)
      IF(KO200)403,402,403
  403 N=KO200
      CO227=1.0/CO16(N)
      IF(CO9(N))406,407,406
  407 CO234=0.
      GO TO 404
  406 CO221=CO199**2.0*(CO7(N)+CO7(KO198))*(CO9(N)+CO9(KO198))*CO15(N)
      CO222=(CO221*.000007098*SIN(CO202/57.296))/COS(CO202/57.296)
      CO225=(CO222*.75*CO15(N))/(CO9(N)**2.)
      CO228=((CO7(N)**2.)*(CO227-1.))/(CO7(KO198)**2.)
      CO230=(4.*CO7(KO198)**2.)*(CO227+1.)*LOG(CO7(KO198)/CO7(N))
      CO232=CO230-(CO7(KO198)**2.*(CO227+3.))+CO7(N)**2.*(4.+CO228)
      CO234=(CO225*CO232)/(CO227+1.+CO228)
  404 IF(CO10(N))405,408,405
  408 CO235=0.
      GO TO 409
  405 CO223=CO199**2.*(CO5(N)+CO5(KO198))*(CO10(N)+CO10(KO198))*CO151(N)
      CO224=(CO223*.000007098*SIN(CO201/57.296))/COS(CO201/57.296)
      CO226=(CO224*.75*CO151(N))/(CO10(N)**2.)
      CO229=((CO5(N)**2.)*(CO227-1.))/(CO5(KO198)**2.)
      CO231=(4.*CO5(KO198)**2.)*(CO227+1.)*LOG(CO5(KO198)/CO5(N))
      CO233=CO231-(CO5(KO198)**2.*(CO227+3.))+CO5(N)**2.*(4.+CO229)
      CO235=(CO226*CO233)/(CO227+1.+CO229)
      CO236=(CO9(N)**2.)*CO234/6.
      CO237=(CO10(N)**2.)*CO235/6.
  409 IF(CO204)410,411,410
  411 CO103(N)=CO103(N)+CO234
      CO105(N)=CO105(N)+CO235
  412 IF (SENSE SWITCH 1) 413,402
  413 PRINT 414,CO236,CO237
  414 FORMAT (16HDIFF BEND MOMENT,F8.0,3HHUB,F8.0,6HSHROUD)
      GO TO 402
  410 CO238=((CO7(KO203)-CO7(N))/CO9(KO203))**3.*(CO204/3.14159)
      CO239=CO238/(CO7(KO203)*CO12(N)*10.**6.)
      CO240=((CO5(KO203)-CO5(N) /CO10(KO203))**3.*(CO204/3.14159)
      CO241=CO240/(CO5(KO203)*CO12(N)*10.**6.)
      CO242=24.*(CO206**2.)*SIN(CO209/57.296)*COS(CO209/57.296)/CO205
      CO209=CO209/57.296
      CO343=CO12(N)*10.**6.
      CO243=(CO242/(CO207**3.))*((CO208*CO209)+(CO206/3.))/CO343
      CO244=(CO206+(CO208*CO209))*CO207*CO205*CO7(KO203)*(CO199**2.)
      CO245=CO244*.00005678*CO152(KO203)
      CO246=(1./CO239)+(1./CO243)
      CO209=CO209*57.296
      CO247=(CO245*COS(CO209/57.296))/(SIN(CO209/57.296)*CO246)
      CO248=(1./CO241)+(1./CO243)
```

```
      C0249=(C0245*COS(C0209/57.296))/(SIN(C0209/57.296)*C0248)
      C0250=(C0247*(C07(K0203)-C07(N))*C0204)/(C0239*C07(N)*6.2831&)
      C0251=(C0249*(C05(K0203)-C05(N))*C0204)/(C0241*C05(N)*6.2831&)
      C0252=1.-(C0250/C0236)
      C0253=1.-(C0251/C0237)
      C0103(N)=C0103(N)+(C0254*C0252)
      C0105(N)=C0105(N)+(C0255*C0253)
      C0236=C0236*C0252
      C0237=C0237*C0253
      C0254=(6.*C0245*COS(C0209/57.296)*C0206)/(C0205*(C0207**2.))
      C0256=C0245/2.0
      C0257=C0245/SIN(C0209/57.296)
      GO TO 412
  402 CONTINUE
      PUNCH 800
      PUNCH 801
      PUNCH 802
      PUNCH 703
      PUNCH 704
      PUNCH 705
      PUNCH 705
      PUNCH 706
      PUNCH 707
      DO 706 N=1,K0198
  706 PUNCH 709,N,C07(N),C0104(N),C0103(N),C082(N)
      PUNCH 708
      PUNCH 708
      PUNCH 710
      C0602=0.
      DO 601 N=1,K0198
  601 C0602=C0602+C011(N)
      IF(C0602)603,603,604
  603 PUNCH 737
      GO TO 605
  604 PUNCH 738
  605 PUNCH 708
      PUNCH 711
      PUNCH 712
      PUNCH 713
      PUNCH 708
      DO 714 N=1,K0198
  714 PUNCH 715,N,C05(N),C0105(N),C0108(N),C083(N)
      PUNCH 716
      PUNCH 717
      IF (C0195) 718,718,719
  718 PUNCH 720
      GO TO 722
  719 PUNCH 721,C0195
  722 PUNCH 708
      PUNCH 708
```

```
      PUNCH 723
      PUNCH 724
      PUNCH 703
      PUNCH 725
      PUNCH 703
      PUNCH 726
      PUNCH 727
      PUNCH 728
      DO 729 N=1,K0198
  729 PUNCH 730,N,C07(N),C0100(N),C099(N),C05(N),C097(N),C096(N,
      PUNCH 703
      PUNCH 703
      PUNCH 731
      PUNCH 732
      PUNCH 733
      PUNCH 734
      PUNCH 703
      DO 735 N=1,K0198
  735 PUNCH 736,N,C06(N),C087(N),C086(N)
      PUNCH 716
      PUNCH 800
      PUNCH 801
      PUNCH 802
      PUNCH 703
      PUNCH 807
      IF (C0197)808,808,809
  808 PUNCH 810,C0199,C0196
      GO TO 811
  809 PUNCH 863,C0199,C0196
  811 PUNCH 703
      PUNCH 703
      PUNCH 812
      PUNCH 813
      PUNCH 814
      PUNCH 815
      DO 852 N=1,K0198
  852 PUNCH 816,N,C07(N),C09(N),C05(N),C010(N),C011(N),C04(N)
      PUNCH 703
      PUNCH 703
      PUNCH 817
      PUNCH 818
      PUNCH 819
      PUNCH 820
      PUNCH 821
      DO 853 N=1, K0198
  853 PUNCH 822,N,C06(N),C03(N),C02(N),C01(N),C08(N),C014(N),C017(N)
      IF(K0200)831,832,831
  831 PUNCH 834
      PUNCH 703
```

```
      PUNCH 835
      PUNCH 836
      PUNCH 703
      C0255=C07(K0198)/C07(K0200)
      PUNCH 837,C07(K0200),C0201,C0202,C0255
      PUNCH 703
      IF(C0204)838,839,838
  839 PUNCH 839
      GO TO 832
  838 PUNCH 840
      PUNCH 703
      PUNCH 841
      PUNCH 842
      PUNCH 843
      PUNCH 844,C07(K0203),C0204,C0205,C0206,C0207,C0208,C0209
  832 CONTINUE
      PUNCH 716
      PUNCH 823
      PUNCH 824
      PUNCH 703
      PUNCH 825
      DO 854 N=1,K0198
  854 PUNCH 826,N,C012(N),C013(N),C016(N),C015(N),C0151(N),C0152(N)
      PUNCH 716
      GO TO 600
      END
```

APPENDIX III

BLANK INPUT DATA SHEETS

A copy of the blank input data sheets used for coding the input of the computer program is shown on the next three pages. Rather than showing the numerical values corresponding to the runs of interest in this format, instructions were included in the program to print the input values as part of the program output. Thus, the input values corresponding to Runs 41 and 44 will be found with the print-outs shown in Appendixes VI and V, respectively, with a different format from that shown here.

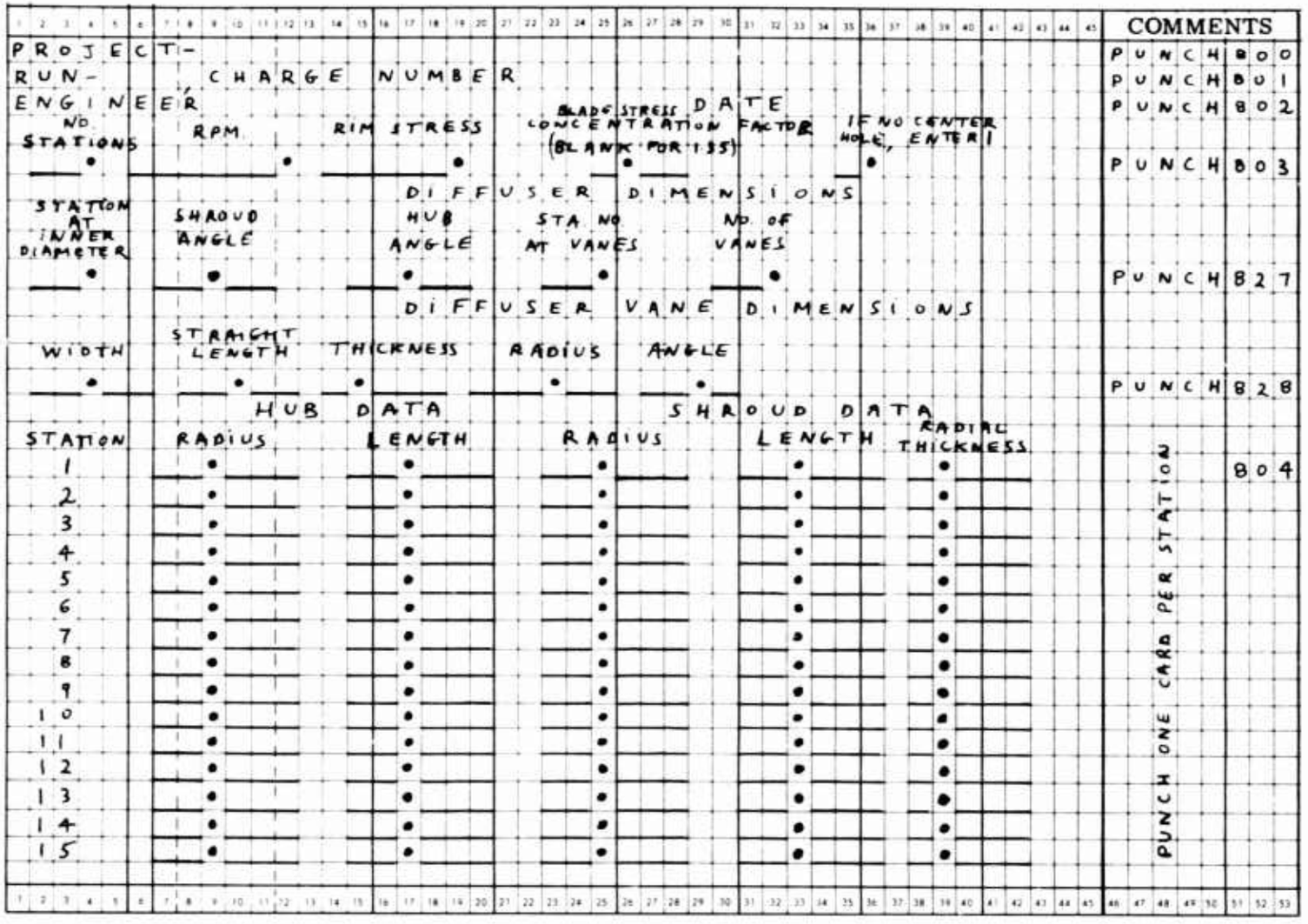
PROJECT-
RUN-
CHARGE NUMBER
ENGINEER
DATE
NO STATIONS
RPM
RIM STRESS
BLADE STRESS CONCENTRATION FACTOR (BLANK FOR 1.35)
IF NO CENTER HOLE, ENTER 1
DIFFUSER DIMENSIONS
STATION AT INNER DIAMETER
SHROUD ANGLE
HUB ANGLE
STA NO AT VANES
NO OF VANES
DIFFUSER VANE DIMENSIONS
WIDTH
STRAIGHT LENGTH
THICKNESS
RADIUS
ANGLE
HUB DATA
SHROUD DATA
STATION
RADIUS
LENGTH
RADIUS
LENGTH
RADIAL THICKNESS
1
2
3
4
5
6
7
8
9
10
11
12
13
14
15
COMMENTS
PUNCH 800
PUNCH 801
PUNCH 802
PUNCH 803
PUNCH 827
PUNCH 828
PUNCH ONE CARD PER STATION
804

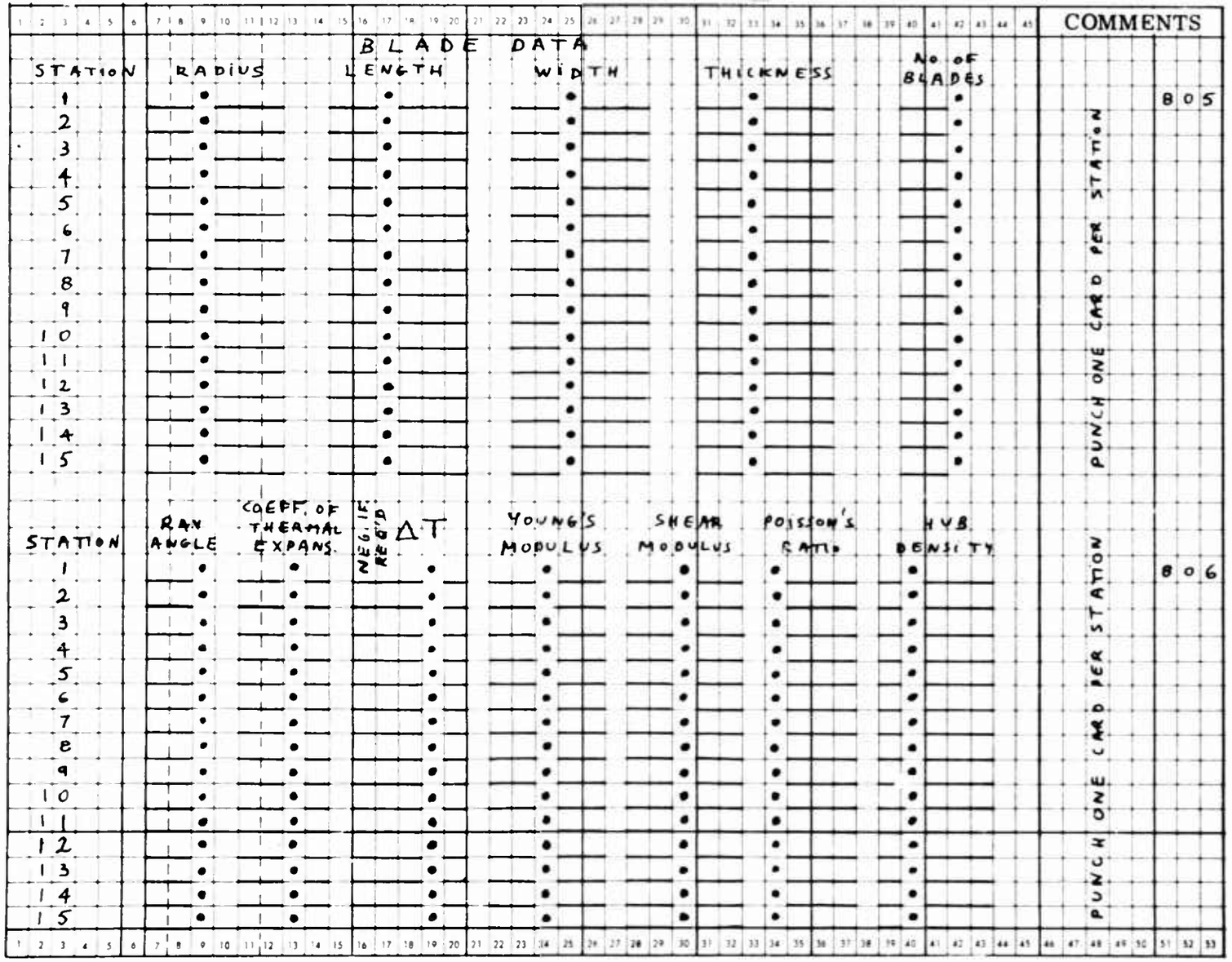
BLADE DATA
STATION
RADIUS
LENGTH
WIDTH
THICKNESS
No. OF BLADES
COMMENTS
PUNCH ONE CARD PER STATION
B 0 5
STATION
RAN ANGLE
COEFF. OF THERMAL EXPANS.
NEG'LE REQ'D
ΔT
YOUNG'S MODULUS
SHEAR MODULUS
POISSON'S RATIO
MVB DENSITY
PUNCH ONE CARD PER STATION
B 0 6
PUNCH ONE CARD PER STATION

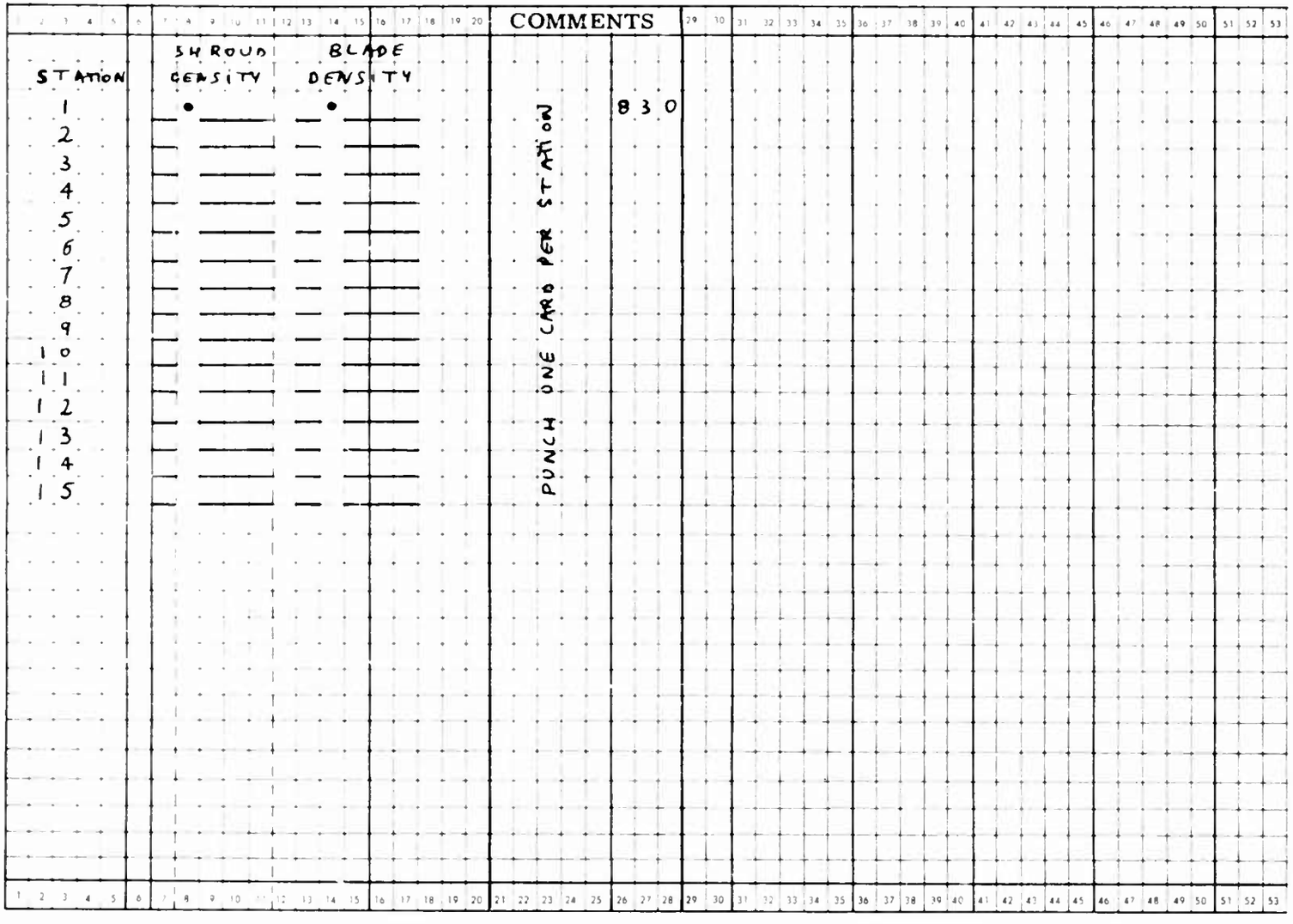
COMMENTS
STATION
SHROUD DENSITY
BLADE DENSITY
1
2
3
4
5
6
7
8
9
10
11
12
13
14
15
PUNCH ONE CARD PER STATION
830

APPENDIX IV

LIST OF FABRICATION DRAWINGS

Title	Drawing No.	Part No.
Assembly	036-1000	-9
Outer Shroud	036-1001	-1
Back Plate	036-1002	-1
Hub Spider	036-1003	-1
Hub Disc	036-1004	-1
Blade	036-1005	-1
Shroud Blade Channel	036-1006	-1
Backplate Blade Channel	036-1006	-3
Fairing Clip	036-1007	-1 and -2
Inner Shroud Fairing	036-1007	-13
Hub Spinner	036-1007	-5
Shroud Doubler	036-1007	-7

APPENDIX V

INPUT AND OUTPUT DATA, FINAL DESIGN (RUN 44)

2
PROJECT-FINAL DESIGN-TSWH-SHROUD-FLANGE
RUN-44 NO RADIAL THICKNESS
ENGINEER BOEHLER DATE-14 OCT.19

INPUT DATA
RPM= 1180. RIM LOAD= . WHEEL HAS CENT.HOLE

STA NO.	HUB RADIUS IN	HUB LENGTH IN	SHROUD RADIUS IN	SHROUD LENGTH IN	SHROUD DEPTH IN	RAY ANGLE DEG
1	1.120	1.520	.000	.000	.000	90.
2	1.250	2.180	13.590	.340	.000	80.
3	1.500	3.280	13.591	.340	.000	80.
4	1.600	3.160	13.592	.690	.000	77.
5	1.870	2.770	13.593	2.010	.000	73.
6	2.670	3.100	13.700	.520	.000	64.
7	2.900	3.000	13.940	.200	.000	60.
8	5.170	.500	14.380	.140	.000	55.
9	7.800	.250	14.940	.100	.000	52.
10	9.540	.230	15.530	.090	.000	49.
11	11.000	.125	16.120	.090	.000	46.
12	19.000	.125	20.740	.100	.000	25.
13	25.510	.125	25.490	.130	.000	.
14	28.000	.125	27.950	.125	.000	.
15	32.188	.125	32.188	.125	.000	.

STA NO.	BLADES RADIUS IN	BLADES LENGTH IN	BLADES WIDTH IN	BLADES THICK IN	NO OF BLADES	COEF.OF EXPANSION MICROIN/IN DEG.F	DELTA T DEG.F
1	.000	.000	.000	.000	.	.0	.
2	8.470	10.300	.600	.072	18.	.0	.
3	8.470	10.300	.600	.072	18.	.0	.
4	8.475	10.440	1.000	.072	18.	.0	.
5	8.480	10.580	2.100	.072	18.	.0	.
6	8.540	11.430	2.340	.072	18.	.0	.
7	8.640	12.160	1.500	.072	18.	.0	.
8	9.760	11.080	1.700	.072	18.	.0	.
9	11.370	9.030	1.500	.072	18.	.0	.
10	12.550	7.860	1.110	.072	18.	.0	.
11	13.570	7.030	3.800	.072	18.	.0	.
12	19.870	4.030	5.520	.072	18.	.0	.
13	25.510	2.940	3.060	.072	18.	.0	.
14	.000	.000	.000	.000	.	.0	.
15	.000	.000	.000	.000	.	.0	.

DIFFUSER DIMENSIONS

INNER RADIUS IN	SHROUD ANGLE DEG	HUB ANGLE DEG	DIAMETER RATIO
25.510	4.25	4.25	1.261

DIFFUSER HAS NO VANES

2

STA NO.	YOUNGS MODULUS	SHEAR MODULUS	POISSONS RATIO	DENSITY		
	MEGAPSI	MEGAPSI		HUB	SHROUD	BLADE
1	10.0	3.8	.337	.098	.098	.098
2	10.0	3.8	.337	.394	.187	.098
3	10.0	3.8	.337	.347	.187	.098
4	10.0	3.8	.337	.316	.187	.098
5	10.0	3.8	.337	.289	.197	.098
6	10.0	3.8	.337	.232	.208	.098
7	10.0	3.8	.337	.199	.200	.098
8	10.0	3.8	.337	.124	.192	.098
9	10.0	3.8	.337	.130	.165	.098
10	10.0	3.8	.337	.127	.147	.098
11	10.0	3.8	.337	.144	.116	.098
12	10.0	3.8	.337	.125	.103	.098
13	10.0	3.8	.337	.118	.100	.098
14	10.0	3.8	.337	.098	.098	.098
15	10.0	3.8	.337	.110	.110	.098

2

PROJECT-FINAL DESIGN-TSMH-SHROUD-FLANGE
RUN-44 NO RADIAL THICKNESS
ENGINEER BOEHLER DATE-14 OCT.19

CALCULATED VALUES OF HUB STRESSES

STATION NO	RADIUS IN	TANGENTIAL STRESS PSI	RADIAL STRESS PSI	RADIAL GROWTH IN
1	1.120	1473.	.	.00516
2	1.250	4166.	349.	.00536
3	1.550	3509.	618.	.00549
4	1.600	3218.	737.	.00547
5	1.870	2664.	964.	.00544
6	2.670	1910.	945.	.00542
7	2.900	1883.	992.	.00544
8	5.170	2522.	3692.	.00566
9	7.800	2771.	3804.	.00116
10	9.540	2582.	3072.	.00147
11	11.000	2737.	3964.	.00154
12	19.000	1998.	1623.	.00275
13	25.510	1452.	2135.	.00259
14	28.000	1189.	408.	.00294
15	32.188	896.	.	.00288

CALCULATED VALUES OF SHROUD STRESSES
SHROUD BENDING BETWEEN BLADES NOT INCLUDED

STATION NO	RADIUS IN	RADIAL STRESS PSI	TANGENTIAL STRESS PSI	RADIAL GROWTH IN
1	.000	.	.	.00000
2	13.590	.	3053.	.00112
3	13.591	.	818.	.00111
4	13.592	.	1064.	.00144
5	13.593	.	1547.	.00210
6	13.700	26.	1813.	.00247
7	13.940	96.	1624.	.00221
8	14.380	200.	1818.	.00251
9	14.940	326.	1778.	.00249
10	15.530	384.	1665.	.00238
11	16.120	546.	2137.	.00314
12	20.740	664.	1907.	.00349
13	25.490	1392.	1490.	.00343
14	27.950	368.	1507.	.00386
15	32.188	.	1165.	.00375

CALCULATED VALUES OF BLADE STRESSES
BLADE STRESS CONCENTRATION FACTOR = 1.00

STA NO.	HUB SIDE OF BLADE RADIUS IN	STRESS PSI SHEAR PSI	TENSILE PSI	SHROUD SIDE OF BLADE RADIUS IN	STRESS PSI SHEAR PSI	TENSILE PSI
1	1.120	.	.	.000	.	.
2	1.250	294.	1668.	13.590	193.	1094.
3	1.500	278.	1580.	13.591	203.	1152.
4	1.630	377.	1512.	13.592	255.	1024.
5	1.870	414.	1356.	13.593	244.	798.
6	2.670	617.	1262.	13.700	342.	702.
7	2.900	779.	1349.	13.940	476.	825.
8	5.170	833.	1189.	14.380	499.	713.
9	7.830	834.	1067.	14.940	518.	663.
10	9.540	878.	1010.	15.530	553.	636.
11	11.000	832.	862.	16.120	333.	345.
12	13.000	1015.	473.	20.740	235.	109.
13	25.510	835.	.	25.490	299.	.
14	28.000	.	.	27.950	.	.
15	32.188	.	.	32.188	.	.

STA NO.	MEAN BLADE RADIUS IN	SHEAR STRESS PSI	TENSILE STRESS PSI
1	.000	.	.
2	8.470	209.	1190.
3	8.470	210.	1192.
4	8.475	271.	1087.
5	8.480	269.	881.
6	8.540	381.	781.
7	8.640	514.	890.
8	9.760	534.	763.
9	11.370	545.	698.
10	12.550	581.	669.
11	13.570	402.	416.
12	19.870	329.	153.
13	25.510	363.	.
14	.000	.	.
15	.000	.	

APPENDIX VI

INPUT, STATION LOCATION AND OUTPUT DATA (RUN 41)

TSWH-.125 SHROUD-FLANGE AND DOUBLER-REV.
RUN FORTY-ONE
BOEHLER JUNE 20,1965

INPUT DATA
RPM= 1180. RIM LOAD= . WHEEL HAS CENT.HOLE

	HUB		SHROUD			RAY ANGLE
STA NO.	RADIUS IN	LENGTH IN	RADIUS IN	LENGTH IN	DEPTH IN	DEG
1	1.125	1.170	.000	.000	.000	90.
2	1.430	2.620	.000	.000	.000	90.
3	1.950	2.140	13.575	1.400	.185	79.
4	2.200	1.940	13.590	.890	.180	75.
5	2.460	1.680	13.600	.955	.180	71.
6	2.730	2.740	13.665	.685	.315	68.
7	3.140	.880	14.010	.200	.315	63.
8	3.500	.840	14.530	.105	.345	58.
9	4.350	.450	14.680	.100	.365	57.
10	7.190	.200	15.390	.072	.500	53.
11	11.000	.100	16.965	.070	.500	46.
12	18.000	.100	21.015	.090	1.000	29.
13	25.517	.100	25.517	.080	1.800	.
14	28.000	.098	28.000	.090	1.200	.
15	33.051	.095	33.051	.100	.700	.

	BLADES					COEF.OF EXPANSION	DELTA T
STA NO.	RADIUS IN	LENGTH IN	WIDTH IN	THICK IN	NO OF BLADES	MICROIN/IN DEG.F	DEG.F
1	.000	.000	.000	.000	.	.0	.
2	.000	.000	.000	.000	.	.0	.
3	7.740	11.840	1.200	.070	18.	.0	.
4	7.870	11.730	1.200	.070	18.	.0	.
5	8.000	11.700	1.530	.070	18.	.0	.
6	8.160	11.680	1.680	.070	18.	.0	.
7	8.450	11.870	.880	.070	18.	.0	.
8	8.780	12.430	1.150	.070	18.	.0	.
9	9.250	11.730	2.200	.070	18.	.0	.
10	11.000	9.430	3.220	.070	18.	.0	.
11	13.590	7.020	3.950	.070	18.	.0	.
12	19.000	4.280	8.040	.070	18.	.0	.
13	25.560	2.940	1.960	.070	18.	.0	.
14	.000	.000	.000	.000	.	.0	.
15	.000	.000	.000	.000	.	.0	.

DIFFUSER DIMENSIONS

INNER RADIUS IN	SHROUD ANGLE DEG	HUB ANGLE DEG	DIAMETER RATIO
25.517	4.25	4.25	1.295

DIFFUSER HAS NO VANES

2

STA NO.	YOUNGS MODULUS	SHEAR MODULUS	POISSONS RATIO	DENSITY		
	MEGAPSI	MEGAPSI		HUB	SHROUD	BLADE
1	10.0	3.8	.337	.098	.000	.000
2	10.0	3.8	.337	.098	.000	.000
3	10.0	3.8	.337	.118	.143	.098
4	10.0	3.8	.337	.118	.143	.098
5	10.0	3.8	.337	.118	.143	.098
6	10.0	3.8	.337	.116	.180	.098
7	10.0	3.8	.337	.130	.212	.098
8	10.0	3.8	.337	.098	.206	.098
9	10.0	3.8	.337	.098	.210	.098
10	10.0	3.8	.337	.098	.167	.098
11	10.0	3.8	.337	.098	.130	.098
12	10.0	3.8	.337	.098	.124	.098
13	10.0	3.8	.337	.098	.119	.098
14	10.0	3.8	.337	.098	.098	.000
15	10.0	3.8	.337	.098	.098	.000

2

TSWH-.125 SHROUD-FLANGE AND DOUBLER-REV.
RUN FORTY-ONE
BOEHLER JUNE 20,1965

CALCULATED VALUES OF HUB STRESSES

STATION	RADIUS IN	TANGENTIAL STRESS PSI	RADIAL STRESS PSI	RADIAL GROWTH IN
1	1.125	1190.	.	.00013
2	1.430	917.	153.	.00012
3	1.950	3109.	1509.	.00050
4	2.200	2906.	1693.	.00051
5	2.460	2714.	1883.	.00051
6	2.730	2256.	2096.	.00051
7	3.140	2919.	3264.	.00057
8	3.500	2650.	2952.	.00059
9	4.350	2831.	5.	.00067
10	7.190	2812.		.00111
11	11.000	2892.	3	.00176
12	18.000	2070.	17	.00264
13	25.517	1491.	2343.	.00313
14	28.000	1189.	461.	.00289
15	33.051	858.	.	.00283

CALCULATED VALUES OF SHROUD STRESSES
SHROUD BENDING BETWEEN BLADES INCLUDED

STATION NO	RADIUS IN	RADIAL STRESS PSI	TANGENTIAL STRESS PSI	RADIAL GROWTH IN
1	.000	.	.	.00000
2	.000	.	.	.00000
3	13.575	.	3023.	.00153
4	13.590	1.	2717.	.00156
5	13.600	2.	3048.	.00180
6	13.665	10.	2252.	.00194
7	14.010	78.	2862.	.00158
8	14.530	238.	4788.	.00197
9	14.680	328.	6717.	.00250
10	15.390	582.	6266.	.00291
11	16.965	709.	6375.	.00312
12	21.015	649.	2815.	.00359
13	25.517	3889.	1509.	.00337
14	28.000	440.	1562.	.00396
15	33.051	.	1160.	.00383

CALCULATED VALUES OF BLADE STRESSES
BLADE STRESS CONCENTRATION FACTOR = 1.00

STA NO.	HUB SIDE OF BLADE RADIUS IN	STRESS PSI SHEAR PSI	TENSILE PSI	SHROUD SIDE OF BLADE RADIUS IN	STRESS PSI SHEAR PSI	TENSILE PSI
1	1.125	.	.	.000	.	.
2	1.430	.	.	.000	.	.
3	1.950	284.	1462.	13.575	158.	816.
4	2.200	360.	1344.	13.590	226.	846.
5	2.460	432.	1256.	13.600	271.	788.
6	2.730	495.	1226.	13.665	301.	746.
7	3.140	695.	1364.	14.010	421.	826.
8	3.500	777.	1243.	14.530	487.	779.
9	4.350	688.	1060.	14.680	411.	634.
10	7.190	681.	903.	15.390	341.	452.
11	11.000	772.	800.	16.965	293.	303.
12	18.000	922.	511.	21.015	199.	110.
13	25.517	872.	.	25.517	290.	.
14	28.000	.	.	28.000	.	.
15	33.051	.	.	33.051	.	.

STA NO.	MEAN BLADE RADIUS IN	SHEAR STRESS PSI	TENSILE STRESS PSI
1	.000	.	.
2	.000	.	.
3	7.740	179.	923.
4	7.870	242.	905.
5	8.000	288.	837.
6	8.160	322.	798.
7	8.450	458.	899.
8	8.780	512.	820.
9	9.250	429.	661.
10	11.000	373.	496.
11	13.590	354.	367.
12	19.000	279.	154.
13	25.560	363.	.
14	.000	.	.
15	.000	.	.

Uncl. ssified
Security lassification

DOCUMENT CONTROL DATA - R&D
(Security classification of title, body of abstract and indexing annotation must be entered when the overall report is classified)

1 ORIGINATING ACTIVITY (Corporate author) Aerophysics Company Washington, D. C. 20036	2a REPORT SECURITY CLASSIFICATION Unclassified 2b GROUP

3 REPORT TITLE

INVESTIGATION OF LIGHTWEIGHT STRUCTURAL DESIGN TECHNIQUES FOR LIGHTWEIGHT FANS

4 DESCRIPTIVE NOTES (Type of report and inclusive dates)

5 AUTHOR(S) (Last name, first name, initial)

Boehler, Gabriel D., Foshag, William F., Deutsch, Edward and Balciunas, John A.

6 REPORT DATE	7a TOTAL NO OF PAGES	7b NO OF REFS
September 1966	154	10

8a CONTRACT OR GRANT NO	9a ORIGINATOR'S REPORT NUMBER(S)
DA 44-177-AMC-250(T) b. PROJECT NO Project 1P125901A142 c. d.	USAAVLABS Technical Report 66-60 9b OTHER REPORT NO(S) (Any other numbers that may be assigned this report)

10 AVAILABILITY/LIMITATION NOTICES

Distribution of this document is unlimited.

11 SUPPLEMENTARY NOTES	12 SPONSORING MILITARY ACTIVITY
	USAAVLABS Department of the Army Fort Eustis, Virginia

13 ABSTRACT

The results of an investigation of the design and fabrication problems of a minimum-weight rotating-diffuser lift system for an air cushion vehicle (ACV) are presented.

A numerical method for the stress analysis of an indeterminate rotating diffuser centrifugal fan structure was reduced to practice and programmed for the IBM 1620 computer. This method was used as a tool for the analytical design of a minimum-weight RD fan. This fan, with a 64.5-inch overall diameter, was built of aluminum and was structurally tested in the fan test facility of the Joy Manufacturing Company, New Philadelphia, Ohio. Stress levels throughout the fan were measured by means of 21 strain gages.

Results of the tests are very encouraging and vindicate the analytical approach to fan design. Based on measured weights and stress levels, it is concluded that RD fans for ACV applications, for ratings between 100 and 1000 horsepower, can be built for 0.5 pound per horsepower.

DD FORM 1 JAN 64 1473

Unclassified
Security Classification

14 KEY WORDS	LINK A		LINK B		LINK C	
	ROLE	WT	ROLE	WT	ROLE	WT
Structural design techniques Lightweight fans Rotating diffuser fans Air cushion vehicles						

INSTRUCTIONS

1. ORIGINATING ACTIVITY: Enter the name and address of the contractor, subcontractor, grantee, Department of Defense activity or other organization *(corporate author)* issuing the report.

2a. REPORT SECURITY CLASSIFICATION: Enter the overall security classification of the report. Indicate whether "Restricted Data" is included. Marking is to be in accordance with appropriate security regulations.

2b. GROUP: Automatic downgrading is specified in DoD Directive 5200.10 and Armed Forces Industrial Manual. Enter the group number. Also, when applicable, show that optional markings have been used for Group 3 and Group 4 as authorized.

3. REPORT TITLE: Enter the complete report title in all capital letters. Titles in all cases should be unclassified. If a meaningful title cannot be selected without classification, show title classification in all capitals in parenthesis immediately following the title.

4. DESCRIPTIVE NOTES: If appropriate, enter the type of report, e.g., interim, progress, summary, annual, or final. Give the inclusive dates when a specific reporting period is covered.

5. AUTHOR(S): Enter the name(s) of author(s) as shown on or in the report. Enter last name, first name, middle initial. If military, show rank and branch of service. The name of the principal author is an absolute minimum requirement.

6. REPORT DATE: Enter the date of the report as day, month, year; or month, year. If more than one date appears on the report, use date of publication.

7a. TOTAL NUMBER OF PAGES: The total page count should follow normal pagination procedures, i.e., enter the number of pages containing information.

7b. NUMBER OF REFERENCES: Enter the total number of references cited in the report.

8a. CONTRACT OR GRANT NUMBER: If appropriate, enter the applicable number of the contract or grant under which the report was written.

8b, 8c, & 8d. PROJECT NUMBER: Enter the appropriate military department identification, such as project number, subproject number, system numbers, task number, etc.

9a. ORIGINATOR'S REPORT NUMBER(S): Enter the official report number by which the document will be identified and controlled by the originating activity. This number must be unique to this report.

9b. OTHER REPORT NUMBER(S): If the report has been assigned any other report numbers *(either by the originator or by the sponsor)*, also enter this number(s).

10. AVAILABILITY/LIMITATION NOTICES: Enter any limitations on further dissemination of the report, other than those imposed by security classification, using standard statements such as:

(1) "Qualified requesters may obtain copies of this report from DDC."

(2) "Foreign announcement and dissemination of this report by DDC is not authorized."

(3) "U. S. Government agencies may obtain copies of this report directly from DDC. Other qualified DDC users shall request through _____."

(4) "U. S. military agencies may obtain copies of this report directly from DDC. Other qualified users shall request through _____."

(5) "All distribution of this report is controlled. Qualified DDC users shall request through _____."

If the report has been furnished to the Office of Technical Services, Department of Commerce, for sale to the public, indicate this fact and enter the price, if known.

11. SUPPLEMENTARY NOTES: Use for additional explanatory notes.

12. SPONSORING MILITARY ACTIVITY: Enter the name of the departmental project office or laboratory sponsoring *(paying for)* the research and development. Include address.

13. ABSTRACT: Enter an abstract giving a brief and factual summary of the document indicative of the report, even though it may also appear elsewhere in the body of the technical report. If additional space is required, a continuation sheet shall be attached.

It is highly desirable that the abstract of classified reports be unclassified. Each paragraph of the abstract shall end with an indication of the military security classification of the information in the paragraph, represented as *(TS)*, *(S)*, *(C)*, or *(U)*.

There is no limitation on the length of the abstract. However, the suggested length is from 150 to 225 words.

14. KEY WORDS: Key words are technically meaningful terms or short phrases that characterize a report and may be used as index entries for cataloging the report. Key words must be selected so that no security classification is required. Identifiers, such as equipment model designation, trade name, military project code name, geographic location, may be used as key words but will be followed by an indication of technical context. The assignment of links, rules, and weights is optional.

5825-66